2020-05-14

Improving the Performance of Dynamic Electromyogram-to-Force Models for the Hand-Wrist and Multiple Fingers

Berj Bardizbanian
Worcester Polytechnic Institute

IMPROVING THE PERFORMANCE OF DYNAMIC ELECTROMYOGRAM-TO-FORCE MODELS FOR THE HAND-WRIST AND MULTIPLE FINGERS

by

Berj Bardizbanian

A Thesis

Submitted to the Faculty

of the

WORCESTER POLYTECHNIC INSTITUTE

in partial fulfillment of the requirements for the

Degree of Doctor of Philosophy

in

Electrical and Computer Engineering,

2020

APPROVED:

_____

Professor Edward A. Clancy, Major Advisor, WPI ECE

_____

Professor Xinming Huang, Committee Member, WPI ECE

_____

Todd R. Farrell, Ph.D., Committee Member, Liberating Technologies, Inc., Holliston, MA

Abstract

Relating surface electromyogram (EMG) activity to force/torque models is used in many areas including: prosthesis control systems, to regulate direction and speed of movement in reaching and matching tasks; clinical biomechanics, to assess muscle deficiency and effort levels; and ergonomics analysis, to assess risk of work-related injury such as back pain, fatigue and skill tests. This thesis work concentrated on improving the performance of dynamic EMG-to-force models for the hand-wrist and multiple fingers. My contributions include: 1) rapid calibration of dynamic hand-wrist EMG-force models using a minimum number of electrodes, 2) efficiently training two degree of freedom (DoF) hand-wrist EMG-force models, and 3) estimating individual and combined fingertip forces from forearm EMG during constant-pose, force-varying tasks.

My calibration approach for hand-wrist EMG-force models optimized three main factors for 1-DoF and 2-DoF tasks: training duration (14, 22, 30, 38, 44, 52, 60, 68, 76 s), number of electrodes (2 through 16), and model forms (subject-specific, DoF-specific, universal). The results show that training duration can be reduced from historical 76 s to 40–60 s without statistically affecting the average error for both 1-DoF and 2-DoF tasks. Reducing the number of electrodes depended on the number of DoFs. One-DoF models can be reduced to 2 electrodes with average test error range of 8.3–9.2% maximum voluntary contraction (MVC), depending on the DoF (e.g., flexion-extension, radial-ulnar deviation, pronation-supination, open-close). Additionally, 2-DoF models can be reduced to 6 electrodes with average error of 7.17–9.21 %MVC. Subject-specific models had the lowest error for 1-DoF tasks while DoF-specific and universal were the lowest for 2-DoF tasks.

In the EMG-finger project, we studied independent contraction of one, two, three or four fingers (thumb excluded), as well as contraction of four fingers in unison. Using regression, we found that a pseudo-inverse tolerance (ratio of largest to smallest singular value) of 0.01 was optimal. Lower values produced erratic models and higher values produced models with higher errors. EMG-force errors using one finger ranged from 2.5–3.8 %MVC, using the optimal pseudo-inverse tolerance. With additional fingers (two, three or four), the average error ranged from 5–8 %MVC. When four fingers contracted in unison, the average error was 4.3 %MVC.

Additionally, I participated in two team projects—EMG-force dynamic models about the elbow and relating forearm muscle EMG to finger force during slowly force varying contractions. This work is also described herein.

Acknowledgements

First and Foremost, I am greatly thankful to my research advisor, Dr. Edward A. Clancy, for his support and guidance thru my academic years at WPI. There is no word to describe his friendly, honest and patient characters. He was the one who lighten my path to success at WPI and I am honored to know somebody like him in my life.

Thank you to my committee, Professor Xinming Huang and D. Todd Farrell, for your advice and feedback on this thesis.

Thank you to my research partners, Chenyun Dai, Ziling Zhu and Jianan Li who gave me a lot of help on my research.

Thank you to Jennifer Keating for her support and friendship thru our Finger-EMG project.

Thank you to my wife, Marghrit, for your patience and support. For taking upon you the caring of our kids during my absence. For understanding the challenges that I was going thru balancing work, family and study.

Thank you to my kids, Noushig, Armig and Chris for embracing my situation as a father, care provider and student. For acknowledging the fact that life requires sacrifice to earn what you are looking for.

Thank you, my parents, Mom and Dad who gave me love and shelter, for teaching me to stand on my own, for you always cared for me. I wish you were with me. Hope you can read this from the New Jerusalem.

And finally Thank you God who strengthen me and held my hand thru all my difficult times "*So do not fear, for I am with you; do not be dismayed, for I am your God. I will strengthen you and help you; I will uphold you with my righteous right hand*" **(Isaiah: 41:10)**

Table of Contents

Table of Figures

Chapter 1: Background and Introduction

1.1 Background on Electromyography (EMG)

Electromyography, which is the study of muscle function through inquiry of the electrical signal of skeletal muscles, has been of scientific interest since 1666 [Basmajian and DeLuca, 1985]. It incorporates central control strategies, signal transmission along nerve fibers and, through chains of complex biochemical events, the production of forces acting on the tendons of the agonist and/or antagonist muscles, moving the bones.

Body movement is a result of muscle contraction [Marieb and Hoehn, 2013]. The type of contraction depends on the muscle tension (force exerted on an object) and load (opposing force exerted on muscle by an object). Two frequently-studied types of contraction are isotonic and isometric (Fig. 1.1). Isotonic contraction involves either concentric or eccentric contraction. A contraction in which the muscle fibers shorten to create force is called concentric. However, when the muscle lengthens during the contraction, then an eccentric contraction is taking place.

An isometric contraction, on the other hand, is one in which the muscle does not change length while contracting. In an isometric contraction, tension is developed but a load is not moved (e.g., pushing against a wall). During this kind of contraction, the maximum tension for the muscle in use can be reached, but the muscle only shortens slightly from applying tension to tendons and ligaments.

Both active and passive muscle force depend on the length of the muscle. Active force peaks when the muscle is around its resting length, and decreases when the muscle is shortened or lengthened (Fig. 1.2). Passive force, on the other hand, works like a rubber band; it's minimal when the muscle is shortened, and increases exponentially as the muscle lengthens.

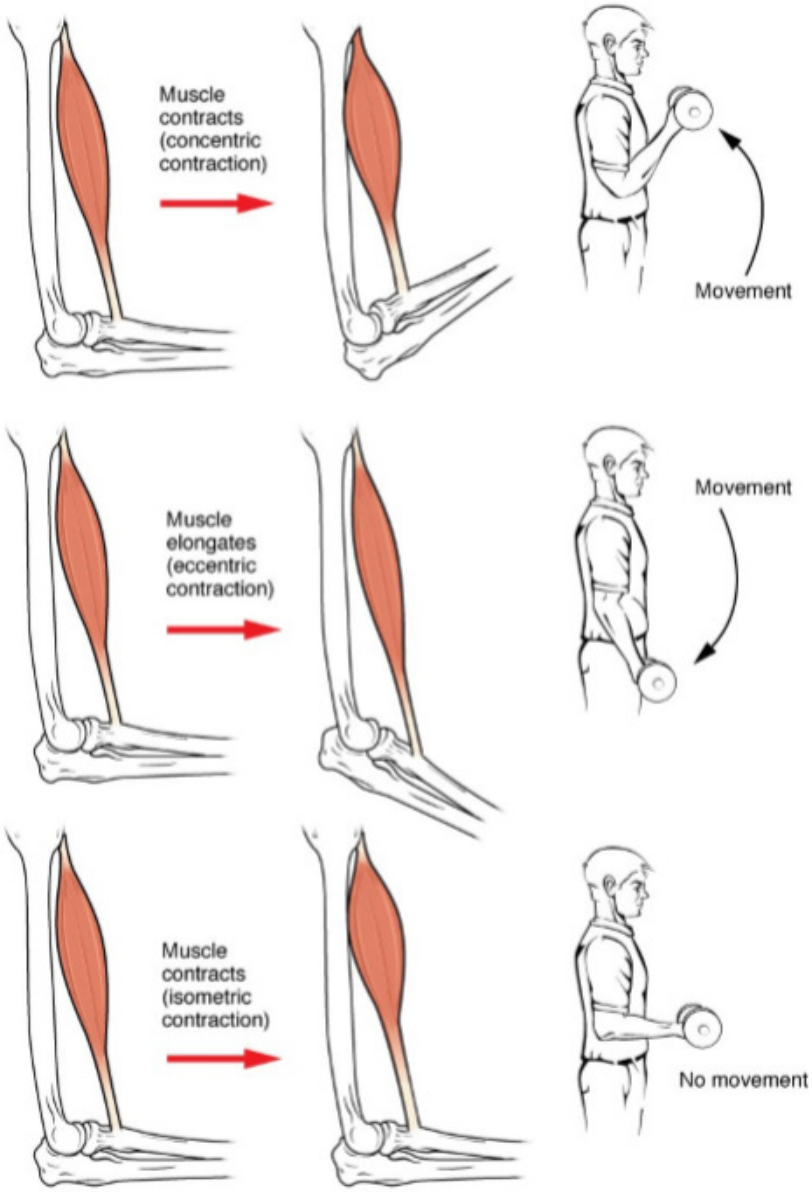

Fig. 1.1. Illustration of concentric, eccentric and isometric contractions [Betts et al., 2017]

Skeletal muscle is made up of bundles of muscle fibers (Fig. 1.3), which in turn are bundles of muscle cells. Each muscle is surrounded by a connective tissue sheath called the epimysium. Fascia, connective tissue outside the epimysium, surrounds and separates the muscles. Portions of the epimysium project inward to divide the muscle into compartments. Each compartment contains a bundle of muscle fibers. Each bundle of muscle fibers is called a fasciculus and is surrounded by a layer of connective tissue called the perimysium. Within the fasciculus, each individual muscle cell, called a muscle fiber, is surrounded by connective tissue called the endomysium.

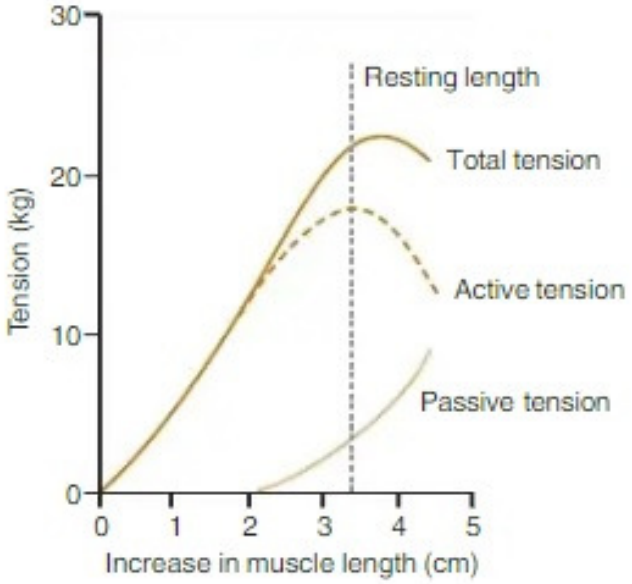

Fig. 1.2. Skeletal Muscle Length-Tension Curves [Barrett et al., 2012]

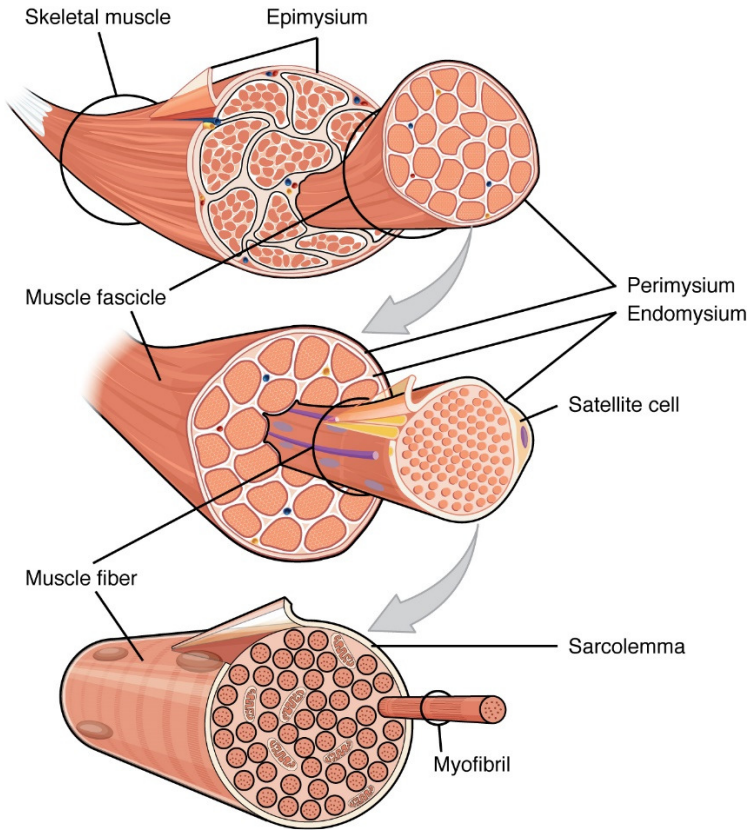

Fig. 1.3. The structure of a skeletal muscle [Betts et al., 2017]

Myofibrils (muscle fibrils) are composed of long proteins including actin, myosin, and titin, and other proteins that hold them together. These proteins are organized into thick and thin filaments called myofilaments, which repeat along the length of the myofibril in sections called sarcomeres. Muscles contract by sliding the thick (myosin) and thin (actin) filaments along each other, thereby shortening the sarcomere length. Energy that is produced in cells by adenosine triphosphate is called ATP energy. ATP energy is essential for many living processes, including muscle contraction and nerve impulses.

People have two general types of skeletal muscle fibers: slow-twitch (type I) and fast-twitch (type II). Slow-twitch muscles tend to be the deeper muscle fibers with slower conduction velocity. They generate more ATP from aerobic metabolism; have slower, less forceful contraction; and are slower to fatigue. Fast twitch muscle fibers produce larger action potentials than those of slow twitch fibers. These muscle fibers fatigue faster but are used in powerful bursts of movements like sprinting. Fast-twitch muscles generate more ATP from glucose (thus, lactic acid is a by-product); produce quicker, more forceful contraction; and are faster to fatigue. The phasic muscles responsible for generating movement in the body contain a higher density of fast-twitch fibers. Strength and power training can increase the number of fast-twitch muscle fibers recruited for a specific movement.

Motor neurons electro-chemically activate muscle fibers. In resting conditions, the concentration of sodium is relatively high outside the muscle cell membrane and relatively low inside the fiber, while potassium concentration is relatively low outside the membrane and relatively high inside of the muscle. When excited via depolarization of the muscle membrane, these relative concentrations flip polarity. As a result, fibers depolarize—which instantiates fiber mechanical contraction and creates a changing electromagnetic field. EMG is the recording of this electromagnetic field, as it propagates within muscle or on the skin surface.

Fig. 1.4 shows the time course of depolarization-repolarization in one individual muscle fiber. The rest potential is often around –70 mV, which is based on the concentration of sodium, potassium and chloride in body cells and fluid. When muscle fibers are activated, the action potential peaks at around +30 mV. The duration of one action potential is usually 2–4 ms or longer. When the overall muscle continues to contract, the same motor unit will successively generate a series of action potentials with quite similar shape.

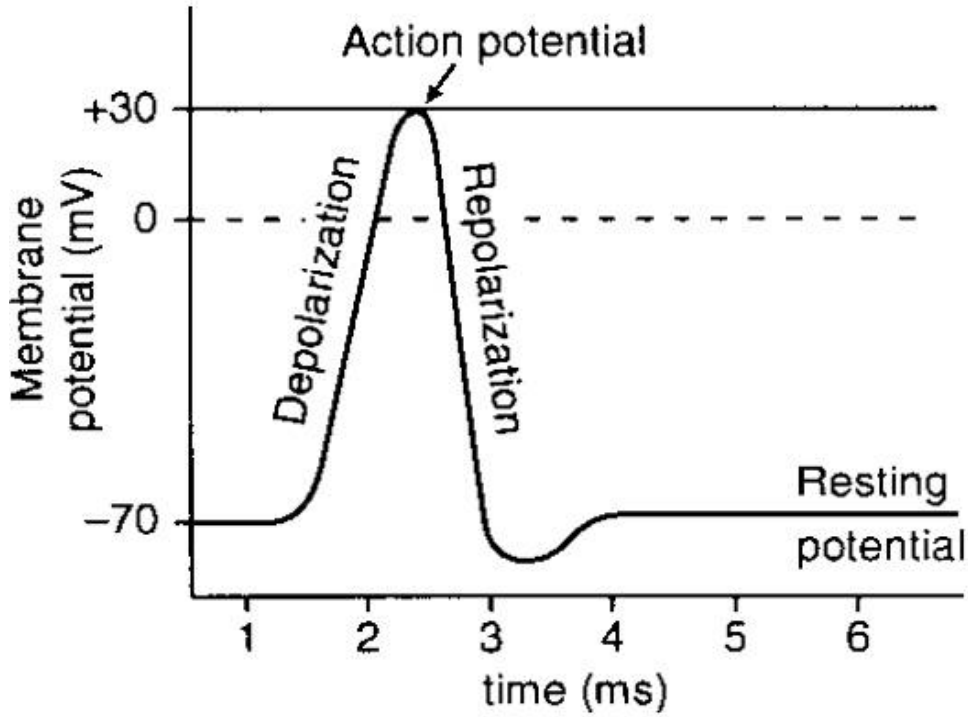

Fig. 1.4. Electrical activity of one individual motor unit [Marieb, 2008]

A motor unit consists of a motoneuron and all of its innervated muscle fibers. When a motoneuron is activated (or "fired"), it results in the near simultaneous discharge of many muscle fibers. The summed electrical activity of all muscle fibers is called the motor unit action potential (MUAP) (Fig. 1.5). The number of motor units recruited has a large impact on the amplitude of EMG. Also, the average frequency with which motor units are activated is called the firing rate. Motor units have initial firing rates of 5–10 pulses per second. As the demand for force increases, firing rate increases and it might exceed 60 pulses per second. For an individual motor unit (and, in general, between motor units) successive firing times are mostly independent and random at low force levels and become more correlated at higher force levels. Muscular force is affected by the pattern of muscular activation, including doublet firing (two successive firings of the same motor in a very short time span, such as 20 ms) or simultaneously fired motor units.

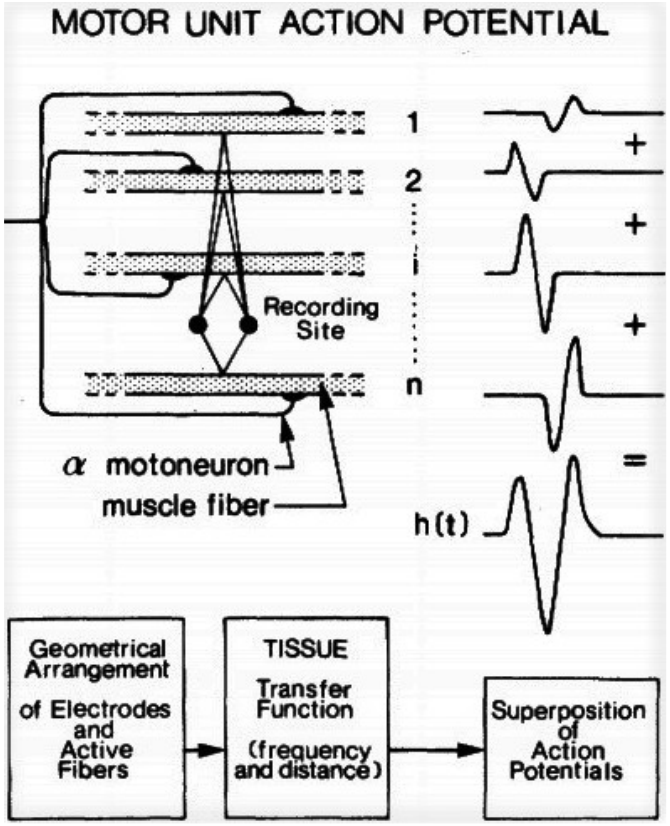

Fig. 1.5. Schematic representation of generation of a motor unit action potential (MUAP) from it constituent muscle fibers [Basmajian and DeLuca, 1985]

One motor unit always generates a similarly shaped action potential for healthy muscles (Fig. 1.6), while different motor units typically produce different action potential shapes; albeit these distinct shapes are still peaked in shape. The shape of a motor unit action potential sometimes may vary due to muscle fatigue or disease [Basmajian and DeLuca, 1985]. When muscle contraction level increases, several different motor units may discharge at the same time. Fig. 1.7 shows this case as the superposition of potentials from individual motor units. When the muscle generates force, each motor unit produces successive motor unit action potentials. This process can be modeled as: the nerve sends a series of stimuli (an impulse train) through its innervated muscle fibers. Then, the EMG output can be regarded as an impulse response train. When many motor units are active at the same time, the EMG recording would be the summation of these impulse response trains. Therefore, the EMG recording looks like a random Gaussian process (i.e., the sum of many mostly-independent, sufficiently identically shaped pulses). Mathematically, equation 1 shows the superposition model of MUAP. Signal $u_i(t)$ is the result of passing the

impulse trains through the shape of the MUAP, *h(t)* (Fig. 1.6), *f* denotes the constant force value, and *s* is the total number of MUAP's present (De Luca and Forrest, 1973). (The firing rate is defined as the average number of MUAPs per second in a MUAP train.)

$$m(t,f) = \sum_{i=1}^{s} u_i(t,f)$$

Equation 1: Model of MUAP

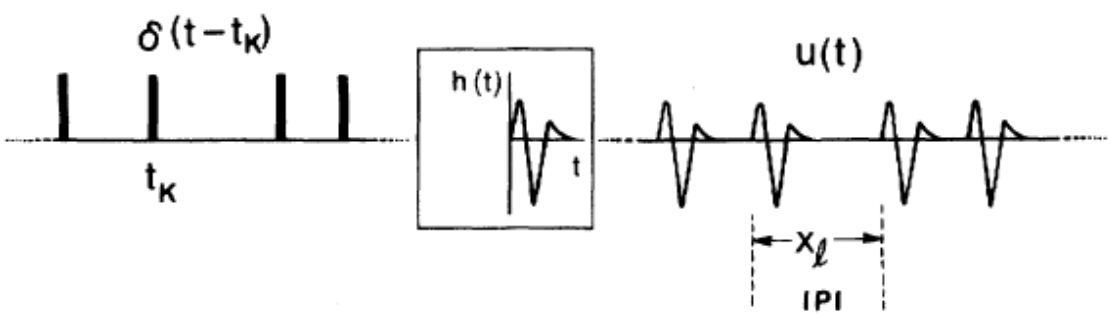

Fig. 1.6. Schematic for motor unit action potential (MUAP) train [DeLuca, 1979]

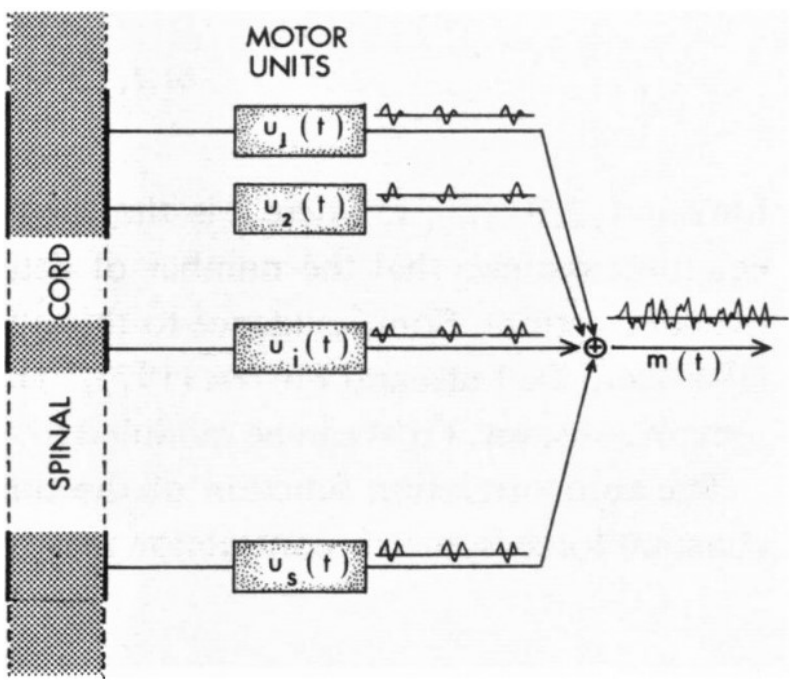

Fig. 1.7. Schematic representation of EMG signal derived from the sum of MUAP trains [DeLuca, 1975]

Merlo et al. [Merlo et al., 2000] modeled the surface EMG signal, $s(t)$, as:

$$s(t) = \sum_j MUAP_j(t) + n(t) = \sum_j \sum_i k_j f(\frac{t - \theta_{ij}}{\alpha_j}) + n(t)$$

Equation 2: Model of surface EMG signal by Merlo et al. [2000]

where k_j is an amplitude factor for the jth motor unit, $f()$ is the shape of the action potential discharge, θ_{ij} is the ith time at which the MUAP occurs, α_j is a scaling factor, and $n(t)$ is additive noise.

The sEMG signal is dependent on the level and duration of contraction, the state of the contraction (static or dynamic), fatigue, and sweat from the skin. The maximum level that a skeletal muscle can contract to is referred to as maximum voluntary contraction (MVC), and contraction levels are typically referred to by the percentage of MVC that they represent. Studies have found that the distribution of the EMG signal is more sharply peaked near zero than a Gaussian distribution, and that at low contraction levels, the signal is more likely to be best modeled as a zero mean Laplacian process [Clancy et. al 2002, Wang et. al 2019].

EMG is acquired either using surface electrodes (Fig. 1.8) or indwelling electrodes (Fig. 1.9). These electrodes are either monopolar (potential difference with respect to a common reference location, with the common reference location often being electrically inactive) or bipolar (potential difference with respect to two electrically active locations). Surface electrodes are a noninvasive and easy to apply method of recording. It involves applying electrolyte gel and rubbing into the skin in lab applications so that it is absorbed to the stratum mucosum to make contact with the derma. Then, the electrode is placed on the muscle under study and held in place by tape or some other means. Disadvantages of using these electrodes include that they can also record EMG from unrelated muscles that is mixed in with the signal of interest (a phenomenon referred to as cross talk), are affected by sweat (if not gelled), and may be more susceptible to motion artifact. Indwelling electrodes record EMG either using single needle or two wires inserted within the muscle. Indwelling EMG has great diagnostic value but is invasive, not appropriate for chronic applications, can be painful, and not appropriate for monitoring many dynamic contractions as occur in human movement.

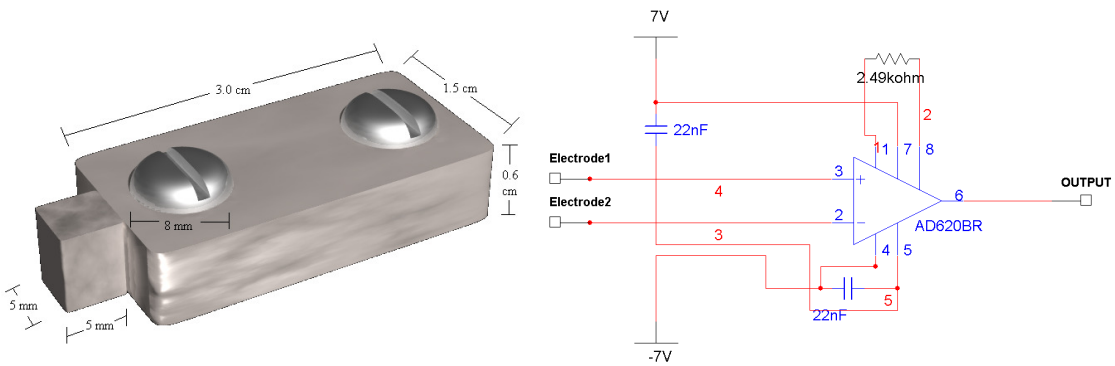

Fig. 1.8. Surface bipolar electrode-amplifier and its electrical circuit [Salini et al., 2003]

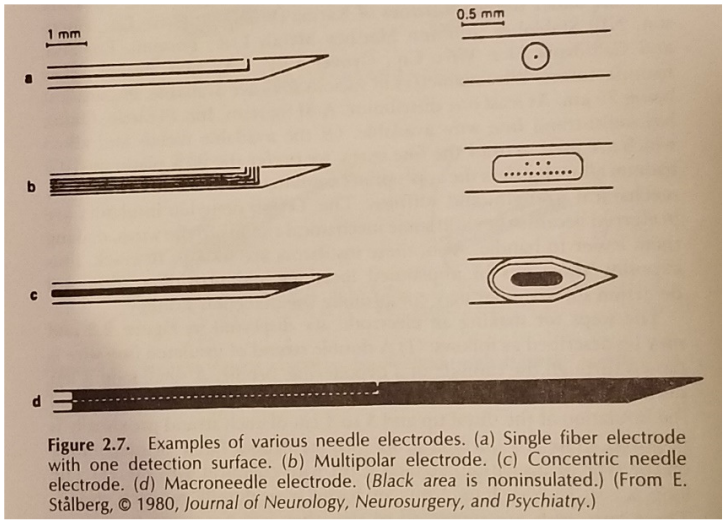

Fig. 1.9. Indwelling electrodes [Stalberg, 1980]

1.2 EMG Processing

Surface EMG was processed across our experiments using five stages: (1) noise rejection/filtering, (2) multiple-channel combination (including gain scaling), (3) demodulation, (4) smoothing and (5) relinearization [Clancy et al., 2002]. This process estimates the time-varying signal standard deviation. The standard deviation of the electrical activity generated by a muscle is commonly referred to as the amplitude of the EMG, which measures the intensity of muscular activation level. Fig. 1.10 shows an example raw EMG signal (in grey) and its EMG amplitude (in blue). When many motor units contract at the same time, the surface EMG signal is the sum of their impulse response trains and can be regarded as an amplitude modulated, zero-mean, random

Gaussian process (see Fig. 1.11). The math expression for this Gaussian process model is: $m[n] = s[n] \cdot v[n]$, where n is the discrete-time sample index, $m[n]$ is raw EMG signal, $s[n]$ is EMG amplitude (i.e., standard deviation) and $v[n]$ is a random process with unit variance. One important feature which can be extracted from the processed EMG signal is EMG amplitude.

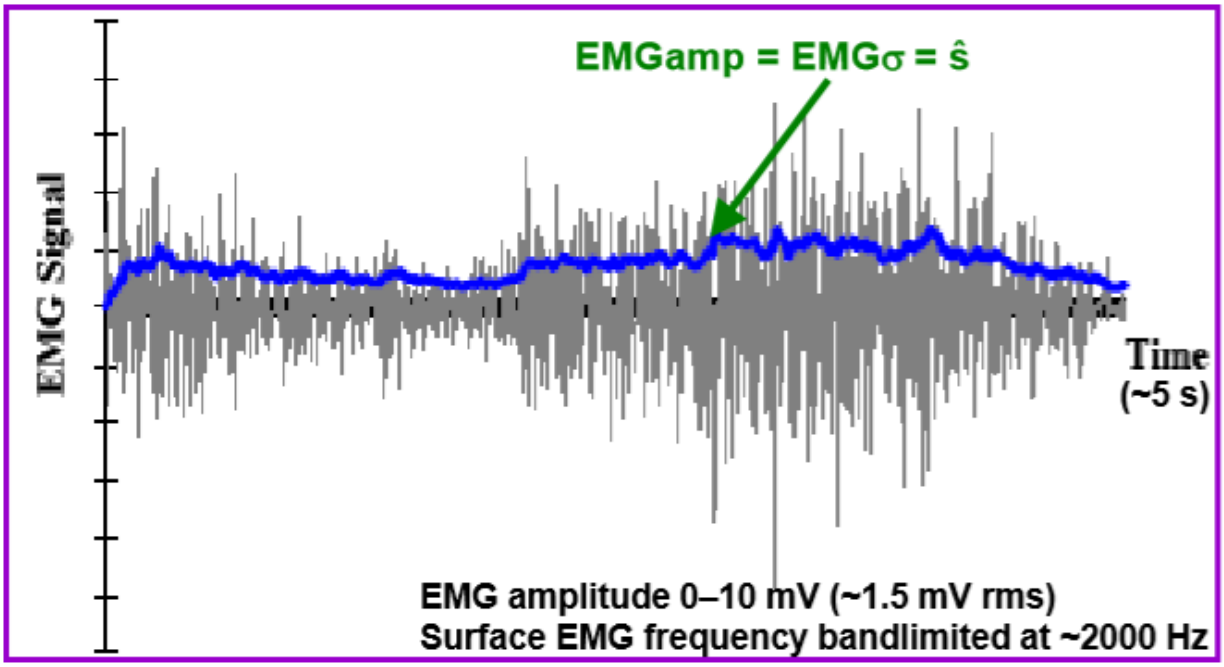

Fig. 1.10. Raw EMG signal (in grey) and its EMG amplitude (in blue) [Clancy, 1991]

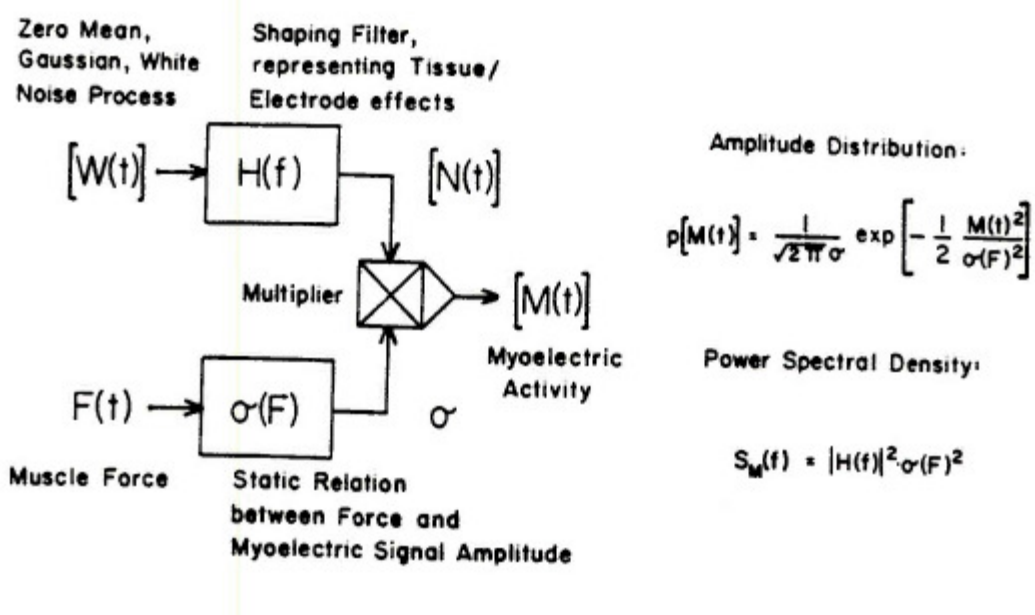

Fig. 1.11. Functional Mathematical model of EMG [Hogan and Mann 1980a]

Fig. 1.12 shows detailed signal processing steps for EMG amplitude estimation. Noise is generated from two sources: inherent and interference [Kamen and Gabriel, 2010]. Inherent noises are initiated at either electrode to skin and electrode to metal interfaces or amplifier noise due to thermal (resistive) and 1/f noises (amplitude is greatest at low frequency, then deceases according to the function 1/f) [Huigen et al., 2002]. Interference noise is induced from the power line (60 Hz) and all the harmonics. Interference is also introduced at lower frequencies due to motion artifacts. In order to attenuate noise, the EMG is highpass filtered at 15 Hz using a 5th order Butterworth filter followed by an IIR notch filter of 1 Hz bandwidth, centered at 60 Hz. To achieve zero phase filtering, forward and reverse time filters were applied off-line. This filtering is followed by a first order demodulation for signal rectification. After demodulation, EMG signals were passed through a noncausal, low pass 9th order Chebyshev Type 1 lowpass filter with an effective cutoff frequency of 0.8*20.48Hz= 16.4 Hz and decimated by a factor of 100, producing a resampled frequency of 40.96 Hz. Finally, relinearization inverts the power law applied during the demodulation stage, returning the signal to units of EMG amplitude.

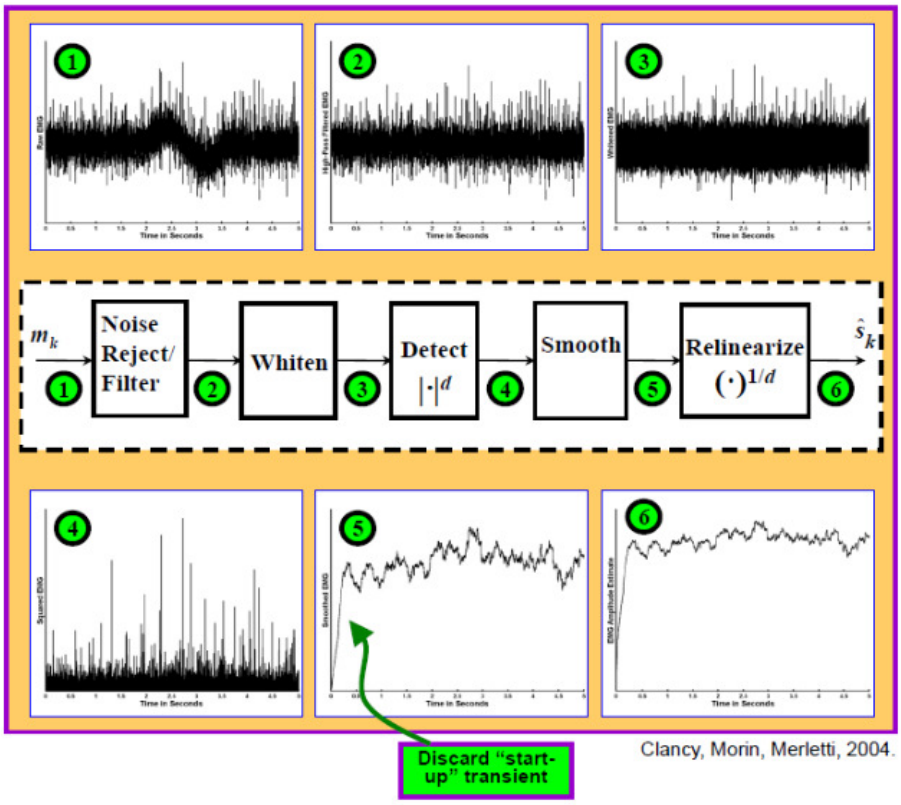

Fig. 1.12. Detailed signal processing procedure of EMG amplitude estimation [Clancy et al. 2002]

EMG amplitude from relevant muscles can be related to one or more joint forces (or moments) using various methods of system identification. Various system identification methods are in use, including least squares and neural network/machine learning approaches [An et al., 1983; Clancy and Hogan, 1997; Clancy et al., 2012; Doheny et al., 2008; Hasan and Enoka, 1985; Heckathorne and Childress, 1981; Hof and Van den Berg, 1981; Hogan and Mann, 1980b; Inman et al., 1952; Lawrence and DeLuca, 1983; Sanger, 2007; Shin et al., 2009; Solomonow et al., 1986; Staudenmann et al., 2009; Thelen et al., 1994; Vredenbregt and Rau, 1973; Staudenmann et al., 2010]. This relation provides a non-invasive tool for applications in many different fields, such as myoelectric control of prosthesis [Parker et al., 2006], clinical biomechanics [Disselhorst-Klug et al., 2009; Doorenbosch and Harlaar, 2003], EMG biofeedback for rehabilitation [Armagan et al., 2003; Holtermann et al., 2010], ergonomic analysis/ task analysis [Hagg et al., 2004; Kumar and Mital, 1996], biomechanical modeling [Karlsson et al., 1992], and measurement in motion control studies [Fukuda et al., 2003].

The EMG to force model that we used throughout our entire project is based on the least squares approach. Equation 3 shows force output at the fingertips or hand-wrist using both linear and nonlinear FIR EMG-force modeling. The model structure was a polynomial nonlinear model of degree D (nonlinear when D>1), the equation for which is shown below [Press et al., 1994]:

$$T_{E-F}[m] = \sum_{d=1}^{D}\sum_{e=1}^{E}\sum_{q=0}^{Q} c_{e,q,d}\sigma_e^d[m-q]$$

Equation 3: EMG-Force Model

- $T_{E\text{-}F}$: Ext-Flx force (or Rad-Uln or Pro-Sup or …)
- m: Decimated discrete time sample index
- E: Number of electrodes (initially set to 16)
- Q: Number of time lags (Q=20, 30, 40)
- $c_{e,q,d}$: Fit coefficients
- σ_e: EMG amplitude
- D: model order

This model can be written as:

$$Ax = b + error$$

Equation 4: Linear Least squares EMG-force model

- $\boldsymbol{A}$ *: design matrix*
- $\boldsymbol{x}$ *: fit coefficient vector*
- $\boldsymbol{b}$ *: output vector*

The solution to this equation is found by minimizing errors in the least square sense by minimizing the square distance between the data and signal vectors through a linear combination of the columns of A [Kay, 1993].

$$min\|Ax - b\|^2$$

Equation 5: Linear Least error minimization

The solution to this equation is:

$$x = (A^T A)^{-1} A^T b = A^\dagger b$$

Equation 6: Calculation of fit coefficients via singular value decomposition to find the pseudo-inverse

where $A^\dagger$ is the Moore-Penrose pseudo-inverse of A, which uses singular value decomposition to compute $A^\dagger$. When calculating $A^\dagger$, the ratio between each individual singular value to the maximum singular value in the design matrix A is limited by a tolerance (Tol). Singular values and vectors below this value are replaced with zero values/vectors after calculating the inverse in the middle section of the above equation [Press et al., 1994].

1.3 My Thesis Contributions

This section introduces my contributions for each of my projects. The projects in which I was the lead investigator during my Ph.D. study were the dynamic-force finger EMG-to-torque with improved methods project, dynamic-force hand-wrist EMG-to-torque with improved methods project for 1-DoF and 2-DoF models. This latter work also included efficiently calibrating and training the EMG-force hand-wrist models.

1.3.1 Finger Project

This thesis research focused on developing signal processing methods that could eventually increase the functionality of prostheses worn by amputees, as well as rehabilitation orthoses worn by stroke victims during rehabilitation. In each case, this thesis investigated the relationship between muscle electrical activity and forces exerted by upper limb.

For the EMG-force work involving the fingers, EMG signals from the forearm were collected on 19 healthy subjects during constant-posture force-varying contractions. Subjects had no known neuromuscular deficits of their right hand, arm, or shoulder. Contraction trials ranged between 30% maximum voluntary contraction (MVC) flexion and 30% MVC extension, and EMG signals were acquired using 12 bipolar surface EMG electrode-amplifiers mounted circumferentially around the forearm. Force was collected using a 100 pound load cell in contact with one or more fingertip. A model was developed to relate EMG amplitude to forces in the fingertip(s) and model performance was compared across all 19 subjects. Deliverables of this

project include a large (*N*=19) dataset (EMG and force recordings) in the forearm/fingers to facilitate the development of signal processing methods that might lead to increased dexterity in prosthetics and orthotics, comprised of:

- Force-varying contractions of each of four fingers (1 Hz bandwidth).
- Additional data related to contraction of multiple fingers at the same time.
- Characterization of model performance for force-varying data versus:
    - The number of electrodes (1 through 12)
    - Model order (D=1, 2)
    - The lag time (Q=20, 30, 40)
    - Filter (whitened, unwhitened)
    - Different tolerance values 0 thru 0.1

Previous literature studies: Existing commercial EMG-controlled prosthetics are mostly limited to rudimentary control: hand close/open/off fixed velocity (Parker et al., 2006) and one degree of freedom of proportional control (Smith et al., 2008). Also, researchers studied classification schemes for discriminating between hand-wrist functions and individual finger movements (Castellini et al., 2009; Khushaba et al., 2012). In our lab, fingertip force estimation from forearm muscle electrical activity from three subjects using electrode arrays of 64 channels was studied by Pu Liu (Liu et al., 2011, 2013). She collected constant-posture, slowly force-varying contraction data and her results showed evidence that surface EMG activity from the forearm encodes multiple degrees of freedom of proportional control information that may be sufficient for use in controlling prosthetic wrists, hands and/or fingers – at least when tested on intact subjects [Liu, 2014].

My contribution in this field: We used 12 bipolar surface electrodes and expanded previous work done by Liu to study 19 more subjects instead of the three she studied. Also, we studied multiple finger models; two independent fingers, three independent fingers and four independent fingers in addition to three finger grip and four finger grip models. (In "grip" models, only one total applied force was measured, not individual finger forces.) Also, we collected data from constant-posture, dynamic force varying contractions using conventional surface electrodes. Our goal was to study how the EMG-force error changes with pseudo-inverse tolerance values and which model yields the lowest error. We found out that the one finger model error ranges from 2.5–3.8 %MVC and

(two, three, four) independent finger models averaged error from 5–8 %MVC. Four finger grip EMG-force error averaged 4.3 %MVC.

1.3.2 Hand-Wrist Project

For EMG-force work involving the hand-wrist, dynamic hand-wrist data had been previously acquired from ten able-bodied subjects [Dai, 2016]. Sixteen conventional bipolar electrodes were mounted circumferentially about the proximal forearm. The hand was secured to a load cell to measure wrist extension-flexion, radial-ulnar deviation or pronation-supination forces. The fingers were secured to a second load cell to measure hand open-close. One-DoF and 2-DoF dynamic contractions (40 s in duration) were collected. The initial 2 s of processed data trials were discarded to compensate for startup transients. Contraction trials ranged between 30% MVC flexion and 30% MVC extension. Backward stepwise selection of the training data sequentially reduced the number of electrodes. RMS error on two separate test trials was evaluated at each step. Training duration was then progressively decreased.

Previous literature studies: Myoelectric prostheses have used surface electromyogram activity from residual muscles to control prosthesis movement, thereby realizing partial replacement of function. Parker et al. (Parker et al., 2006) used one degree of freedom with and without proportional control at a time, with mode switching. Other researchers (Englehart and Hudgins, 2003; Parker, Englehart, 2006; Powell et al., 2014) studied multifunction pattern recognition. (Kuiken et al., 2004; Kuiken et al., 2009) used targeted muscle reinnervation surgery which is costly and requires a long recovery. Alternatively, some researchers utilized a large quantity of specialized electrodes (64–192) and acquired multi–DoF data. The large electrode array was mainly intended to extract more information and decrease the error in EMG-force/kinematics estimation. However, these arrays are not practical for commercial prostheses (Liu et al., 2013; Muceli and Farina, 2012; Muceli et al., 2014). In our lab, Dai (Dai at al 2016, 2017) studied 1-DoF and 2-DoF system identification and the minimum number of electrodes that is needed to extract enough EMG information from the subject to estimate EMG-force models.

My contribution in this field: My research concentrates on two broad subjects: rapid calibration of dynamic EMG-force models and efficiently training their 1-DoF and 2-DoF models. Reducing the number of electrodes is reasonable, but doing so in a real device is the ultimate goal. We don't

want to collect long durations of calibration data, but do not know what data duration is needed. That is why I first studied the effect of reducing the training duration on EMG-force error. Our collected data had 38 s of useful information per trial and we were training using two trials (76 s) and testing on two trials. So, we studied 14, 22, 30, 38, 44, 52, 60, 68 and 76 s of calibration duration. All durations above 44 s used two equally length trials. For example, the 60 s duration study used two 30 s trials for calibration. Durations below 44 s used data from only one trial since, if only shorter durations were necessary, users would likely acquire such data more simply via a single trial. This evaluation helped us examine whether one training trial per contraction type is sufficient or if multiple trials are necessary. We applied the reduced duration study along with study of a reduced number of electrodes, 16 down to 2. So, we generalized Dai's original experiment. Then we asked: what is the optimum best fit parameters that can be extracted from the collected data and how can we calibrate the gains? For this work, we studied four different models: subject specific full duration, where the full system dynamics were calibrated for each subject using a full trial; subject specific reduced duration, where the full system dynamics were calibrated for each subject using reduced trial durations; DoF specific model, where the system dynamics were fixed per each DoF, but gain was calibrated for each subject; and universal model, where the system dynamics were fixed for all trials, but gain was calibrated for each subject. From our study, we concluded that 2-DoF models in which the dynamics were universal across all subjects generally performed 15–21% better than models in which the complete dynamics were trained to each subject. This result was surprising as customized models have historically provided better results. Also, training durations can be reduced, but it depends on the DoF. For example, statistical evaluation showed that Opn-Cls with Flx-Ext can be reduced to 44 s while Opn-Cls with Rad-Uln can be reduced only to 60 s. Further time reduction may be appropriate in some applications if some decrement in performance is acceptable.

1.3.3 Collaborative Work

With Chenyun Dai: Comparison of Constant-Posture Force-Varying EMG-Force Dynamic Models About the Elbow. Used three techniques to improve current models. First, we additionally extracted waveform length, slope sign change rate and zero crossing rate, from raw EMG signals instead of EMG amplitude only. Second, used each EMG channel separately, rather than previous studies which combine multiple channels from biceps (and separately from triceps) into a

combined processed EMG. Third, used an exponential power law model to replace the previous polynomial model. The three new methods were individually compared with the current "best" model. Then, examined if combining pairs of these various improvement techniques provides an additive benefit. Each of the individual improvement techniques showed a better performance ($p<0.05$ and ~10–15% error improvement) than the previously existing "optimal" model.

With Jennifer Keating: Relating Forearm Muscle Electrical Activity to Finger Forces. For this Master's thesis project, we studied slowly force-varying contraction of each of the four fingers and for multiple fingers at the same time, classification of various hand grips/wrist contractions. A model was used to relate forearm extension/flexion EMG amplitudes during slowly force varying contractions to forces in the fingertips. Characterization of model performance vs. the number of electrodes used by identifying the best electrode sets per subject for electrode sets of sizes 6–12.

1.4 Summary of My Ph. D. Research and Introduction to Remaining Chapters

The remaining chapters describe all of my Ph.D. projects in detail in the form of published, accepted, submitted and in-development journal or conference manuscripts. Chapter 2 describes the finger project. It describes in detail the methods that were used to collect dynamic force data from nineteen subjects' individual (Index, Middle, Ring, Pinky excluding the thumb) and combined fingers. In addition, we studied one, two, three, and four independent finger models and a four finger grip model. This chapter will be published as a conference paper. Chapters 3–5 focus on hand-wrist EMG-force studies. They study calibration of dynamic EMG-force models using the minimum number of electrodes. Each chapters was/will be published as a conference paper. Chapter 6 is the collaborative work about the dynamic elbow project. It studies the comparison of constant posture force-varying EMG-force dynamic models about the elbow. This chapter was published as a journal paper.

REFERENCES

An KN., Cooney WP, Chao EY., Askew LJ. and Daube JR. "Determination of forces in extensor pollicis longus and flexor pollicis longus of the thumb," J Appl Physiol, vol. 54, pp. 714–719, 1983.

Armagan O., Tascioglu F., Oner C. Electromyographic biofeedback in the treatment of the hemiplegic hand: aplacebo-controlled study. Am J Phys Med Rehabil 2003; 82: 856–861.

Barrett KE., Barman SM., Boitano S., Brooks HL. Ganong's Review of Medical Physiology, 24th Edition, McGrawHill Lang Medical Publictions: Los Altos, California, pp. 105-108, 2012.

Basmajian J. and De Luca C. Muscles Alive Their Functions Revealed by Electromyography (5th edition), Baltimore, MD: Williams and Wilkins, 1985.

Betts JG., et al. Anatomy and Physiology, openstax, Houston, TX, pp. 392-432, 2017.

Buchanan TS, Lloyd DG., Manal K., and Besier TF. "Neuromusculoskeletal modeling: Estimation of muscle forces and joint moments and movements from measurements of neural command," J Appl Biomech, vol. 20, no. 4, pp. 367–395, 2004.

Castellini C. and van der Smagt P. "Surface EMG in Advanced Hand Prosthetics," Bio. Cyber, vol. 100, pp. 35-47, 2009.

Clancy EA. Stochastic Modeling of the Relationship Between the Surface Electromyogram and Muscle Torque. Ph.D. Thesis, Massachusetts Institute of Technology, January 1991.

Clancy EA, Farry KA. "Adaptive Whitening of the Electromyogram to Improve Amplitude Estimation," IEEE Transactions on Biomedical Engineering, Vol. 47, No. 6, June 2000.

Clancy EA., Hogan N. "Relating agonist-antagonist electromyograms to joint torque during isometric, quasi-isotonic, nonfatiguing contractions," IEEE Trans Biomed Eng 44(10):1024–1028, 1997.

Clancy EA., Liu L., Liu P. and Moyer DV. "Identification of Constant-Posture EMG-Torque Relationship About the Elbow Using Nonlinear Dynamic Models," IEEE Transactions on Biomedical Engineering, Vol. 59, No. 1, pp. 205–212, 2012.

Clancy EA., Morin EL. and Merletti R. "Sampling, Noise-Reduction and Amplitude Estimation Issues in Surface Electromyography," Journal of Electromyography and Kinesiology, Vol. 12, No. 1, pp. 1–16, 2002.

Dai C. "Studies of the relationship between the surface electromyogram, joint torque and impedance," Ph.D. Thesis, Worcester Polytechnic Institute, 2016.

Dai C., Martinez-Luna C., Hunt T., Zhu Z., Farrell TR. and Clancy EA. "System Identification of Two Degrees of Freedom EMG-Force at the Hand-Wrist Using Dynamic Models," Proceedings of the Twenty First Congress of the International Society of Electrophysiology and Kinesiology, Chicago, IL, July 5–8, 2016.

Dai C., Martinez-Luna C., Hunt T., Zhu Z., Farrell TR. and Clancy EA. "Two-DoF, Dynamic, EMG-Based Estimation of Hand-Wrist Forces with a Minimum Number of Electrodes," Myoelectric Controls and Upper Limb Prosthetics Symposium, Fredericton, New Brunswick, Canada, 15–18 August, 2017.

De Luca CJ. and Van Dyk EJ. "Derivation of some parameters of myoelectric signals recorded during sustained constant force isometric contractions," Biophys. J., vol. 15, pp. 1167-1180, 1975.

De Luca CJ., and Forrest WJ. “Some properties of motor unit action potential trains recorded during constant force isometric contractions in man”. Kybernetik. 12(3):160, 1973

DeLuca C. "Physiology and mathematics of myoelectric signals," IEEE Trans Biomed Eng 26(6): 313–325, 1979.

Disselhorst-Klug C., Schmitz-Rode T., and Rau G. "Surface electromyography and muscle force: Limits in sEMG-force relationship and new approaches for applications," Clin. Biomech., vol. 24, pp. 225–235, 2009.

Doheny EP., Lowery MM., FitzPatrick DP. and O'Malley MJ "Effect of elbow joint angle on force-EMG relationships in human elbow flexor and extensor muscles," J Electromyogr Kinesiol, vol. 18, pp. 760–770, 2008.

Doorenbosch CAM. and Harlaar J. "A clinically applicable EMG-force model to quantify active stabilization of the knee after a lesion of the anterior cruciate ligament," Clin. Biomech., vol. 18, pp. 142–149, 2003.

Englehart K. and Hudgins B. "A robust, real-time control scheme for multifunction myoelectric control," IEEE Trans. Biomed. Eng., vol. 50, pp. 848– 854, 2003.

Fukuda O., Tsuji T., Kaneko M., Otsuka A. A human-assisting manipulator teleoperated by EMG signals and arm motions. IEEE Trans Robot Autom 2003; 19: 210–222.

Geiger SR., Adrian RH., Peachey LD. Skeletal Muscle, Bethesda, Md.: American Physiological Society; Baltimore, pp. 150-175, 1983.

Hagg GM., Melin B., Kadefors R. Applications in Ergonomics. In: R. Merletti, P. A. Parker, editors. Electromyography: Physiology, Engineering, and Noninvasive Applications. Hoboken, NJ: John Wiley & Sons, Inc., 2004: 343–363.

Hasan Z. and Enoka RM. "Isometric torque-angle relationship and movement-related activity of human elbow flexors: Implications for the equilibrium-point hypothesis," Exp. Brain Res., vol. 59, pp. 441–450, 1985.

Heckathorne CW. and Childress DS. "Relationships of the surface electromyogram to the force, length, velocity, and contraction rate of the cineplastic human biceps," Am. J. Phys. Med., vol. 60, pp. 1–19, 1981.

Hof AL. and Van den Berg J. "EMG to force processing I: An electrical analogue of the Hill muscle model," J. Biomech., vol. 14, pp. 747–758, 1981.

Hogan N. and Mann RW. "Myoelectric signal processing: Optimal estimation applied to electromyography—Part I: Derivation of the optimal myoprocessor," IEEE Trans. Biomed. Eng., vol. 27, pp. 382–395, 1980.

Holtermann A., Mork PJ., Andersen LL., Olsen HB. Sogaard K., The use of EMG biofeedback for learning of selective activation of intra-muscular parts within the serratus anterior muscle: A novel approach for rehabilitation of scapular muscle imbalance. J Electromyogr Kinesiol 2010; 20:359–365.

Hudgins B., Parker P., and Scott RN. "A new strategy for multifunction myoelectric control," IEEE Trans. Biomed. Eng., vol. 40, pp. 82–94, 1993.

Huigen E., Peper A., and Grimbergen CA. Investigation into the origin of the noise of surface electrodes, Medical and Biological Engineering and computing 40: 332 – 338, 2002.

Inman VT., Ralston HJ., Saunders JB., Feinstein B. and Wright EW. "Relation of human electromyogram to musculuar tension," EEG Clin. Neurophysiol., vol. 4, pp. 187–194, 1952.

Jiang N., Muceli S., Graimann B., and Farina D. "Effect of arm position on the prediction of kinematics from EMG in amputees," Med. Biol. Eng. Comput., vol. 51, pp. 143–151, 2013.

Jiang N., Vest-Nielsen JLG., Muceli S., and Farina D. "EMG-based simultaneous and proportional estimation of wrist/hand kinematics in unilateral trans-radial amputees," J. NeuroEng. Rehabil., vol. 9:42, 2012.

Kamavuako EN., Englehart KB., Jensen W., and Farina D. "Simultaneous and proportional force estimation in multiple degre es of freedom from intramuscular EMG," IEEE Trans. Biomed. Eng., vol. 59, pp. 1804–1807, 2012.

Kamen G., Gabriel DA. "Essentials of Electromyography" Human Kinetics, pp. 141-149, 2010.

Karlsson J., Peterson L., Andreasson G., Hogfors C. The unstable ankle: a combined EMG and biomechanical modeling study. Int J Sport Biomech 1992; 8: 129–144.

Khushaba RN., Kodagoda S., Takruri M., and Dissanayake G. "Toward improved control of prosthetic fingers using surface electromyogram (EMG) signals," Exp. Sys. App., vol. 39, pp. 10731–10738, 2012

Kuiken TA., Dumanian GA., Lipschutz RD., Miller LA., and Stubblefield KA., "The use of targeted muscle reinnervation for improved myoelectric prosthesis control in a bilateral shoulder disarticulation amputee," Prosthet. Orthot. Int., vol. 28, pp. 245–253, 2004.

Kuiken TA., Li G., Lock BA., Lipschutz RD., Miller LA., Stubblefield KA. "Targeted muscle reinnervation for real-time myoelectric control of multifunction artificial arms," J. Am. Med. Assoc., vol. 301, pp. 619–628, 2009.

Kumar S. and Mital A. Electromyography in Ergonomics. Briston, PA: Taylor & Francis, pp. 297-306, 1996.

Lawrence JH. and De Luca CJ. "Myoelectric signal versus force relationship in different human muscles," J. Appl. Physiol.: Respirat. Environ. Exercise Physiol., vol. 54, pp. 1653–1659, 1983.

Liu P. "Experimental Investigations of EMG-Torque Modeling for the Human Upper Limb," Ph.D. Thesis, Worcester Polytechnic Institute, 2014.

Liu P., Brown DR., Clancy EA., Martel F., and Rancourt D. "EMG-force estimation for multiple fingers," IEEE Sig. Proc. Med. Biol. Symp., 2013.

Liu P., Brown DR., Martel F., Rancourt D. and Clancy EA "EMG-to-force Modeling for Multiple Fingers," in Proc. of Bioengineering Conference (NEBEC), 2011 IEEE 37th Annual Northeast, New York, Troy.

Liu P., Liu L., Martel F., Rancourt D. and Clancy EA "Influence of joint angle on EMG-torque model during constant-posture quasi-constant-torque contractions.," Journal of Electromyography and Kinesiology, vol. 23, pp. 1020-1028, 2013.

Marieb EN., Hoehn K. Anatomy & Physiology. 5th ed, Boston, Pearson, pp. 281-290, 2013.

Merlo A., Farina D. and Merletti R. "A fast and reliable technique for muscle activity detection from surface EMG signals," IEEE Trans. Biomed. Eng., vol. 47, no. 6, pp. 748-756, 2000.

Muceli S. and Farina D. "Simultaneous and proportional estimation of hand kinematics from EMG during mirrored movements at multiple degrees-of-freedom," IEEE Trans. Neural Sys. Rehabil. Eng., vol. 20, pp. 371–378, 2012.

Muceli S., Jiang N., and Farina D. "Extracting signals robust to electrode number and shift for online simultaneous and proportional myoelectric control by factorization algorithms," IEEE Trans. Neural Sys. Rehabil. Eng., vol. 22, pp. 623–633, 2014.

Nielsen JL., Holmgaard S., Jiang N., Englehart KB., Farina D., and Parker P. "Simultaneous and proportional force estimation for multifunction myoelectric prostheses using mirrored bilateral training," IEEE Trans. Biomed. Eng., vol. 58, pp. 681–688, 2011.

Parker P., Englehart K., and Hudgins B. "Myoelectric signal processing for control of powered limb prostheses," J. Electromyo. Kinesiol., vol. 16, pp. 541–548, 2006.

Powell MA, Kaliki RR., and Thakor NV. "User training for pattern recognition-based myoelectric prostheses: Improving phantom limb movement consistency and distinguishability," IEEE Trans. Neural Sys. Rehabil. Eng., vol. 22, pp. 522–532, 2014.

Press WH, Flannery BP, Teukolsky SA, Vetterling WT, 1994. Numerical Recipies in C. 2nd ed. New York: Cambridge Univ. Press, p. 671–681.

Salini CA., Tranquili JA., Prakash P. Adaptive whitening in electromyogram amplitude estimation for epoch-based applications. Major Qualifying Project, Worcester Polytechnic Institute, January, 2003.

Sanger TD. "Bayesian filtering of myoelectric signals," J. Neurophysiol., vol. 97, pp. 1839–1845, 2007.

Shin D., Kim J., Koike Y. A Myokinetic Arm Model for Estimating Joint Torque and Stiffness from EMG Signals during Maintained Posture. J Neurophysiol 2009; 101: 387–401

Smith RJ, Tenore F., Huberdeau D., Etienne-Cummings R. and Thakor NV "Continuous Decoding of Finger Position from Surface EMG Signals for the Control of Powered Prostheses," Proc. 30th An. Int. Conf. IEEE EMBS, pp. 197-200, 2008.

Smith RJ, Huberdeau D., Tenore F. and Thakor NV. "Real-Time Myoelectric Decoding of Individual Finger Movements for a Virtual Target Task," Proc. 31st Ann. Int. Conf. IEEE EMBS, pp. 2376-2379, 2009.

Solomonow M., Guzzi A., Baratta R., Shoji H. and D'Ambrosia R. "EMG-force model of the elbows antagonistic muscle pair," Am. J. Phys. Med., vol. 65, pp. 223–244, 1986.

Stalberg E. Macro EMG, a new recording technique, Journal Neural Neurosurg Psychiatry 43:475-482, 1980.

Staudenmann D., Roeleveld K., Stegeman DF., and van Dieen JH. "Methodological aspects of EMG recordings for force estimation—A tutorial and review," J Electromyogr Kinesiol, vol. 20, pp. 375–387, 2010.

Thelen DG., Schultz AB., Fassois SD. and Ashton-Miller JA. "Identification of dynamic myoelectric signal-to-force models during isometric lumber muscle contractions," J. Biomech., vol. 27, pp. 907–919, 1994.

Vredenbregt J. and Rau G. "Surface electromyography in relation to force, muscle length and endurance," New Developments Electromyogr. Clin. Neurophysiol., vol. 1, pp. 607–622, 1973.

Wang H., Rajotte K. J., Wang H., Dai C., Zhu Z., Bhuiyan M., Huang X. and Clancy EA. "Optimal Estimation of EMG Standard Deviation (EMGσ) in Additive Measurement Noise Model-Based Derivations and their Implications," IEEE Transactions on Neural Systems and Rehabilitation Engineering, Vol. 27, No. 12, pp. 2328–2335, 2019.

Author's Initial Submitted Copy: Berj Bardizbanian, Jennifer Keating, Xinming Huang and Edward A. Clancy, "Estimating Individual and Combined Fingertip Forces from Forearm EMG During Constant-Pose, Force-Varying Tasks," *Annual International Conference of the IEEE Engineering in Medicine and Biology Society*, Vol. 42, 2020, accepted for publication.

Chapter 2: Estimating Individual and Combined Fingertip Forces From Forearm EMG During Constant-Pose, Force-Varying Tasks

Berj Bardizbanian, Jennifer Keating, Xinming Huang and Edward A. Clancy

***Abstract*—Numerous applications in areas such as ergonomics assessment, clinical biomechanics and motor control research would benefit from accurately modeling the relationship between forearm EMG and fingertip force, using conventional electrodes. Herein, we describe a methodological study of relating 12 conventional surface EMGs, applied circumferentially about the forearm, to fingertip force during constant-pose, force-varying (dynamic) contractions. We studied independent contraction of one, two, three or four fingers (thumb excluded), as well as contraction of four fingers in unison. Using regression, we found that a pseudo-inverse tolerance (ratio of largest to smallest singular value) of 0.01 was optimal. Lower values produced erratic models and higher values produced models with higher errors. EMG-force errors using one finger ranged from 2.5–3.8% maximum voluntary contraction (MVC), using the optimal pseudo-inverse tolerance. With additional fingers (two, three or four), the average error ranged from 5–8 %MVC. When four fingers contracted in unison, the average error was 4.3 %MVC.**

2.1 Introduction

Relating surface electromyogram (sEMG) activities of the forearm muscles to fingers has been the interest of many researchers. Only a few studies involving the fingers have considered multi-finger proportional force estimation via EMG, e.g., (Castellini and van der Smagt, 1009; Smith et al., 2009). Single-use EMG-force models (i.e., a new model is trained each time electrodes are

applied) are used in various areas, including ergonomics assessment, clinical biomechanics, and motor control research.

Our own preliminary work (Liu et al., 2013) showed promising results that electrical activity in the forearm, acquired via a 64-channel high-density array, may be used to estimate forces applied at the fingertips. We acquired data from four subjects producing constant-posture, slowly force-varying (*non-dynamic*) contractions. This work did not account for the influences of localized muscle fatigue, electrode movement and day-to-day variations. Spatial filters were used to derive EMG channels and an EMG-force model was generated to relate muscle activity to fingertip force via least squares regression. But, the use of specialized high-density arrays is not conducive to most biomechanics studies.

In the continuing research reported herein, 12 conventional electrodes were placed equidistant (circumferentially) about the forearm of each subject. System identification techniques (regularized least squares regression) were used to model EMG-torque in one finger or multiple fingers working in unison, during constant-pose, force-varying (*dynamic*) tasks. See (Bardizbanian, in preparation) for a more complete report of this work.

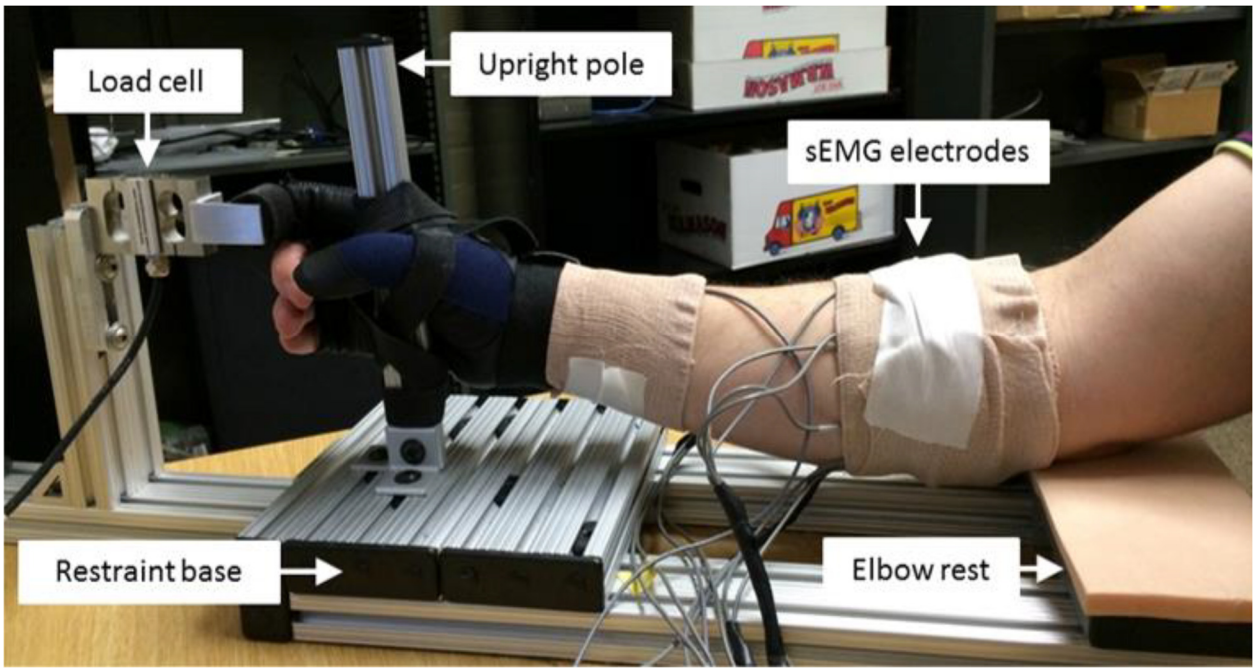

Fig. 2.1. Index finger secured to restraint. Velcro strap wrapped around the finger secures it to the load cell, which measures finger flexion/extension force. Gloved hand is Velcro-attached to the upright pole. Twelve surface EMG electrode amplifiers are secured around the circumference of the forearm; reference electrode is mounted on the head of the radius.

2.2 Methods

2.2.1 Experimental Apparatus and Subject Set-Up

Each bipolar electrode-amplifier consisted of a pair of 8 mm diameter stainless steel electrode contacts separated by a distance of 10 mm (edge to edge), connected to an instrumentation amplifier (CMRR > 100 dB over the passband). A signal conditioner then bandlimited the signals between 15–1800 Hz, and provided selectable gain. Raw EMG were digitized at 4096 Hz with 16-bit resolution.

A single-finger restraint (Fig. 2.1) was custom-built with modular framing (10 Series Profiles, 80/20 Inc., Columbia City, IN, U.S.A.), and rigidly clamped to a table. The finger attachment was bolted to a force transducer (LC101-100 load cell; Omega Engineering, Inc., Stamford, CT, USA) to enable measurement of flexion and extension forces of one selected finger. A bridge amplifier/signal conditioner module (DMD465-WB; Omega Engineering, Inc., Stamford, CT, USA) was used to amplify and de-noised the load cell signal. The force channel was digitized at 4096 Hz with 16-bit resolution. A similar grip restraint (Clancy et al., 2006) was custom-built for simultaneous co-activation of three or four fingers, with net force measured by a single load cell.

Experimental procedures were approved by the New England IRB; all subjects provided written informed consent. The subject's dominant forearm was cleaned with an alcohol wipe and conductive gel was applied. Then, 12 bipolar sEMG electrode-amplifiers were placed circumferentially, equidistant around the forearm, oriented parallel to the muscle fibers. The proximal edge of each bipolar electrode was mounted three fingers breadth from the antecubital fossa with a reference electrode attached over the head of the radius.

After donning a glove, the subject's palm was arranged perpendicular to the table and then secured to the front of a restraint using Velcro, to stabilize the hand during contraction trials. Next, subjects were instructed to support their forearm on the cushioned elbow rest plate via contact at the olecranon process, with their arm extending along the sagittal plane. For finger trials, each finger was individually fixed to the restraint; while for grip trials, four fingers (thumb excluded) were simultaneously fixed to the restraint.

Subjects performed muscle contractions by interacting with a computer screen GUI. A vertical blue line displayed a computer-controlled target that guided the subject to complete different experimental tasks by exerting force on the load cell. A real-time feedback signal from the load cell was shown as a second red vertical line. Both lines were bounded within two fixed white vertical lines representing each subject's 50% maximum voluntary contraction (MVC). The *x*-axis location of each feedback line (positive and negative) corresponded to extension-flexion forces, respectively.

2.2.2 Experimental Data Collection

Nineteen able-bodied human subjects (nine males, ten females; aged 23 to 62 years) each participated in one experiment. Subjects initially sat at the single-finger restraint and performed two 5-s 100% MVCs per finger, in each of flexion and extension, the average peaks of which were used as the subject's MVCs. Next, they performed a 0% MVC (rest contraction) and separate flexion and extension 30% MVCs (for each finger) for 10 s each, utilizing force feedback on a computer screen.

Subjects then performed three dynamic target tracking contractions per finger, each 45 s in duration. The random target was a 1 Hz band-limited, white and uniform random process which moved randomly between ±(|30 %MVC Ext| + |30 %MVC Flx|)/2, with subjects tracking this movement by controlling the load cell force. A minimum two-minute rest interval was provided between contractions to limit fatigue.

After completing the single-finger trials, the subject was arranged into the grip restraint in a similar manner. In four-finger grip trials, all four fingers (thumb excluded) were secured to the apparatus. The same steps were followed to collect grip EMG and force data as were followed for single-finger efforts.

2.2.3 Analysis—Signal Processing

All signal processing was performed using MATLAB, with filtering applied in the forward, then reverse time directions, to achieve zero phase. To produce estimates of EMG standard deviation (EMGσ), the sampled EMG were highpass filtered (f_c=15 Hz, 5th-order Butterworth) and 2nd-order IIR notch filtered (bandwidth 1 Hz) at the power line frequency and all harmonics (to attenuate power line interference). This filtering was followed by a first order demodulator (i.e., rectifier).

After demodulation, EMG signals were passed through a low pass 9th-order Chebyshev Type 1 filter with an effective cutoff frequency of 16.8 Hz, and then decimated by a factor of 100, producing a resampled frequency of 40.96 Hz. This low pass filter served as the initial smoothing stage of the EMGσ processor. The original sampling rate of 4096 Hz is necessary for acquiring the raw EMG, but is not appropriate once EMGσ has been estimated (Clancy, Bida, 2006; Ljung, 1999). The force signal was similarly decimated, and then normalized to 100% MVC flexion.

2.2.4 Analysis—Models

EMGσ values were related to force output at the fingertips using a nonlinear FIR dynamic EMGσ-force model structure for each EMG channel, as:

$$F[m] = \sum_{d=1}^{D=2} \sum_{q=0}^{Q=20} \sum_{c=1}^{C=12} f_{d,c} EMG\sigma_c^d\,[m-q] \tag{1}$$

where $F[m]$ is the force at decimated sample index m, $f_{d,c}$ are the fit parameters, c is the EMG channel, $D=2$ is the degree of the polynomial nonlinearity, and parameter $Q=20$ sets the signal lags. Fit parameters were found via least squares, regularized via the pseudo-inverse approach, in which singular values of the design matrix were removed if the ratio of their magnitude to that of the largest singular value was less than an empirically defined tolerance Tol.

Five different EMG-force model sets (one, two, three, and four independent fingers; and four finger "grip") were studied. Each model was studied for all combinations of pseudo-inverse tolerance ($0.01 \leqslant Tol \leqslant 0.1$ in 0.005 increments). For all models, two trials were used for training and one for testing (ignoring the first 2 s of each trial to account for filter start-up transients), with three-fold cross-validation. Performance was measured as the average RMS error (expressed in %MVC) between actual and EMGσ-estimated force, across the three cross-validated test trials.

For one independent finger, separate EMGσ-force analysis was conducted for each of the four fingers (index, middle, ring, pinky), using only the single-finger contraction trials for each respective finger (12 EMGσ inputs, one force output). Twelve-input, one-output modeling was also performed using the four-finger grip data. For two independent fingers, separate analysis was conducted for each of the six combinations of two fingers, using 12-input, two-output models (i.e., separate $f_{d,c}$ parameters per finger). Training trials from each of the two fingers were combined, with the unused "true" finger force assigned to zero. RMS error was assessed on both testing trials

(again assigning the "true" force of the unused finger to be zero), and then averaged. Similarly, for three independent fingers, separate analysis was conducted for each of the four combinations of three fingers (12-input, three-output models), combining training and testing trials for the relevant fingers (assigning "true" forces in unused fingers to zero). Finally, only one combination of four independent fingers existed. This 12-input four-output model used all single-finger training and testing trials, assigning "true" forces in unused fingers to zero.

2.2.5 Statistics

Differences in model performance were tested utilizing multivariate repeated measures ANOVA (RANOVA) using SPSS version 25, assessing all possible interactions. Interactions were not significant, unless noted below. When degree of sphericity, ε, was <0.75, degrees of freedom were adjusted by the Greenhouse-Geisser method; for $0.75 \leqslant \varepsilon < 1$, the Huynh-Feldt method was used. For brevity, when related comparisons are summarized, degrees of freedom are reported without adjustment, since the adjusted values vary within each comparison. Tukey *post hoc* pair-wise comparisons were conducted with Bonferroni correction. A significance level of $p = 0.05$ was used.

2.3 Results

2.3.1 One Independent Finger Models

Fig. 2.2 shows average errors per each one-finger model, versus tolerance. The trend was for increasing error values as tolerance increased. Using all one-finger model results, a one-way RANOVA was computed for each finger (index, middle, ring, pinky) [factor: tolerance]. The main effect of tolerance was significant [$F(18,324) \geqslant 3.94$, $p \leqslant .03$], except for middle finger [$F(18,324)=0.75$, $p=0.8$]. Tukey *post hoc* comparisons were computed. In summary, a tolerance value of 0.01 gave the lowest error for index and pinky fingers, while 0.02 gave the lowest error for ring finger.

2.3.2 Two Independent Finger Models

Fig. 2.3 shows average errors per each two-finger model, versus tolerance. As in the case of one-finger, all models trended toward increasing error values as tolerance increased. Using all two-finger model results, a one-way RANOVA was computed for each two finger combination (index-middle, index-ring, index-pinky, middle-ring, middle-pinky, ring-pinky) [factor:

tolerance]. The main effect of tolerance was significant [F(18,324)⩾5, p⩽0.02], except for index-middle [F(18,324)=1.747, p=0.2]. Tukey *post hoc* comparisons were computed. In summary, a tolerance value of 0.01 always exhibited the lowest average error and was always statistically different from the error exhibited when using higher tolerance values.

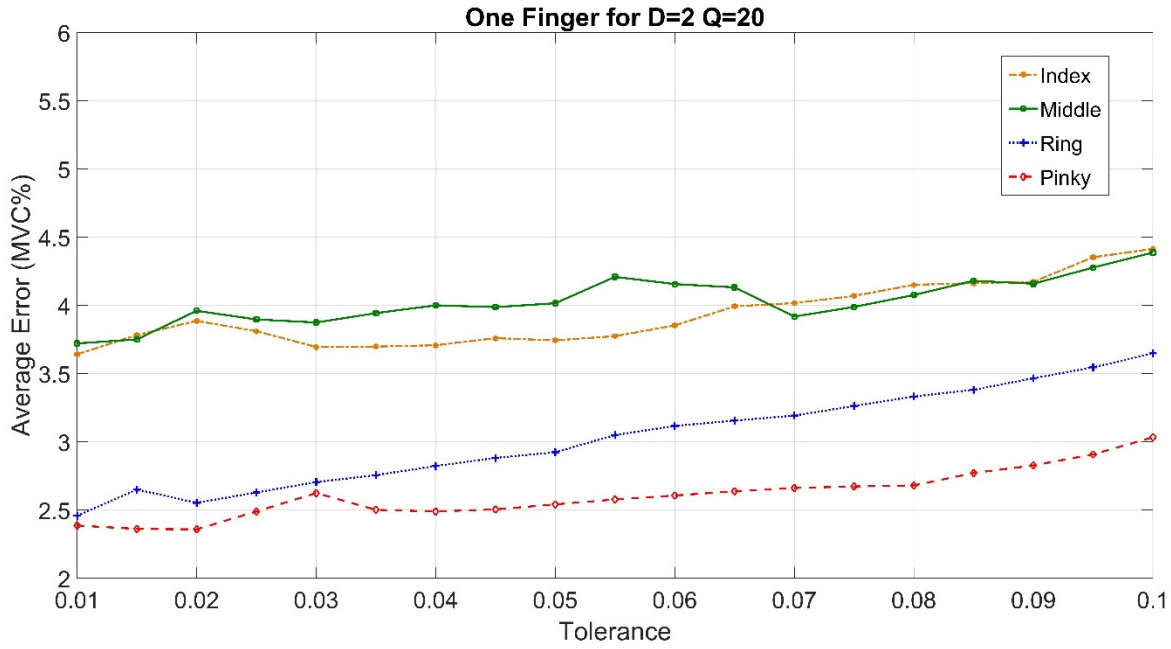

Fig. 2.2. Average error (%MVC) for one-finger models.

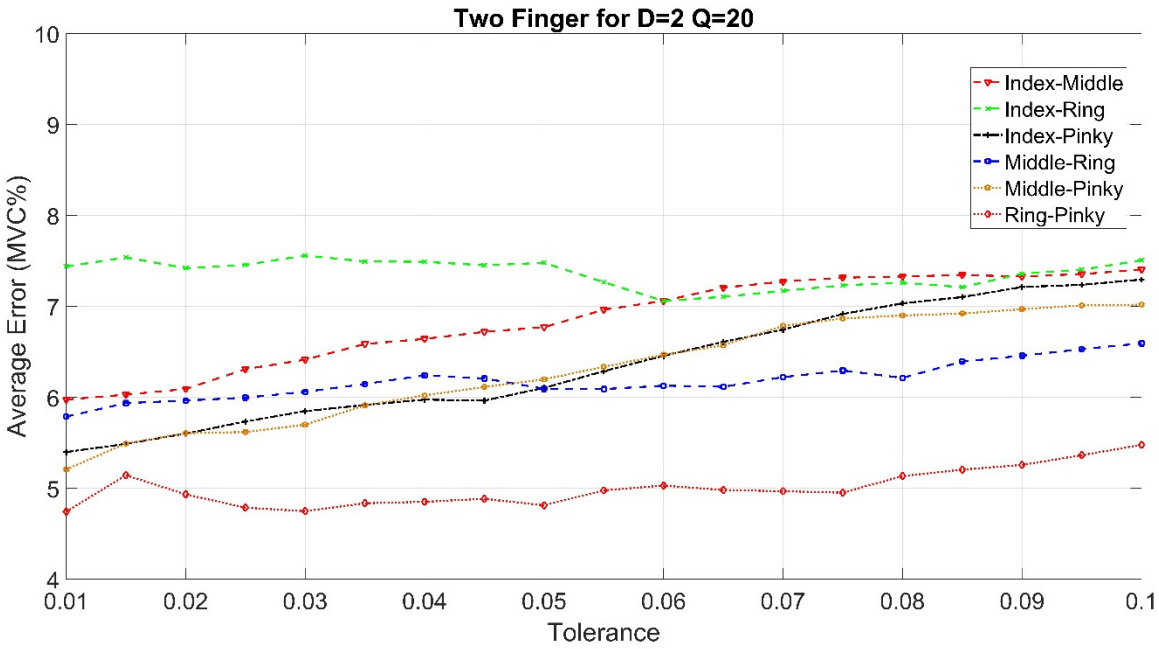

Fig. 2.3. Average error (%MVC) for two finger models.

2.3.3 Three Independent Finger Models

Fig. 2.4 shows average errors per each three-finger model, versus tolerance. The trend was for increasing error values as tolerance increased. Using all three-finger model results, a one-way RANOVA was computed for each three-finger combination (index-middle-ring, index-middle-pinky, index-ring-pinky, middle-ring-pinky) [factor: tolerance]. The main effects of tolerance was always significant [$F(18,324) \geqslant 20$, $p \leqslant 0.001$]. Tukey *post hoc* comparisons were computed. In summary, a tolerance value of 0.01 always exhibited the lowest average error and was always statistically different from the error exhibited when using higher tolerance values.

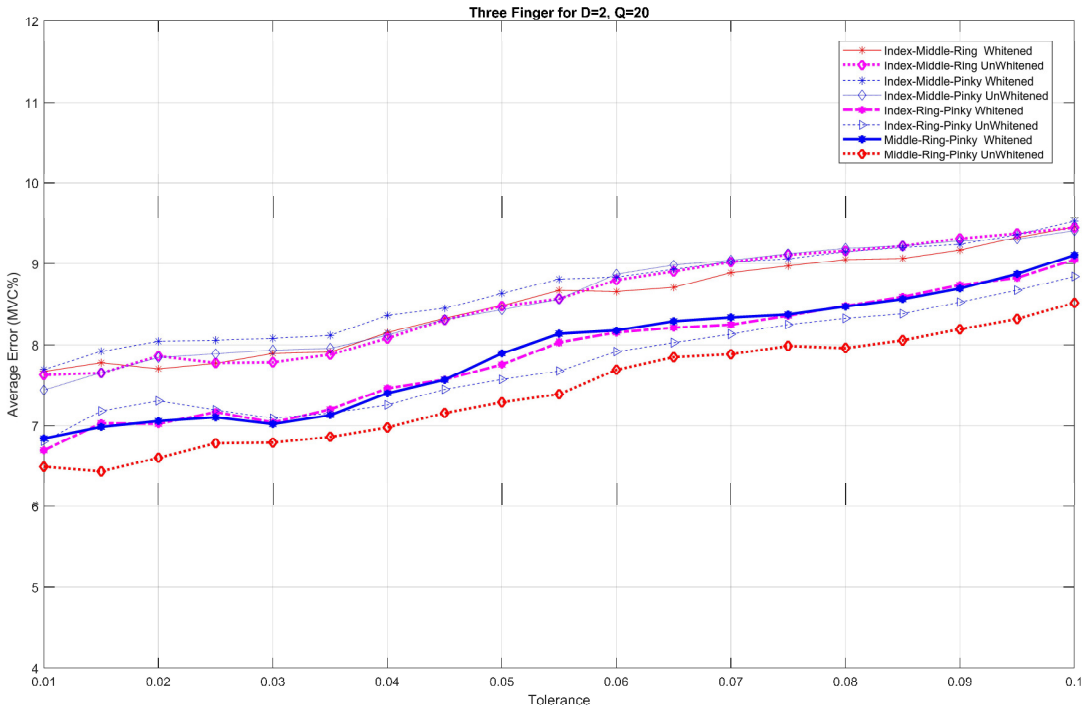

Fig. 2.4. Average error (%MVC) for three-finger models.

2.3.4 Four Independent Finger Models

Fig 2.5 shows sample time-series results of the actual versus estimated force for the four-finger case. Fig. 2.6 shows average errors for the four-finger models, versus tolerance. Again, the models trended towards increasing error as tolerance increased. Using all four-finger model results, a one-way RANOVA was computed [factor: tolerance]. The main effect of tolerance was significant [$F(18,324)=23$, $p=0.0001$]. Tukey *post hoc* comparisons were computed. In summary, the tolerance value of 0.01 exhibited the lowest mean and was significantly different from all other values.

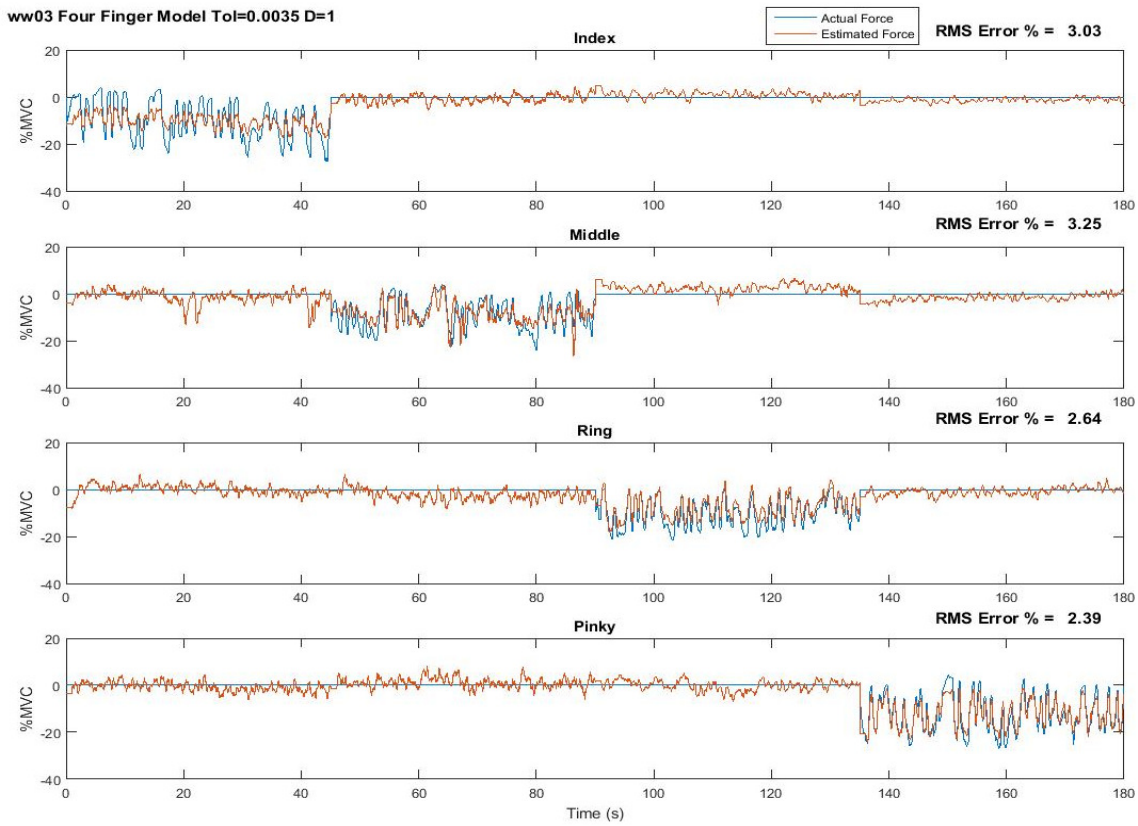

Fig. 2.5. Estimated force versus actual force, four-finger study. Blue line is measured force

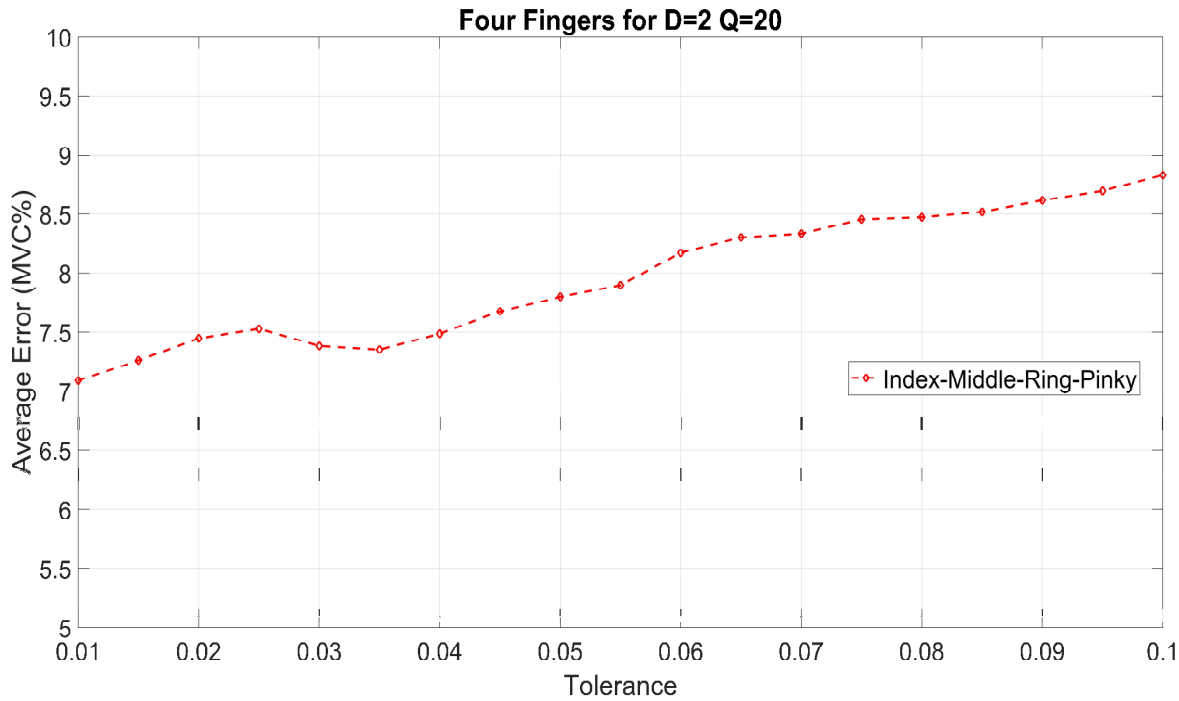

Fig. 2.6. Average error (%MVC) for four-finger models.

2.3.5 Four-Finger "Grip" Models

For this analysis, subjects had applied one force using all four fingers simultaneously. Using the results of four finger grip models, a one-way RANOVA was computed [factor: tolerance]. The main effect of tolerance was significant [$F(18,324)=33$, $p=0.001$]. Tukey *post hoc* comparisons found that a tolerance value of 0.01 had the lowest error and was statistically different from all other tolerance values. At this tolerance, the average error was 4.3 %MVC.

2.4 Discussion

This study was of modest size ($N=19$) and primarily evaluated system identification techniques for regression modeling of EMG-force in one or more fingers during constant-pose, dynamic-force contractions. For this conference report, we primarily analyzed the influence of pseudo-inverse tolerance on error performance, finding that a value of 0.01 (ratio of largest singular value in the design matrix to smallest singular value) was best, with higher values performing progressively poorer. This optimal value is at the edge of our reported range. We did, however, study values below 0.01, finding erratic model behavior. Hence, it was pragmatic to limit our range of analysis to a tolerance value no lower than 0.01. This tolerance value is similar to optimal tolerance values found in dynamic EMG-force models of the elbow joint and of the wrist joint (Clancy et al., 2012; Dai et al., 2019).

At the optimal pseudo-inverse tolerance value of 0.01, rather accurate EMG-force models were formed. Model performance is best visualized in the time-series plot of Fig. 2.5. In this plot, each finger is sequentially activated. When activated, the dynamic force profile is well estimated by the EMG-based model. When a finger is *not* activated (3/4 of the time), its EMG-based estimate is near zero. Hence, the individual fingers seem well identified by the models, demonstrating that conventional EMG electrodes may be suitable for identification of individual finger actuation.

There are many limitations to this work that can be pursued in the future. We limited ourselves to constant-pose contraction, since EMG-force is known to vary with joint angle. We limited ourselves to non-fatiguing contractions, since EMG-force is known to vary during fatigue. We utilized 12 electrodes about the complete circumference of the forearm. Fewer electrodes might provide similar performance. Active control of the hand is the result of a coordinated effort of extrinsic and intrinsic musculature. The contribution of extrinsic extensor and flexor muscles is

prominent in changing the shape of the hand by manipulating fingers, while intrinsic muscles are responsible for maintaining the different configurations of the hand, i.e., flattening or cupping the palm to grasp objects of different sizes and shapes. We only studied extrinsic muscles.

In summary, using 12 conventional EMG electrodes placed circumferentially about the forearm, EMG-force errors using one finger during these dynamic tasks ranged from 2.5–3.8 %MVC, using the optimal pseudo-inverse tolerance. With additional fingers (two, three or four), the average error ranged from 5–8 %MVC. When four fingers contracted in unison, the average error was 4.3 %MVC. All of this performance was found using an optimal pseudo-inverse tolerance of 0.01 in our regression operation.

REFERENCES

Bardizbanian B, in preparation. Improving the Performance of Dynamic Electromyogram-to-Force Models for the Hand-Wrist and Multiple Fingers. Ph.D. Thesis, Worcester Polytechnic Institute

Castellini C, van der Smagt P, 1009. Surface EMG in advanced hand prosthetics. Bio Cyber 100:35–47.

Clancy EA, Bida O, Rancourt D, 2006. Influence of advanced electromyogram (EMG) amplitude processors on EMG-to-torque estimation during constant-posture, force-varying contractions. J Biomech 39:2690–2698.

Clancy EA, Liu L, Liu P, Moyer DV, 2012. Identification of constant-posture EMG-torque relationship about the elbow using nonlinear dynamic models. IEEE Trans Biomed Eng 59:205–212.

Dai C, Zhu Z, Martinez-Luna C, Hunt TR, Farrell TR, Clancy EA, 2019. Two degrees of freedom, dynamic, hand-wrist EMG-force using a minimum number of electrodes. J Electromyo Kinesiol 47:10–18.

Liu P, Brown DR, Clancy EA, Martel F, Rancourt D, 2013. EMG-force estimation for multiple fingers. IEEE Sig Proc Med Biol Symp.

Ljung L, 1999. System Identification: Theory for the User. Upper Saddle River, NJ: Prentice-Hall, p. 1–8, 408–452, 491–519.

Smith RJ, Huberdeau D, Tenore F, Thakor NV, 2009. Real-time myoelectric decoding of individual finger movements for a virtual target task. Ann Int Conf IEEE EMBS:2376–2379.

Author's Copy: B. Bardizbanian, Z. Zhu, J. Li, C. Dai, C. Martinez-Luna, X. Huang, T. Farrell and E. A. Clancy "Calibration of Dynamic Hand-Wrist EMG-Force Models using a Minimum Number of Electrodes," *2018 IEEE Signal Processing in Medicine and Biology Symposium (SPMB)*, Temple University, Philadelphia, PA, 1 December 2018.

Chapter 3: Calibration of Dynamic Hand-Wrist EMG-Force Models Using a Minimum Number of Electrodes

3.1 Introduction

EMG-force models are used in many areas, including: prosthesis control (Mann and Reimers, 1970; Parker et al., 2006) (to command the direction and speed of movement), clinical biomechanics (Disselhorst-Klug et al., 2009; Doorenbosch and Harlaar, 2003) (to assess healthy muscle timing and effort levels), and ergonomics analysis (Hagg et al., 2004; Kumar and Mital, 1996) (to assess risk of injury). Advanced EMG–force models incorporate subject-specific and task-specific dynamics, and are calibrated from contractions with time durations of upwards of 1–2 minutes. For various models, we studied EMG-force estimation error vs. calibration duration for two degree-of-freedom (2-DoF) hand-wrist contractions. We also studied the role of number of electrodes on EMG-force estimation error. Reducing the calibration duration and/or number of electrodes makes EMG-force modeling more accessible, by reducing task time and equipment cost.

3.2 Methods

Similar to (Clancy et al., 2017; Zhu et al., 2017), 16 conventional bipolar electrodes were circumferentially mounted about the proximal forearm (nine subjects). The dominant hand was secured to a three-axis load cell to measure wrist extension-flexion (Ext-Flx), radial-ulnar deviation (Rad-Uln) and pronation-supination (Pro-Sup) forces/moment. The fingers of the same hand were secured to a second single-axis load cell to measure hand open-close (Opn-Cls) force. A PC produced 40 s duration uniform random (0.75 Hz, white, bandlimited) force targets on-screen either along one of these four contraction dimensions per trial (1-DoF), or as 2-DoF contractions comprised of the hand paired with one wrist dimension. Effort ranged over 0–30% maximum

voluntary contraction (MVC). Separately for each subject, linear, FIR (20th order), and 2-DoF regression models related EMG standard deviation (EMGσ) to force using two 1-DoF and two 2-DoF training trials. Initially, all 16 electrodes and 76 s of data were inputs. Thereafter, the number of electrodes was sequentially reduced using a backward stepwise selection procedure on the training data. RMS error on two separate test trials was evaluated at each step. For each number of electrodes, training duration was also progressively decreased and tested. We repeated this complete analysis, instead using only one filter per DoF pair, ensemble-averaged across subjects, but gain-normalized for each subject. That is, only electrode gains were calibrated for each subject. Finally, a "universal" fixed dynamic model (ensemble-averaged across all subjects and DoFs) was compared. Again, only the gain of each electrode was calibrated.

3.3 Results

Fig. 3.1 shows summary test error results for one of the three DoF pairs. Error results for the other DoF pairs were quite similar. Models using either one electrode or a 6 s calibration duration exhibited noticeably higher error, causing significant statistical interactions. Since these two parameter extremes represented unrealistic values, they were excluded from further analysis. Using the remaining RMS error results, a three-way RANOVA was computed for each DoF pair (Factors: Model—subject-specific, one per DoF pair, universal; Electrodes—2–16; Training Duration—14, 22, 30, 38, 44, 52, 60, 68 and 76 s). All main effects were significant, without interactions ($F>8.5$, $p<0.02$).

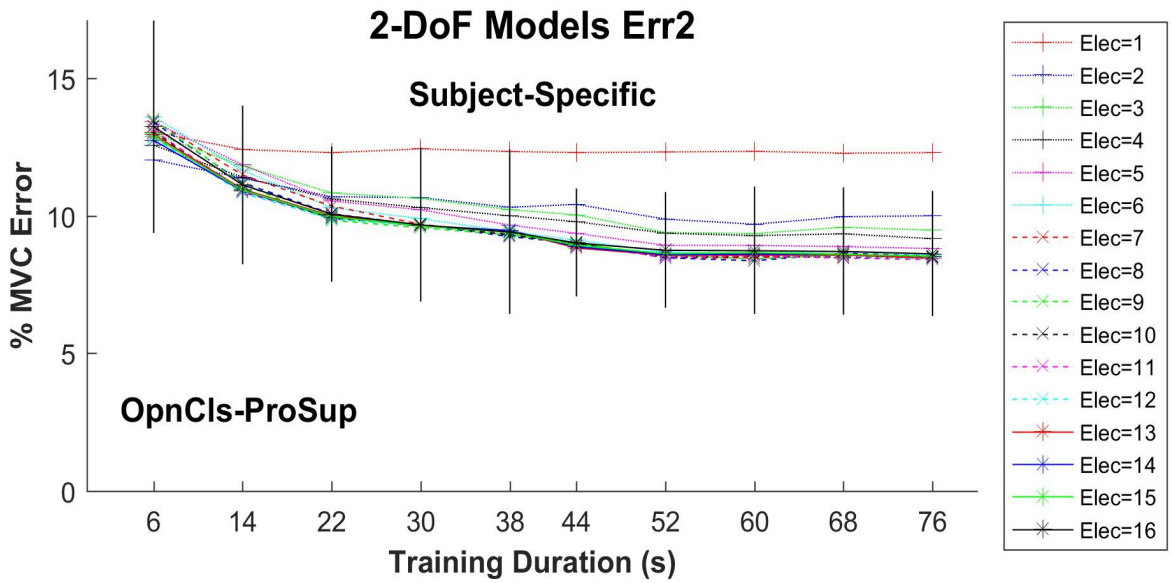

Fig. 3.1. Two-DoF summary error results: subject-specific models, Opn-Cls & Pro-Sup pair vs. training duration for each number of backward selected electrodes. Markers show means. Vertical lines show standard deviations only for 16-electrode models. Standard deviations for other numbers of electrodes were similar.

Tukey *post hoc* comparisons first found a significant difference in RMS error between universal filtering, DoF-specific filtering and subject-specific filtering. The simpler universal filtering had lower mean error. Second, there was no significant RMS error difference for durations of ≥44 s for Opn-Cls with Flx-Ext, ≥52 s for Opn-Cls with Rad-Uln, and ≥60 s for Opn-Cls with Pro-Sup. Finally, RMS error using ≥7 electrodes was not significantly different for Opn-Cls with Flx-Ext, ≥8 electrodes for Opn-Cls with Pro-Sup, and ≥10 electrodes for Opn-Cls with Rad-Uln. Future work in this area should recognize that these statistical differences need to be weighted vs. their clinical significance/strength in a given application.

[†]Supported by NIH award R43 HD076519. Content solely the authors' responsibility & does not necessarily represent NIH views.

REFERENCES

Clancy EA, Martinez-Luna C, Wartenberg M, Dai C, Farrell T, 2017. Two degrees of freedom quasi-static EMG-force at the wrist using a minimum number of electrodes. J Electromyogr Kinesiol 34:24–36.

Disselhorst-Klug C, Schmitz-Rode T, Rau G, 2009. Surface electromyography and muscle force: Limits in sEMG-force relationship and new approaches for applications. Clin Biomech 24:225–235.

Doorenbosch CAM, Harlaar J, 2003. A clinically applicable EMG-force model to quantify active stabilization of the knee after a lesion of the anterior cruciate ligament. Clin Biomech 18:142–149.

Hagg GM, Melin B, Kadefors R, 2004. Applications in ergonomics. In: Merletti R, Parker PA, editors. Electromyography: Physiology, Engineering, and Noninvasive Applications: IEEE Press/Wiley-Interscience, p. 343–363.

Kumar S, Mital A, 1996. Electromyography in Ergonomics. Briston, PA: Taylor & Francis.

Mann RW, Reimers SD, 1970. Kinesthetic sensing for the EMG controlled "Boston Arm". IEEE Trans Man-Mach Sys 11:110–115.

Parker P, Englehart K, Hudgins B, 2006. Myoelectric signal processing for control of powered limb prostheses. J Electromyo Kinesiol 16:541–548.

Zhu Z, Wartenberg M, Clancy EA, Martinez-Luna C, Farrell T, 2017. A pilot study of two degrees of freedom dynamic EMG-force at the wrist using a minimum number of electrodes. IEEE Sig Proc Med Biol Sym. Philadelphia, PA.

Author's Copy: Edward (Ted) A. Clancy, Berj Bardizbanian, Ziling Zhu, Chenyun Dai, Carlos Martinez-Luna and Todd Farrell, "Advancements in Rapid Calibration of Dynamic EMG-Force Models at the Hand/Wrist Using a Minimum Number of Electrodes," *Proceedings of the Twenty Second Congress of the International Society of Electrophysiology and Kinesiology,* Dublin, Ireland, June 29–July 2, 2018.

Chapter 4: Advancement In Rapid Calibration of Dynamic EMG-Force Models At The Hand/Wrist Using a Minimum Number of Electrodes

4.1 ABSTRACT

BACKGROUND: The association between EMG standard deviation (EMGσ) and muscle force is used in various applications, including: "direct" control of myoelectric prostheses, clinical biomechanics and ergonomics analysis. Advanced models of the EMGσ–force relationship calibrate subject-specific dynamics based on force-varying training sets using time durations of upwards of 1–2 minutes. For one degree of freedom (1-DoF) hand-wrist contraction, we studied the duration of data required to train dynamic models as well as the need for subject-specific models. Shorter training would be advantageous for all applications. We also studied the relationship between estimation error and the number of electrodes.

4.2 METHODS

For 9 healthy subjects, 16 conventional bipolar electrodes were mounted circumferentially about the proximal forearm. The hand was secured to a load cell to measure wrist extension-flexion, radial-ulnar deviation or pronation-supination forces. The fingers were secured to a second load cell to measure hand open-close. A screen target produced 38 s duration random, uniformly distributed, dynamic (0.75 Hz, white, bandlimited) force targets along one of these four contraction dimensions per trial. Effort ranged over 0–30% MVC. Separately for each subject; linear, FIR (20th order), 1-DoF regression models relating EMGσ to force were trained using 2 trials. Initially, all 16 electrodes were used as inputs. Thereafter, backward stepwise selection of the training data sequentially reduced the number of electrodes. RMS error on two separate test trials was evaluated

at each step. Training duration was then progressively decreased. Finally, a “universal” fixed dynamic model that was not subject-specific (except for each electrode gain) was compared to models with subject-specific dynamics.

4.3 RESULTS

Using all 76 s of training data for calibration, each DoF found that stepping down to fewer than two electrodes was unacceptable, and retaining more than two electrodes provided limited benefit. This result was expected and consistent with existing prosthesis practice. With 2 electrodes, the average test error ranged from 8.3–9.2 %MVC, depending on the DoF. Error increased as the training duration decreased, particularly for durations less than one full trial (38 s). With just 6 s of training data, the average test error was 13–16 % MVC. Average errors were nearly identical when this entire process was repeated with a fixed, universal dynamic filter (and, thus, only a zero-order gain was fit via regression). Additionally, the approach using a universal filter selected similar electrodes via the backward stepping procedure.

4.4 CONCLUSION

For these experimental conditions, all subjects shared similar dynamics. Thus, a simple, more robust (parsimonious) system identification procedure was found in which only channel gain required training. With our approach thus far, substantial duration training trials are still required.

Funding: NIH 2R42HD076519.

Author's Initial Submitted Copy: Berj Bardizbanian, Ziling Zhu, Jianan Li, Xinming Huang, Chenyun Dai, Carlos Martinez-Luna, Benjamin E. McDonald, Todd R. Farrell and Edward A. Clancy, "Efficiently Training Two-DoF Hand-Wrist EMG-Force Models," *Annual International Conference of the IEEE Engineering in Medicine and Biology Society*, Vol. 42, 2020, accepted for publication.

Chapter 5: Efficiently Training Two-DoF Hand-Wrist EMG-Force Models

Berj Bardizbanian, Ziling Zhu, Jianan Li, Xinming Huang, Chenyun Dai, Carlos Martinez-Luna, Benjamin E. McDonald, Todd R. Farrell and Edward A. Clancy

5.1 Abstract

Single-use EMG-force models (i.e., a new model is trained each time the electrodes are donned) are used in various areas, including ergonomics assessment, clinical biomechanics, and motor control research. For one degree of freedom (1-DoF) tasks, input-output (black box) models are common. Recently, black box models have expanded to 2-DoF tasks. To facilitate efficient training, we examined parameters of black box model training methods in 2-DoF force-varying, constant-posture tasks consisting of hand open-close combined with one wrist DoF. We found that approximately 40–60 s of training data is best, with progressively higher EMG-force errors occurring for progressively shorter training durations. Surprisingly, 2-DoF models in which the dynamics were universal across all subjects (only channel gain was trained to each subject) generally performed 15–21% better than models in which the complete dynamics were trained to each subject. In summary, lower error EMG-force models can be formed through diligent attention to optimization of these factors.

*Research supported by U.S. NIH (award R43HD076519). Content solely authors' responsibility and does not necessarily represent official NIH views.

B. Bardizbanian, Z. Zhu, J. Li, X. Huang, E. A. Clancy (phone: +1-508-831-5778) are with Worcester Polytechnic Institute (WPI), Worcester, MA 01609. E-mail: [berj, zzhu2, jli6, xhuang, ted]@wpi.edu.

C. Dai is with Fudan University, Shanghai, China. E-mail: chenyundai@fudan.edu.cn.

C. Martinez-Luna, B. E. McDonald, T. R. Farrell are with Liberating Technologies, Inc. (LTI), Holliston, MA 01746. E-mail: [carlos.martinez, benjamin.mcdonald, todd.farrell]@liberatingtech.com.

5.2 INTRODUCTION

Over the past several decades, numerous investigators have studied the dynamic system relationship between the conventional surface electromyogram (EMG) and muscle force/joint torque (Buchanan et al., 2004; Staudenmann et al., 2010). Much of this modeling trains an EMG-force model for single-use (i.e., a new model is trained each time the electrodes are applied), applicable to areas such as ergonomics assessment, clinical biomechanics, scientific studies relating EMG to joint mechanical impedance, and motor control research. Single-use EMG-force calibration is appropriate, as there is evidence of inter-day decrements in performance when an EMG-force model is not re-calibrated (Oskouei et al., 2013). Some emerging studies have introduced the use of large, high-density surface EMG arrays (Hahne et al., 2014; Liu et al., 2013a; Muceli and Farina, 2012). But, these arrays generally remain rather complex and expensive for biomechanics investigations, and are presently impractical for most commercial applications of EMG.

In one modeling paradigm, EMG-force dynamics are assumed (e.g., length-tension and force-velocity relationships) and only the gains of each EMG channel are optimized (Buchanan, Lloyd, 2004; Hof and Van den Berg, 1981). This "Hill-style" paradigm is simpler and of particular benefit in multi-joint studies for which training of system dynamics would be a daunting task. Alternatively, the "black box" system identification paradigm trains subject- and muscle-specific EMG-force models (Clancy et al., 2012; Doheny et al., 2008; Hashemi et al., 2013; 2015; Hashemi et al., 2012; Hof and Van den Berg, 1981; Liu et al., 2015). Because these models adapt to the specific subject and/or muscle, they would generally be hypothesized to be more accurate than Hill-style models, but require longer training trials (Ljung, 1999) and more effort to program. For simplicity, most early work in this area focused on linear models of single-joint systems. Non-linear models, however, have been shown to improve the relationship (Dai et al., 2017; Hashemi, Morin, 2012; Vredenbregt and Rau, 1973).

Recently, there has been increased interest in expanding these black box models to multi-joint applications, for example to two degree of freedom (DoF) systems in the upper limb (Clancy et al., 2017; Dai et al., 2019; Hahne, Biessmann, 2014; Hahne et al., 2018). In doing so, several technical questions related to system identification are encountered. Previously (Dai, Zhu, 2019), we studied 2-DoF EMG-force in the hand-wrist, finding lower errors when training sets included both 1-DoF and 2-DoF trials. Further, we studied the required number of conventional electrodes, when placed

eqidistant about the circumference of the proximal forearm. Using backward stepwise selection of 16 electrodes, we found that error was optimized with 6 electrodes. Of course, backward selection of electrode sites may have limited utility in single-use EMG-force studies, since all 16 electrodes must still be applied.

These insights narrow the range of system identification methods that need be considered when conducting single-use EMG-force studies. However, other modeling questions remain: determining the necessary duration of training data used to form the EMG-force relationship and choosing the specificity of the model (subject-specific vs. DoF-specific models of dynamics vs. a "universal" Hill-style model of dynamics used for all subjects and muscles). Herein, we examine these questions when relating forearm surface EMG to hand open-close (Opn-Cls) combined with one of three wrist DoFs—either extension-flexion (Ext-Flx) force, radial-ulnar (Rad-Uln) force, or pronation-supination (Pro-Sup) moment. See (Bardizbanian, in preparation) for a more complete report of this work.

5.3 Methods

5.3.1 Experimental Data and Apparatus

5.3.1.1 Data Collection—Setup

The WPI IRB approved reprocessing of previously acquired data from able-bodied subjects (5 males, 4 females; aged 27±9.7 years) (Dai, Zhu, 2019). Subjects sat at the experimental apparatus (see (Dai, Zhu, 2019), Figs. 1–3) with their dominant hand cuffed to a 6-DoF load cell, to measure wrist force/torque. Separately, Opn-Cls grip force was measured by a single-axis load cell by securing to the thumb on one side and the distal aspects of the four fingers on the opposite side. The shoulder was flexed 45° forward from the anatomical position along the sagittal plane, the wrist was in a neutral position and the palm of the hand was perpendicular with the plane of the floor. The elbow was supported.

Skin about the forearm was scrubbed with an alcohol wipe and electrode gel was applied. Sixteen bipolar EMG electrodes were applied equidistant and circumferentially about the forearm: their mid-point was located 5 cm distal to the elbow crease. Bipolar electrodes were 5 mm diameter, stainless steel, hemispherical contacts separated 1 cm edge-to-edge, oriented along the forearm's long axis. A gelled reference electrode was secured on the ventral forearm. Each EMG signal was

differentially amplified (30–500 Hz pass band, CMRR > 100 dB over the pass band). Load cell force/moment was displayed in real-time as a blue arrowhead on a computer screen. The arrowhead displayed 4 DoFs: *x*-axis location for Ext-Flx force, *y*-axis location for Rad-Uln force, rotation for Pro-Sup moment, and size for hand Opn-Cls force. A second red arrowhead displayed a computer-controlled target. Four load cell signals and 16 EMG channels were each sampled at 2048 Hz with 16-bit resolution.

5.3.1.2 Data Collection—Contractions

All contractions were constant-posture, with a two-minute rest interval between each. After warm-up, maximum voluntary contraction (MVC) was measured separately for both directions of each of the 4 DoFs. Next, subjects produced 5 s constant-force 50% MVC contractions for each direction within a DoF.

Then, subjects completed 1-DoF *dynamic* tracking trials, separately for each DoF (randomized order). Feedback only displayed the specified DoF. For Rad-Uln, the target moved randomly between ±(|30 %MVC Rad| + |30 %MVC Uln|)/2. The random target movement was a 0.75 Hz band-limited, white and uniform random process. Four trials of 40 s duration each were completed. The equivalent trials were completed for the three remaining DoFs (16 trials total); except that the maximum force was reduced to 15 %MVC for Opn-Cls due to excessive hand open fatigue found during preliminary testing.

Lastly, subjects tracked *dynamic* 2-DoF targets: hand Opn-Cls paired with one wrist DOF (Ext-Flx, Rad-Uln or Pro-Sup). The same random target style was used, with independent random instances per DoF. Four trials of 40 s duration were completed for each DoF combination (12 trials total).

5.3.2 Analysis: Signal Preprocessing

Data analysis was performed offline in MATLAB. Time-varying EMG standard deviation (EMGσ[n], for discrete-time sample n) was estimated for each channel. Raw EMG were highpass filtered (5th-order Butterworth, f_c=15 Hz), notch filtered to attenuate power-line interference (2nd-order IIR filter at 60 Hz, notch bandwidth of 1 Hz), rectified, lowpass filtered at 16 Hz (Chebyshev Type 1 filter, 9th-order, 0.05 dB peak-to-peak passband ripple), and downsampled to 40.96 Hz (Clancy et al., 2006; Ljung, 1999). Each force/moment signal was normalized by its corresponding MVC level pair. For example, Rad-Uln was normalized by: $(|MVC_{Rad}| + |MVC_{Uln}|)/2$.

5.3.3 Analysis: One-DoF Models

5.3.3.1 Subject-Specific, Full-Duration Model:

One-DoF modeling only utilized 1-DoF trials. EMGσ values were related to force/moment—separately for each DoF—via regression (20th- order linear dynamic model (Clancy, Liu, 2012; Dai, Zhu, 2019); 2 or 16 electrodes used in the fit, where values less than 16 were arrived at using backward stepwise selection (Clancy, Martinez-Luna, 2017; Dai, Zhu, 2019)). Model training used the least squares pseudo-inverse method (Press et al., 1994), with singular values of the design matrix removed if the ratio of their magnitude to that of the largest singular value was less than 0.01 (Clancy, Liu, 2012). Note that backward selection down to 2 electrodes has previously been shown to perform as well as 16 electrodes for these 1-DoF tasks (Clancy, Martinez-Luna, 2017; Dai, Zhu, 2019). Two trials were used for training, and two for testing (RMS error between the estimated and measured torques, expressed in %MVC, after discarding the first 2 s of each trial). Training and testing trials were then exchanged (two-fold cross-validation), with the average of these two folds reported.

5.3.3.2 Subject-Specific, Reduced-Duration Model:

The above procedure was repeated while utilizing less than the full available training time, thus varying the time duration used for training. In this manner, we could evaluate model performance vs. training duration. For training durations of 14, 22, 30 and 38 s, only the necessary initial portion of the first training trial was used, and the second training trial was ignored. For training durations of 44, 52, 60, 68 and 76 s, equal durations of both training trials were used (half of the training duration derived from each trial). As above, model testing used both full testing trials, with the two-fold cross-validation results averaged.

5.3.3.3 DoF-Specific Model:

General dynamic models, one per DoF, were next constructed. Two trials were used to train subject-specific models for each subject. After backward selecting down to the channels preferred for EMG-force estimation, the fit coefficients define a FIR filter, which is inherently lowpass in shape (Clancy et al., 2016; Hof and Van den Berg, 1981; Inman et al., 1952; Koirala et al., 2015; Winter, 2005; Winter and Yack, 1987). These filters were each normalized to a gain of one at 0 Hz—expressing the EMGσ-force dynamics, absent of the gains for each EMG channel. A total of

36 gain-normalized filters were formed per DoF (nine subjects, two EMG channels per subject, two cross-validations). The ensemble mean coefficient values of these filters (one filter per DoF) were.

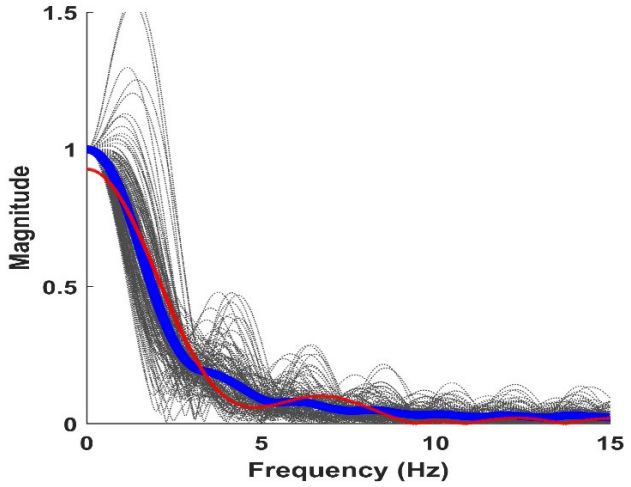

Fig. 5.1. Each of 144 magnitude responses of the 1-DoF models is shown in grey (nine subjects, two EMG channels per subject, two cross-validations, 4 DoFs). Thick blue line is the average and thin red line is the universal FIR filter fit to these responses.

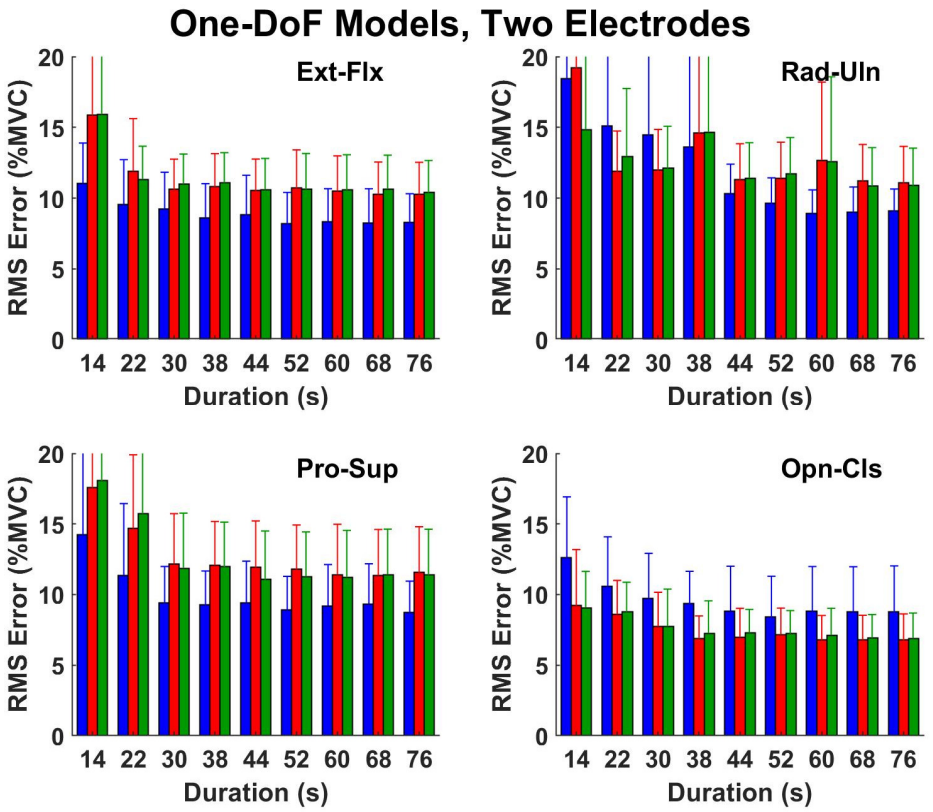

Fig. 5.2. One-DoF summary results for each DoF vs. training duration. Mean error plus one standard deviation shown for 2-electrode models. (Some error bars cropped by y-axis scaling.) Subject-specific models in blue, DoF-specific models in red, universal models in green.

This DoF-specific filter was used, in place of the dynamics provided by subject-specific filters by appending them to the EMG pre-processing (after the decimation step). This evaluation assessed if subject-specific, EMG channel-specific calibration of dynamics could be replaced with one dynamic filter per DoF. Once the DoF-specific filters were formed, the training trials were used to calibrate *only* the gains of each EMG channel. Testing was performed on the remaining two trials. Backward stepwise selection from 16 down to 2 electrodes was performed, with only results for 2 and 16 EMG channels reported (with cross-validation). This analysis was completed for each of the DoFs and training durations.

5.3.3.4 Universal Model:

This analysis was similar to the prior analysis, except that the 36 DoF-specific filter coefficients were ensemble averaged into one "universal" filter (Fig. 5.2) to assess if one filter shape could capture all dynamics for all DoFs. Again, analysis was completed for all training durations and only the results for 2 and 16 EMG channels are reported.

5.3.4 Analysis: Two-DoF Models

Similar 2-DoF EMG-force models were evaluated (with backward stepwise selection to 6 EMG channels and two-fold cross-validation) for each of Opn-Cls paired with one wrist DoF, always estimating 2 DoFs simultaneously. Each EMG channel contributed to both DoFs. Model training always combined both 1-DoF trails and the corresponding 2-DoF trial. Model testing was performed only using the 2-DoF trials. Note that backward selection down to 4–6 electrodes has previously been shown to perform nearly as well as 16 electrodes for these 1-DoF tasks (Clancy, Martinez-Luna, 2017; Dai, Zhu, 2019).

5.3.5 Statistics

Performance differences were tested statistically with SPSS 25 using multivariate RANOVA. Interactions were not significant, unless noted. When degree of sphericity ε was <0.75, degrees of freedom was adjusted by the method of Greenhouse-Geisser; and when $0.75 \leq \varepsilon < 1$, by the method of Huynh-Feldt (Girden, 1992). When multiple comparisons are summarized, degrees of freedom are reported without adjustment. Tukey *post hoc* comparisons were conducted using Fisher's least significant difference (LSD). A significance level of $p = 0.05$ was used.

5.4 Results

5.4.1 One-DoF Models

Fig. 5.2 shows summary test error results vs. training duration for the 1-DoF models using 2 electrodes. All models experienced lower mean error as training duration increased from 14 s, with less improvement as training duration grew. Using all the results of 1-DoF models, a four-way RANOVA was computed [factors: model (subject-specific, DoF-specific, universal), number of electrodes (2, 16), duration (14, 22, 30, 38, 44, 52, 60, 68, 76 s) and DoF (Flx-Ext, Rad-Uln, Pro-Sup, Opn-Cls)]. Since there was a significant two way interaction term involving model and DoF [$F(2.5, 20.0) = 6.1$, $p_{GG}=0.006$], three way RANOVA's were implemented fixing each DoF. The main effects were significant for model [$F(2,16)>77$, $p\leq0.03$], except for Rad-Uln [$F(2,16)=3.5$, $p=0.06$]; significant for duration [$F(8,64)>5$, $p\leq0.04$]; but not significant for number of electrodes [$F(1,8)<6$, $p\geq0.05$].

Tukey *post hoc* comparisons were computed for all significant differences. In summary, when comparing the 1-DoF models, the subject-specific model generally had the lowest errors. There was a clear trend for higher %MVC errors at shorter training durations versus longer durations. For example, training with 14 s always exhibited higher error than ≥ 30s and training with 22 s always exhibited higher error than ≥ 68s. Performance improvement plateaued at longer durations (e.g. there was no statistically significant improvement for durations beyond 30 s for Rad-Uln and Opn-Cls, or beyond 60 s for Ext-Flx and Pro-Sup). With two backward selected electrodes, a training duration of 60 s and subject specific modeling, average ± standard deviation errors (% MVC) were: 8.34 ± 2.32 for Ext-Flx, 8.92 ± 9.65 for Rad-Uln, 9.2 ± 2.93 for Pro-Sup and 8.81 ± 3.18 for Opn-Cls.

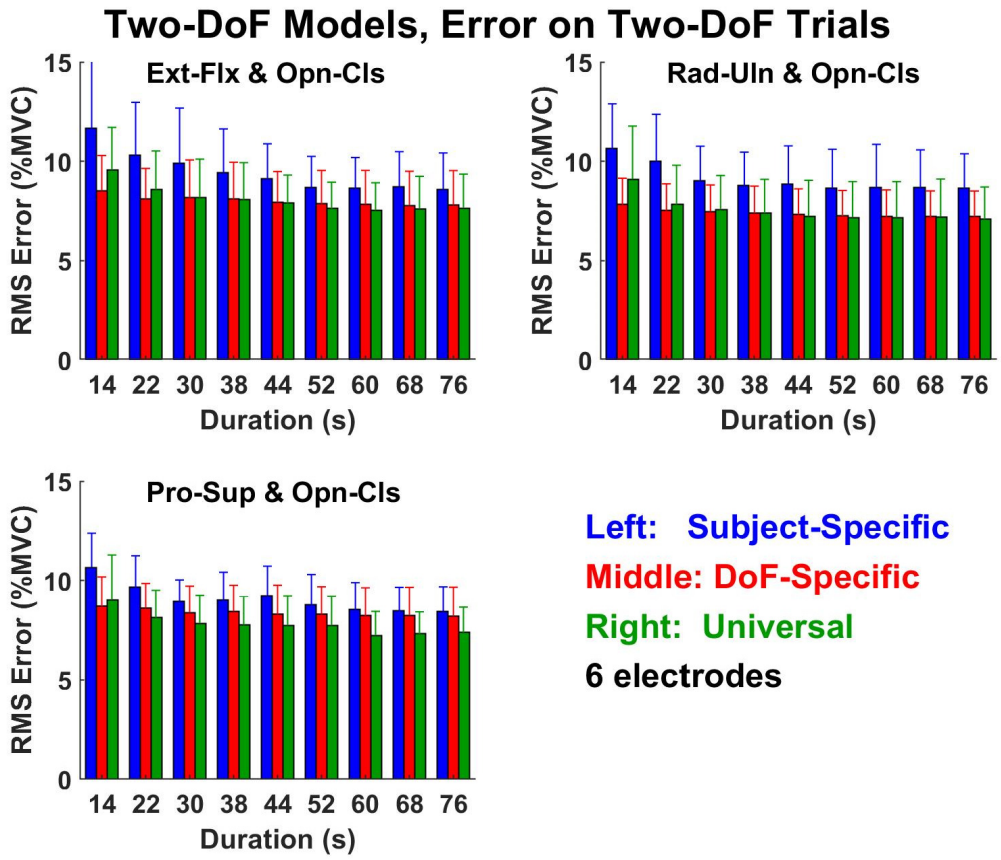

Fig. 5.3. Two-DoF summary results for each DoF pair vs. training duration, when assessing on 2-DoF trials. Mean error plus one standard deviation shown for 6-electrode models.

5.4.2 Two-DoF Models Assessed on Two-DoF Trials

Fig. 5.3 shows summary test error results vs. training duration for the 2-DoF models using 6 electrodes. All models experienced clearly lower error as training duration increased from 14 s, with less improvement as training duration grew. Using all the results of 2-DoF models, a four-way RANOVA was computed [factors: model (subject-specific, DoF-specific, universal), number of electrodes (6, 16), duration (14, 22, 30, 38, 44, 52, 60, 68, 76 s) and DoF pair (Opn-Cls with Flx-Ext, Opn-Cls with Rad-Uln, Opn-Cls with Pro-Sup). There were significant interactions involving model and duration [$F(16,128)=17$, $p=0.0001$]. Unfortunately, fixing a second factor did not eliminate interactions. Thus, we continued to pursue the non-interacting factors within this four-way RANOVA. These other main effects were significant for number of electrodes [$F(1,8)=16$,

p=0.004] and not significant for DoF pair [F(2,16)=0.6, p=0.6]. Tukey *post hoc* comparisons found that using 6 electrodes had a significantly higher mean error than using 16 electrodes.

To examine the model and duration factors, we next performed Tukey pair-wise comparisons for each combination of these factors (with Bonferroni correction). Considering duration: subject-specific models with durations below 38 s always had higher errors than those with durations above 68 s; and DoF-specific and universal models with durations below 30 s always had higher errors than respective models with durations above 68 s. Considering model: subject-specific models always had 15–21% *higher* error than the other two models (except at a duration of 60 s—likely an anomaly), and DOF-specific models did not differ from universal models.

5.5 Discussion

5.5.1 Parameter Selection for Efficient EMG-Force Training

This research focused on two technical details related to forming 2-DoF EMG-force models at the hand-wrist. First, we examined the duration of training used to form the EMG-force relationship. For single-use applications, it is most useful to be able to train models quickly. With all 1-DoF models, error decreased in an exponential fashion as training duration increased. These changes were consistently statistically significant at the shorter durations (where the slope of error vs. duration was largest), but less so at the longer training durations (where more statistical power would be required in order to identify the smaller presumed differences). Most of the error reduction occurred with durations up to 40–60 s. These hand-wrist results are consistent with 1-DoF EMG-force results in the elbow (Clancy, Liu, 2012), wherein 52 s of training data for similar dynamic models were found to reduce error compared to 26 s. For our 2-DoF models, a similar exponential trend was found (error decaying with increased training duration), but the rate of error decay was not as steep. This difference in rate may reflect that the final error was, on average, larger for the 2-DoF trials. These results are generally consistent with system identification theory, in which the necessary training duration is proportional to the number of fit parameters (2-DoF models have more fit parameters) and that error reduces less than linearly as the training size progressively increases (Ljung, 1999).

Second, we researched the specificity of the model (subject-specific vs. DoF-specific vs. universal). A universal model is similar to a Hill model in that the dynamics are pre-assigned. For 1-DoF models, subject-specific models clearly performed best, in general, reducing error by 11–24% compared to universal models. But, for 2-DoF models, universal models actually performed *better* than subject-specific models, in general, by 15–21%. Model training for 2-DoF models uses twice as many fit parameters and requires that subjects complete 2-DoF tasks. Thus, perhaps it is simply more difficult to identify these more complex models, leading to poorer model fits in the subject-specific models (which do not combine training across DoF and subject). Note that our universal models were still formed from data specific to our muscles studied, arm pose and training-testing trajectories. Hence, generic models (e.g., Hill style) that are not tuned in this manner (i.e., simply selected, for example, as second-order lowpass dynamics—a common selection) might be expected to perform poorer. Thus, our results do not directly suggest that Hill style models will outperform subject-specific models in all cases.

5.5.2 Limitations and Extensions

First, our sample size was limited and we studied a single joint. Second, we limited our contractions to being constant posture. It is well established that EMG-force varies with joint angle (e.g., the length-tension curve (Doheny, Lowery, 2008; Hashemi, Morin, 2013; Liu, Liu, 2015; Liu et al., 2013b; Rack and Westbury, 1969; Vredenbregt and Rau, 1973)). Thus, conditions of this work should be extended to varied angle in the future. Third, the method of electrode site selection by backward stepping produces a locally optimum solution, but not necessarily a global optimum. And, this solution is limited by the sites imposed by the original equal-spaced application of the 16 electrodes. Alternative schemes exists, including schemes based on muscle anatomy (Fougner et al., 2014). Fourth, these results present a conundrum for single-use applications: much fewer than 16 electrodes provide minimum error performance, but the complete set of 16 electrodes must be mounted in order to determine the optimal electrode sites. For single-use applications, it may be as effective to simply use the full 16-channel electrode system and forgo any backward selection of EMG channels. Finally, in order to focus on efficient training of EMG-force models, we limited our models to be linear and did not pre-whiten our EMG data. Non-linear models have been shown to produce better EMG-force relationships (Dai, Bardizbanian, 2017; Hashemi, Morin, 2012; Vredenbregt and Rau, 1973). Further, EMG pre-whitening has been shown to reduce the variance of the EMGσ estimate (Clancy and Hogan, 1994; Hogan and Mann, 1980), resulting in reduced

EMG-force error (Clancy and Hogan, 1997; Clancy, Liu, 2012; Dai, Bardizbanian, 2017). Each of these methods can be incorporated in future work.

5.6 Conclusion

We studied efficient training of 2-DoF EMG-force models using conventional EMG electrodes. We found that EMG-force error reduced as training duration increased, for durations up to 40–60 s. Improvement in performance was greatest at the lower training durations. And, subject-specific models performed best when forming 1-DoF models, but (generally) worst when forming 2-DoF models.

REFERENCES

Bardizbanian B, in preparation. Improving the Performance of Dynamic Electromyogram-to-Force Models for the Hand-Wrist and Multiple Fingers. Ph.D. Thesis, Worcester Polytechnic Institute

Buchanan TS, Lloyd DG, Manal K, Besier TF, 2004. Neuromusculoskeletal modeling: Estimation of muscle forces and joint moments and movements from measurements of neural command. J Appl Biomech 20:367–395.

Clancy EA, Bida O, Rancourt D, 2006. Influence of advanced electromyogram (EMG) amplitude processors on EMG-to-torque estimation during constant-posture, force-varying contractions. J Biomech 39:2690–2698.

Clancy EA, Hogan N, 1994. Single site electromyograph amplitude estimation. IEEE Trans Biomed Eng 41:159–167.

Clancy EA, Hogan N, 1997. Relating agonist-antagonist electromyograms to joint torque during isometric, quasi-isotonic, non-fatiguing contractions. IEEE Trans Biomed Eng 44:1024–1028.

Clancy EA, Liu L, Liu P, Moyer DV, 2012. Identification of constant-posture EMG-torque relationship about the elbow using nonlinear dynamic models. IEEE Trans Biomed Eng 59:205–212.

Clancy EA, Martinez-Luna C, Wartenberg M, Dai C, Farrell T, 2017. Two degrees of freedom quasi-static EMG-force at the wrist using a minimum number of electrodes. J Electromyogr Kinesiol 34:24–36.

Clancy EA, Negro F, Farina D, 2016. Single-channel techniques for information extraction from the surface EMG signal. In: Merletti R, Farina D, editors. Surface Electromyography: Physiology, Engineering, and Applications: John Wiley & Sons, Inc., p. 91–125.

Dai C, Bardizbanian B, Clancy EA, 2017. Comparison of constant-posture force-varying EMG-force dynamic models about the elbow. IEEE Trans Neural Sys Rehabil Eng:1529–1538.

Dai C, Zhu Z, Martinez-Luna C, Hunt TR, Farrell TR, Clancy EA, 2019. Two degrees of freedom, dynamic, hand-wrist EMG-force using a minimum number of electrodes. J Electromyo Kinesiol 47:10–18.

Doheny EP, Lowery MM, FitzPatrick DP, O'Malley MJ, 2008. Effect of elbow joint angle on force-EMG relationships in human elbow flexor and extensor muscles. J Electromyogr Kinesiol 18:760–770.

Fougner AL, Stavdahl O, Kyberd PJ, 2014. System training and assessment in simultaneous proportional myoelectric prosthesis control. J NeuroEng Rehabil 11:75.

Girden ER, 1992. ANOVA: Repeated Measures. Sage Publications, p. 21.

Hahne JM, Biessmann, F., Jiang N, Rehbaum H, Farina D, Meinecke FC, et al., 2014. Linear and nonlinear regression techniques for simultaneous and proportional myoelectric control. IEEE Trans Neural Sys Rehabil Eng 22:269–279.

Hahne JM, Schweisfurth MA, Koppe M, Farina D, 2018. Simultaneous control of multiple functions of bionic hand prostheses: Performance and robustness in end users. Sci Robot 3:eaat3630.

Hashemi J, Morin E, Mousavi P, Hashtrudi-Zaad K, 2013. Surface EMG force modeling with joint angle based calibration. J Electromyogr Kinesiol 23:416–424.

Hashemi J, Morin E, Mousavi P, Hashtrudi-Zaad K, 2015. Enhanced dynamic EMG-force estimation through calibration and PCI modeling. IEEE Trans Neural Sys Rehabil Eng 23:41–50.

Hashemi J, Morin E, Mousavi P, Mountjoy K, Hashtrudi-Zaad K, 2012. EMG-force modeling using parallel cascade identification. J Electromyogr Kinesiol 22:469–477.

Hof AL, Van den Berg J, 1981. EMG to force processing I: An electrical analogue of the Hill muscle model. J Biomech 14:747–758.

Hogan N, Mann RW, 1980. Myoelectric signal processing: Optimal estimation applied to electromyography—Part II: Experimental demonstration of optimal myoprocessor performance. IEEE Trans Biomed Eng 27:396–410.

Inman VT, Ralston HJ, Saunders JB, Feinstein B, Wright EW, 1952. Relation of human electromyogram to musculuar tension. EEG Clin Neurophysiol 4:187–194.

Koirala K, Dasog M, Liu P, Clancy EA, 2015. Using the electromyogram to anticipate torques about the elbow. IEEE Trans Neural Sys Rehabil Eng 23:396–402.

Liu P, Brown DR, Clancy EA, Martel F, Rancourt D, 2013a. EMG-force estimation for multiple fingers. IEEE Sig Proc Med Biol Symp.

Liu P, Liu L, Clancy EA, 2015. Influence of joint angle on EMG-torque model during constant-posture, torque-varying contractions. IEEE Trans Neural Sys Rehabil Eng 23:1039–1046.

Liu P, Liu L, Martel F, Rancourt D, Clancy EA, 2013b. Influence of joint angle on EMG-torque model during constant-posture quasi-constant-torque contractions. J Electromyo Kinesiol 23:1020–1028.

Ljung L, 1999. System Identification: Theory for the User. Upper Saddle River, NJ: Prentice-Hall, p. 1–8, 408–452, 491–519.

Muceli S, Farina D, 2012. Simultaneous and proportional estimation of hand kinematics from EMG during mirrored movements at multiple degrees-of-freedom. IEEE Trans Neural Sys Rehabil Eng 20:371–378.

Oskouei HA, Paulin MG, Carman AB, 2013. Intra-session and inter-day reliability of forearm surface EMG during varying hand grip forces. J Electromyo Kinesiol 23:216–222.

Press WH, Flannery BP, Teukolsky SA, Vetterling WT, 1994. Numerical Recipies in C. 2nd ed. New York: Cambridge Univ. Press, p. 671–681.

Rack PMH, Westbury DR, 1969. The effects of length and stimulus rate on tension in the isometric cat soleus muscle. J Physiol 2014:443–460.

Staudenmann D, Roeleveld K, Stegeman DF, van Dieen JH, 2010. Methodological aspects of EMG recordings for force estimation—A tutorial and review. J Electromyogr Kinesiol 20:375–387.

Vredenbregt J, Rau G, 1973. Surface electromyography in relation to force, muscle length and endurance. New Developments Electromyogr Clin Neurophysiol 1:607–622.

Winter DA, 2005. Biomechanics and Motor Control of Human Movement, 3rd edition. Hoboken, NJ: John Wiley & Sons, Inc., p. 203–260.

Winter DA, Yack HJ, 1987. EMG profiles during normal human walking: Stride-to-stride and inter-subject variability. Electroenceph Clin Neurophysiol 67:402–411.

Author's Copy. This chapter has been published as: Chenyun Dai, Berj Bardizbanian, and Edward A. Clancy, "Comparison of Constant-Posture Force-Varying EMG-Force Dynamic Models About the Elbow," IEEE Transactions on Neural Systems and Rehabilitation Engineering 25(9):1529–1538, 2017.

Chapter 6: Comparison Of Constant-Posture Force-Varying EMG-Force Dynamic Models About The Elbow

Chenyun Dai, Berj Bardizbanian, and Edward A. Clancy, *Senior Member, IEEE*

6.1 Abstract

Numerous techniques have been used to minimize error in relating the surface electromyogram (EMG) to elbow joint torque. We compare the use of three techniques to further reduce error. First, most EMG-torque models only use estimates of EMG standard deviation as inputs. We studied the additional features of average waveform length, slope sign change rate and zero crossing rate. Second, multiple channels of EMG from the biceps, and separately from the triceps, have been combined to produce two low-variance model inputs. We contrasted this channel combination with using each EMG separately. Third, we previously modeled nonlinearity in the EMG-torque relationship via a polynomial. We contrasted our model vs. that of the classic exponential power law of Vredenbregt and Rau [Vrendenbregt and Rau, 1973]. Results from 65 subjects performing constant-posture, force-varying contraction gave a "baseline" comparison error (i.e., error with none of the new techniques) of 5.5 ± 2.3% maximum flexion voluntary contraction (%MVC$_F$). Combining the techniques of multiple features with individual channels reduced error to 4.8 ± 2.2 %MVC$_F$, while combining individual channels with the power-law model reduced error to 4.7 ± 2.0 %MVC$_F$. The new techniques further reduced error from that of the baseline by ≈15%.

***Index Terms*—Biological system modeling, electromyogram, EMG-force, multiple-channel EMG**

C. Dai (e-mail: cdai@wpi.edu), B. Bardizbanian (e-mail: berj@wpi.edu) and E. A. Clancy (e-mail: ted@wpi.edu) are with the Electrical and Computer Engineering Department, Worcester Polytechnic Institute, Worcester, MA 01609 USA.

6.2 INTRODUCTION

Since at least the work of Inman *et al.* in 1952 [Inman et al., 1952], the surface electromyogram (EMG) has been investigated as an estimator of muscle force/joint torque. Much of the early work studied the linearity of the relation using agonist muscle EMG during constant-posture, quasi-constant force contractions ("quasi-static") [Vrendenbregt and Rau, 1973, Inman et al., 1952, Lawrence and DeLuca 1983, Hasan and Enoka 1985, Heckathorne and Childress 1981]. During the intervening years, numerous studies (see review in [Staudenmann et al., 2010]) have expanded the experimental conditions and reduced the error in the EMG-torque relationship through various improvements, including: modeling both agonist and antagonist muscle activity [Messier et al. 1971, An et al. 1983, Solomonow et al. 1986, Clancy and Hogan 1997], accounting for subject-to-subject differences in the relationship [Hasan and Enoka 1985, Thelen et al. 1994], reducing variability in the estimate of EMG standard deviation (EMGσ) by whitening the EMG signal and/or (for large muscle groups) utilizing multiple-channel EMGσ–torque estimators [Hogan and Mann 1980, Harba and Lynn 1981, Clancy and Hogan 1994-1995, Potvin and Brown 2004, Staudenmann et al. 2005-2006-2009, Hashemi et al. 2015], modeling EMG-torque dynamics [Hashemi et al. 2015, Gottieb and Agarwal 1971, Sanger 2007, Hashemi et al. 2012], incorporating a range of joint angles [Hof and Van den Berg 1981, Doheny et al. 2008, Hashemi et al. 2013, Liu et al. 2013-2015], and applying robust system identification methods [Thelen et al. 1994, Hashemi et al. 2015-2012, Clancy et al. 2006-2012]. The various techniques are relevant in several areas in which a noninvasive EMG-torque estimate is useful, such as prosthesis control [Mann and Reimers 1970, Parker et al. 2006], clinical biomechanics [Doorenbosch and Harlaar 2003, Disselhorst et al. 2009] and ergonomics assessment [Kumar and Mital 1996, Hagg et al. 2004].

In a related problem in EMG-based prosthetics control, multiple EMG features have been used as inputs to the task of classifying distinct movement classes. In particular, Hudgins *et al.* [Hudgins et al. 1993] (see [Micera et al. 2010] for a review) added to EMGσ the features of slope sign change rate (SSC), zero crossing rate (ZC) and average waveform length (WL). Only recently has the success of these "additional" features in the EMG classification problem led to their investigation as model inputs in the EMG-torque problem [Nielsen et al. 2011, Kamavuako et al. 2012, Jiang et al. 2012,-2013, Ameri et al. 2014].

In this study, we report on three techniques for continuing performance improvement in the

EMG-torque relationship. First, most past studies using dynamic models of EMG-torque have exclusively utilized EMGσ as the input EMG feature. Thus, we look at the applicability of adding the additional features of Hudgins *et al.*, comparing models with and without their inclusion. Second, for large muscles, EMGσ variability has been reduced by combining the information from multiple electrodes into one EMGσ estimate [Hogan and Mann 1980, Harba and Lynn 1981, Clancy and Hogan 1995]. This method of channel combination is optimal assuming that the underlying muscle contains the same information across its multiple electrode locations, varying only due to the stochastic nature of motor unit firing times. However, there is evidence that large muscles—this research studies the biceps and triceps muscles—contain some degree of control based on neuromuscular compartments [English et al. 1993, Tiu et al. 2014, Windhorst et al. 1989]. As such, combining EMG sites to produce a feature estimate would no longer be justified. Thus, we contrast combining EMG sites to estimate a feature vs. extracting features from each individual electrode. Third, our own dynamic EMG-torque models have incorporated the static power-law nonlinearity described by Vredenbregt and Rau [Vredenbregt and Rau, 1973] via the use of a polynomial relation [Liu et al. 2015, Clancy et al. 2012]. This method simplifies the mathematics, allowing the use of *linear* least squares estimation, but can require many parameters—which can have its own detrimental effects [Ljung 1999]. Other authors have captured a nonlinear relationship with other model forms, e.g., parallel-cascade models [Hashemi et al. 2012] and neural networks [Nielsen et al. 2011, Jiang et al. 2012, Ameri et al. 2014, Muceli and Farina 2012]. Therefore, we directly compared use of the power-law nonlinearity of [Vredenbregt and Rau, 1973] (requiring parameter estimation via *nonlinear* least squares) to that of the polynomial model. Finally, we examined if combining pairs of these various improvement techniques provides an additive benefit. We also varied the dynamic model order (i.e., number of time lags) and the tolerance value associated with the Moore-Penrose inverse method used to linear least squares fit model parameters. These parameters influence EMG-force errors [Clancy et al. 2012] and thus should be optimized within each of the three primary techniques studied in this work.

6.3 Methods

6.3.1 Experimental Subjects, Apparatus and Methods

Experimental data from 54 subjects acquired during three prior experiments [Liu et al. 2015, Clancy et al 1999, Clancy et al 2000] were combined with the data from 11 new subjects to form a pool of 65 total subjects. The new data collection and all analysis was approved and supervised by the WPI Institutional Review Board. Each of the 65 subjects provided written informed consent for their respective experiment. For the new data collection (similar methods were used in the prior experiments), subjects were seated and strapped via three belts into the custom-built straight-back chair shown in Fig. 6.1, with their right shoulder abducted 90°, the angle between their upper arm and forearm 90°, their forearm oriented in a parasaggital plane, and their supinated right wrist (palm perpendicular to the floor) tightly cuffed to a load cell (Vishay Tedea-Huntleigh Model 1042, 75 kg full scale). Skin above the biceps and triceps muscles was vigorously scrubbed with an alcohol wipe and a bead of electrode gel was massaged into the overlying skin. Four custom-built bipolar EMG electrode-amplifiers were applied in a transverse row across each of the biceps and triceps muscle groups, midway between the elbow and the midpoint of the upper arm (to avoid the innervation zone proximally and the tendon distally), centered along the muscle mid-line. Each electrode-amplifier had a pair of 8 mm diameter, stainless steel, hemispherical contacts separated 1 cm edge-to-edge, oriented along the muscle's long axis. The distance between adjacent electrode-amplifiers was ~1.75 cm. A reference electrode was gelled and secured to the lateral aspect of the upper arm, between the flexion and extension electrodes. All electrodes were secured in place on the right arm with elastic bandages. Custom electronics amplified and filtered each EMG signal (CMRR > 90 dB at 60 Hz; 8th-order Butterworth highpass at 15 Hz; 4th-order Butterworth lowpass at 1800 Hz) before being sampled at 4096 Hz with 16-bit resolution. The RMS EMG signal level at rest (representing equipment noise plus ambient physiological activity) was on average 5.0 ± 7.3% of the RMS EMG at 50% maximum voluntary contraction (MVC) for these 11 new subjects. The load cell (torque) signal was synchronously sampled at 4096 Hz with 16-bit resolution.

All contractions were constant-posture. Subjects were provided a warm-up period. Separate extension and flexion MVCs were then measured in which subjects took 2–3 seconds to slowly ramp up to MVC and maintained that force for two seconds. The average load cell value during

the contraction plateau was taken as the MVC. Five second duration, constant-force contractions at 50% MVC extension, 50% MVC flexion and at rest (arm removed from the wrist cuff) were next recorded. These contractions were used to calibrate whitening filters and to gain-normalize the EMG and force data [Clancy et al. 2000, Prakash et al. 2005], as further described below. Then, three tracking trials of 30 s duration were recorded during which the subjects used the load cell as a feedback signal to track a computer-generated torque target. The target moved on the screen in the pattern of a bandlimited (1 Hz) uniform random process, spanning 50% MVC extension to 50% MVC flexion. Three minutes of rest were provided between trials to avoid cumulative fatigue.

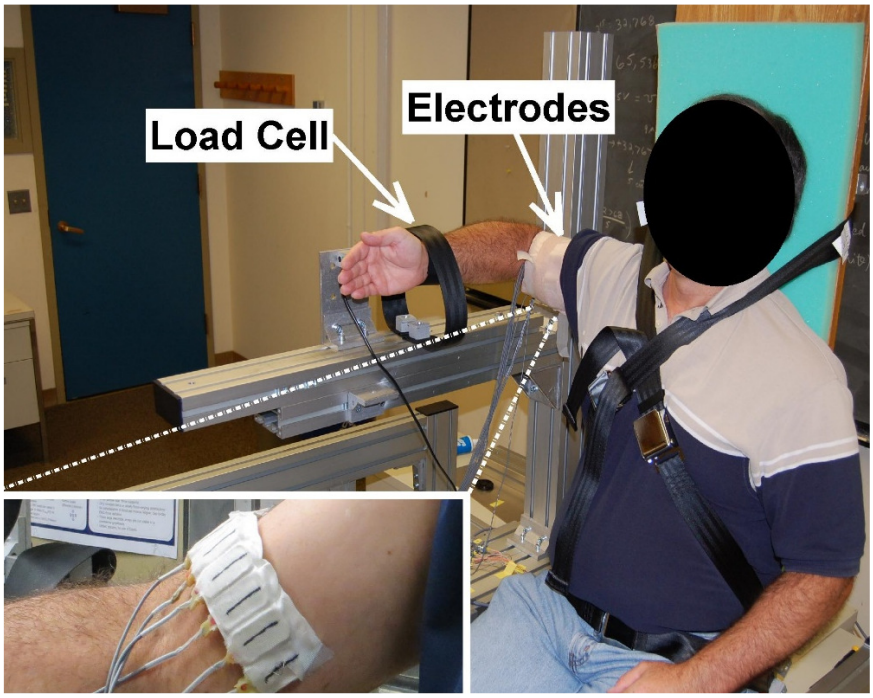

Fig. 5.4. Subject seated in the experimental apparatus with right arm cuffed at the wrist to the load cell and electrodes applied over the biceps and triceps muscles. Inset shows six electrodes positioned transversely across the biceps muscles (with securing bandage removed for visualization). Middle four electrodes used for the analysis reported herein. Triceps electrodes were arranged similarly.

6.3.2 Methods of Analysis

Analysis was performed offline in MATLAB. All EMG filters were designed as specified below, then applied in the forward and reverse time directions to achieve zero phase and the square of the magnitude response. Each EMG channel was powerline notch filtered (2nd-order IIR notch filter

at the fundamental and each harmonic, bandwidth ≤ 1.5 Hz), since whitening at high frequencies is particularly susceptible to powerline interference. These filters attenuate powerline noise with limited reduction in signal statistical bandwidth [Bendat and Piersol 1971]. Each EMG channel was then highpass filtered to reject motion artifacts (5th-order Butterworth, 15 Hz cutoff) and whitened using the adaptive whitening algorithm of [Clancy et al. 2000] and [Prakash et al. 2005]. Features were next extracted from each of the eight whitened EMG signals. EMGσ[n] was formed by rectifying each signal and WL[n] was computed as the absolute difference between adjacent samples [Hudgins et al. 1993, Micera et al. 2010, Liu et al. 2013], where n was the discrete-time sample index at the sampling rate of 4096 Hz. ZC[n] and SSC[n] [Hudgins et al. 1993, Micera et al. 2010, Liu et al. 2013] were formed by assigning a value of one to each sample corresponding to a thresholded zero crossing/slope sign change, and a value of zero otherwise. For each electrode, the noise threshold used for ZC and SSC was 3% of the RMS of a rest contraction. Two different EMG channel selection options were studied: (1) features from the four biceps and, separately, triceps channels were each ensemble averaged to form four-channel feature estimates (for EMGσ and WL, the channels were gain normalized prior to doing so [Clancy and Hogan 1995]), or (2) features from each of the eight individual EMGs were retained separately. EMG features and the torque measurement were next lowpass filtered at 16 Hz, then downsampled to 40.96 Hz. This rate is fast enough to capture the system dynamics while also eliminating high-frequency noise outside of the torque signal band that can confound the ensuing system identification [Clancy et al. 2006, Ljung 1999]. Note that the lowpass filter stage prevents aliasing when downsampling, while simultaneously smoothing (/averaging) the EMG features. Further smoothing is inherently customized to each subject, provided by the dynamic models (described in the next paragraph). Hence, the dynamic models optimize the final lowpass cutoff frequency (and shape) in order to minimize EMG-torque error [Koirala et al. 2015].

The decimated extension and flexion EMG features from each subject (inputs) were related to their respective elbow torque (output) via one of two dynamic models. The first "quadratic" model incorporated a second degree polynomial (based on prior optimization of a subset of these data [Clancy et al. 2012], and consistent with the nonlinearity in the EMG-force curve at the elbow [Vrendenbregt and Rau 1973]):

$$T[m] = \sum_{q=0}^{Q} \sum_{f=1}^{F} \sum_{e=1}^{E} \left\{ c_{1,q,f,e} V_{f,e}[m-q] + c_{2,q,f,e} V_{f,e}^{2}[m-q] \right\}, \qquad (1)$$

where m was the decimated discrete-time sample index, $T[m]$ the measured torque, Q the number of time lags in the model (to provide dynamics), F the number of EMG features included (EMGσ was always included; optionally either one or all of the remaining three features was included), E the number of EMG channels (E=2 was used when the four biceps and four triceps channels were combined into two channels; E=8 was used when eight individual channels were retained), c_i were the fit coefficients, and $V[\cdot]$ were the EMG feature values. The fit coefficients were estimated using regularized (Moore-Penrose inverse) linear least squares, in which singular values of the design matrix were discarded if their ratio to the largest singular value was less than a selected tolerance value (*Tol*) [Clancy et al. 2012, Press et al. 1994]. Thus, the EMG features, and their squared values, were least squares fit to torque.

The second "power-law" model was:

$$T[m] = \sum_{q=0}^{Q} \sum_{f=1}^{F} \sum_{e=1}^{E} c_{q,f,e} V_{f,e}^{r_{f,e}} [m-q], \qquad (2)$$

where r was also a fit parameter equal to a continuous-valued exponent applied to the feature value. This exponent directly implemented the EMG-force nonlinearity of Vredenbregt and Rau [Vredenbregt and Rau, 1973]. The fit coefficients (c_i, r_i) were fit using nonlinear least squares. Anecdotally, initial solution guesses for r of 0.5, 1 and 2 were evaluated, with the c_i coefficients then initialized via linear least squares (using a pseudo-inverse tolerance of 0.005). Only the r = 1 value converged rapidly for most subjects. When each of these three r values led to convergence, they arrived at the same minimum soution. Thus, r = 1 was used as the initial guess value. This initial guess value happens to be the optimal linear solution.

Of the three available tracking trials, two were used for training and one for testing. Since the nonlinear minimizations were time-intensive and the sample size was already quite large for an EMG-torque study (65 subjects), cross-validation was not used. Error is reported as the test set RMS error between the actual and EMG-estimated torque, normalized to maximum flexion torque for each subject. The first and last 2 s of data were excluded to account for filter startup and tail transients[1]. We investigated combinations of: model orders between Q=5 to 40, five distinct EMG feature selections (EMGσ only, EMGσ paired with each of the other three features and all four features), two EMG channel selections (a four-channel biceps EMGσ with a four-channel triceps

[1] In real-time applications, all processing would be conducted using causal filters, eliminating the need to exclude any tail transients. (They would not exist.) The startup transient would occur at device power-up and thus not interfere with regular device operation.

EMGσ, or retaining all eight individual electrodes), two models (quadratic and power-law), and various pseudo-inverse linear least squares tolerance values (starting at *Tol*=0.1 and decrementing by 0.002 to 10^{-3}, and 10^{-4} and 10^{-5}). Note that we did not investigate every combination of model order and pseudo-inverse tolerance vs. the other parameters, since doing so would have been prohibitively time-consuming and the influence of model order and tolerance has already been characterized in prior work [Clancy et al. 2012]. Rather, tolerance was fixed at *Tol*=0.005 while model order was varied; and model order was fixed at *Q*=15 while tolerance was varied.

Finally, for comparison to conventional EMG-torque models, we also investigated cascade of a fixed, second-order Butterworth filter (cut-off frequency of 1.5 Hz , as optimized for a subset of these data in prior work [Koirala et al. 2015]) after each of the extension and flexion EMGσ signals, as derived from single-channel unwhitened EMG (selecting one of the central electrodes on each muscle). The gains of both filters (i.e., the fit coefficients for the Butterworth model) were calibrated from the test data using linear least squares (*Tol* = 0.005, two training trials, one test trial).

Statistical evaluation used multivariate ANOVA (significance level of $p = 0.05$), with *post hoc* pair-wise comparisons conducted using Tukey's honestly significant difference test (which adjusts for multiple comparisons).

6.4 Results

Our strategy was to individually compare the three study techniques of EMG features, EMG channel combination and model vs. our "baseline" best prior technique [Clancy et al. 2012] comprised of the EMGσ feature only, four-channel EMG processors and the quadratic polynomial model. As appropriate, we also assessed performance as a function of dynamic model order (Q) and pseudo-inverse tolerance (Tol). Then, we assessed improvement (beyond that found due to one study technique) when pairs of study techniques were combined. We do not report results from all three study techniques combined, since the nonlinear minimization frequency failed to converge—presumably due to the large number of features encountered when using all (five) features and eight individual EMG channels. Note that for several analyses, model order was fixed at Q=15 and the pseudo-inverse tolerance was fixed at Tol=0.005. These fixed values were determined based on prior analysis of a portion of these data [Clancy et al.

2012] (and are consistent with our results reported herein). Example time-series EMG-torque estimates are shown in Fig. 6.2. For comparison, the conventional Butterworth model had average ± std. dev. RMS error of 8.9 ± 3.0 %MVC_F.

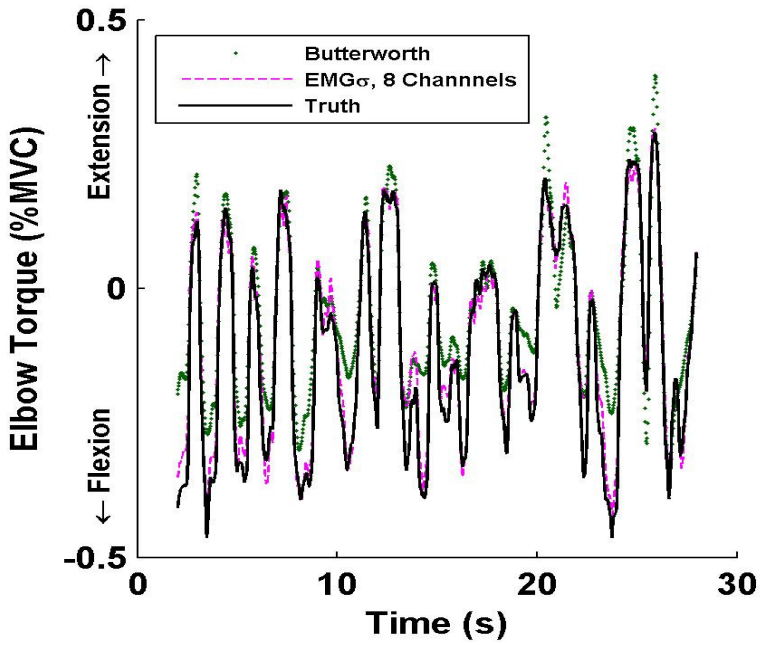

Fig. 5.5. Example EMGσ-torque estimation results for selected models. Butterworth model (2 Hz lowpass filter cut-off) exhibited an RMS error of 10.2 %MVC. Eight-channel EMGσ model (Q = 15 order, pseudo-inverse tolerance of Tol = 0.005) exhibited an RMS error of 4.5 %MVC. "Truth" refers to the recorded load cell values. Subject LA04, trial 45.

6.4.1 Baseline Technique vs. One Improvement Technique

<u>EMG Feature Set:</u> We began by comparing the results between the baseline technique (EMGσ only, four-channel EMG and quadratic model) vs. EMG feature set. Fig. 6.3, top, shows average error results vs. dynamic model order (Q) with pseudo-inverse tolerance fixed at Tol=0.005. Error reduced rapidly as model order initially increased and the full feature set showed the lowest error. A two-way ANOVA (Factors: model order, feature set) was significant for both main effects ($p < 10^{-3}$), without interaction. *Post hoc* Tukey evaluation of model order found that lower orders exhibited higher errors than the highest orders for orders Q=5 through 8. Results for model orders 9–40 did not differ. *Post hoc* Tukey differences were also found as a function of the feature set: EMGσ had higher error than either EMGσ+WL or the full set. At Q=15, the baseline technique error (mean ± std.) was 5.5 ± 2.3 %MVC_F. Fig. 6.3, bottom, shows results vs. pseudo-inverse

tolerance (*Tol*) with model order fixed at Q=15. Error reduced rapidly as tolerance decreased, and the full feature set showed the lowest error. To avoid the interactions at the larger tolerance values, a two-way ANOVA (Factors: tolerance, feature set[2]) omitted tolerance values above 0.011. This comparison was only significant for the main effect of feature set (p=0.01), without interaction. *Post hoc* Tukey comparisons only found differences between the EMGσ-only feature vs. the full feature set. Overall, the full feature set generally produced lower errors.

EMG Channel Selection: Next, we compared results between the baseline technique vs. individual EMG channels. Fig. 6.4, top, shows results vs. model order Q (*Tol* fixed at 0.005). Error reduced as model order initially increased and the individual EMG channels had lower error. A two-way ANOVA (Factors: model order, EMG channel selection) was significant for both main effects ($p<10^{-6}$), without interaction. *Post hoc* Tukey evaluation of model order found that lower orders had higher errors than the highest orders for orders Q=5 through 7. Results for model orders 8–40 did not differ. *Post hoc* Tukey evaluation of EMG channel selection found individual EMG channels to have lower error. Fig. 6.4, bottom, shows results vs. tolerance (Q fixed at 15). For consistency, a two-way ANOVA (Factors: tolerance, EMG channel selection) omitted tolerance values above 0.011. This comparison was only significant for the main effect of EMG channel selection ($p<10^{-6}$, no interaction), with *post hoc* Tukey evaluation finding individual EMG channels to have lower error. Overall, using eight separate channels—as opposed to extension/flexion four-channel processors—consistently led to lower error.

Power-Law Model: Then, we compared results between the baseline technique and the power-law model. Fig. 6.5 shows these results vs. model order (Q), with *Tol*=0.005 selected for the quadratic model. Tolerance was not examined as a separate factor, as it is not varied with the power-law model. Error using the power-law model was consistently lower than that of the

[2] Note that a three-way ANOVA with factors model order, tolerance and feature set was not pursued since results from all combinations of model order and tolerance were not computed (see Methods). Instead, model order and tolerance were analyzed in separate two-way ANOVAs (here and also below).

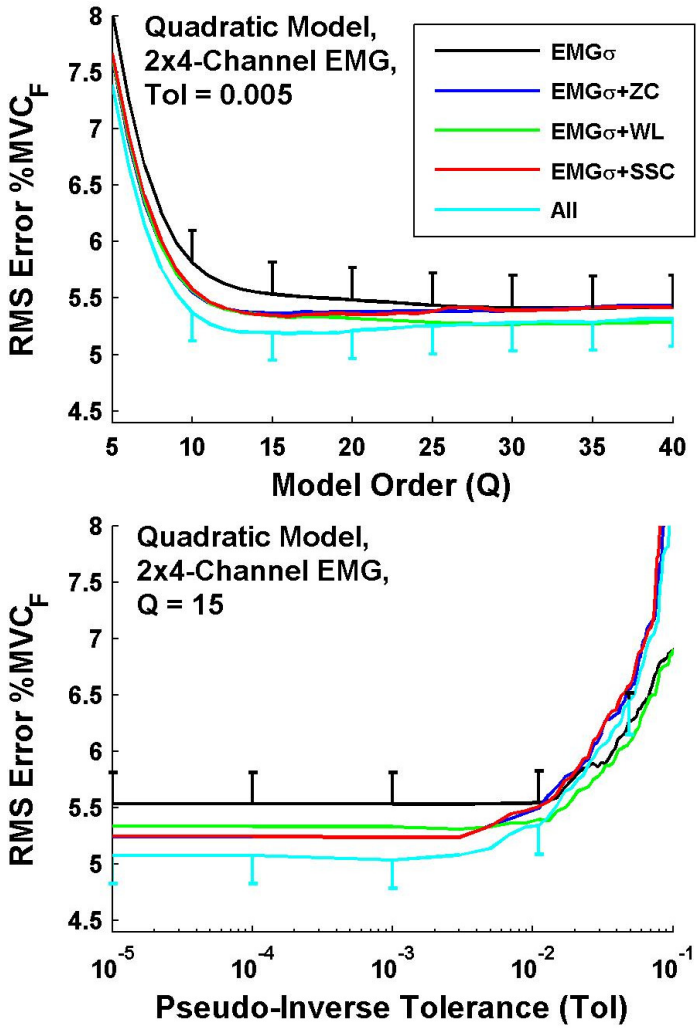

Fig. 5.6. Baseline Model vs. EMG Channel Selection: Average RMS errors from 65 subjects, EMGσ-only feature set. Single-sided standard error bars shown for selected Q values. Top: Results vs. quadratic model order (Q), using pseudo-inverse tolerance of Tol= 0.005. Bottom: Results vs. pseudo-inverse tolerance, with quadratic model order Q=15.

baseline model. A two-way ANOVA (Factors: model order, model type) was significant for both main effects ($p<10^{-6}$), without interaction. *Post hoc* Tukey evaluation of model order found that lower orders exhibited higher errors than the highest orders for orders Q=5 through 7. Results for model orders 8–40 did not differ. *Post hoc* Tukey evaluation of model form found lower errors with the power-law model. Overall, the power-law model produced lower errors.

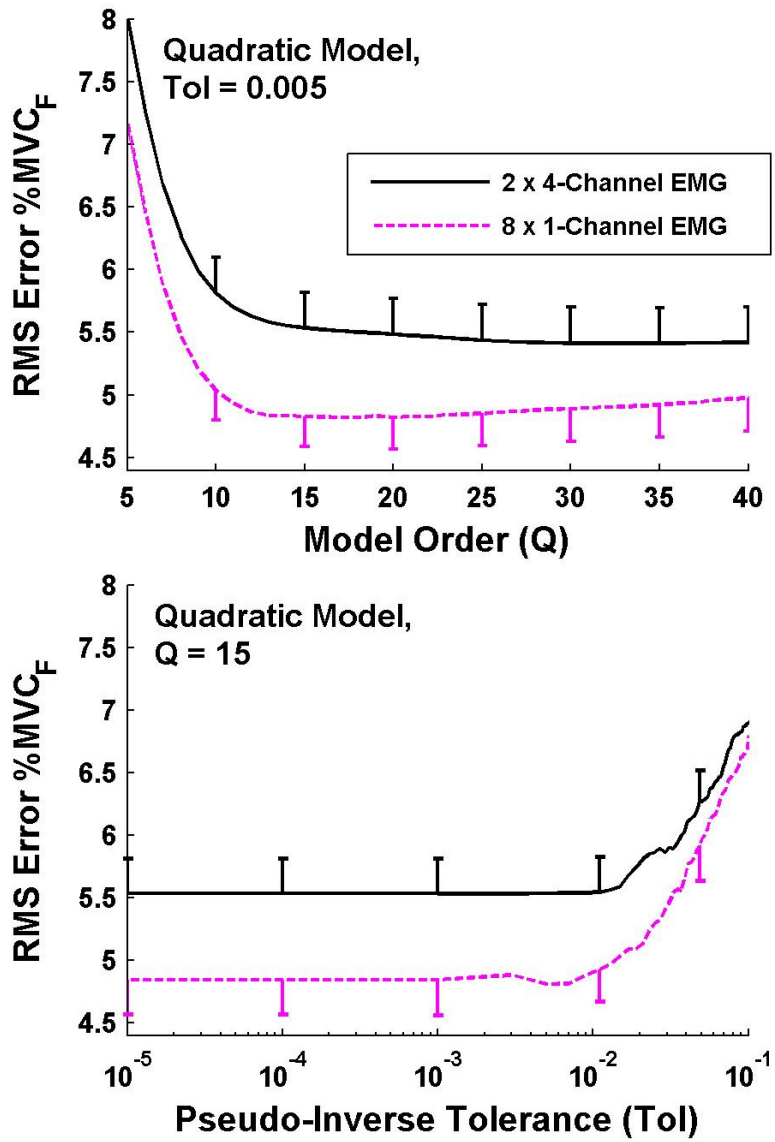

Fig. 5.7. Baseline Model vs. Feature Set: Average RMS errors from 65 subjects, four-channel EMG. Legend refers to both plots. Single-sided standard error bars shown for two of five feature sets (standard errors were similar for the other three feature sets) for selected Q values. Top: Results vs. quadratic model order (Q), using pseudo-inverse tolerance of Tol=0.005. Bottom: Results vs. pseudo-inverse tolerance, with quadratic model order Q=15.

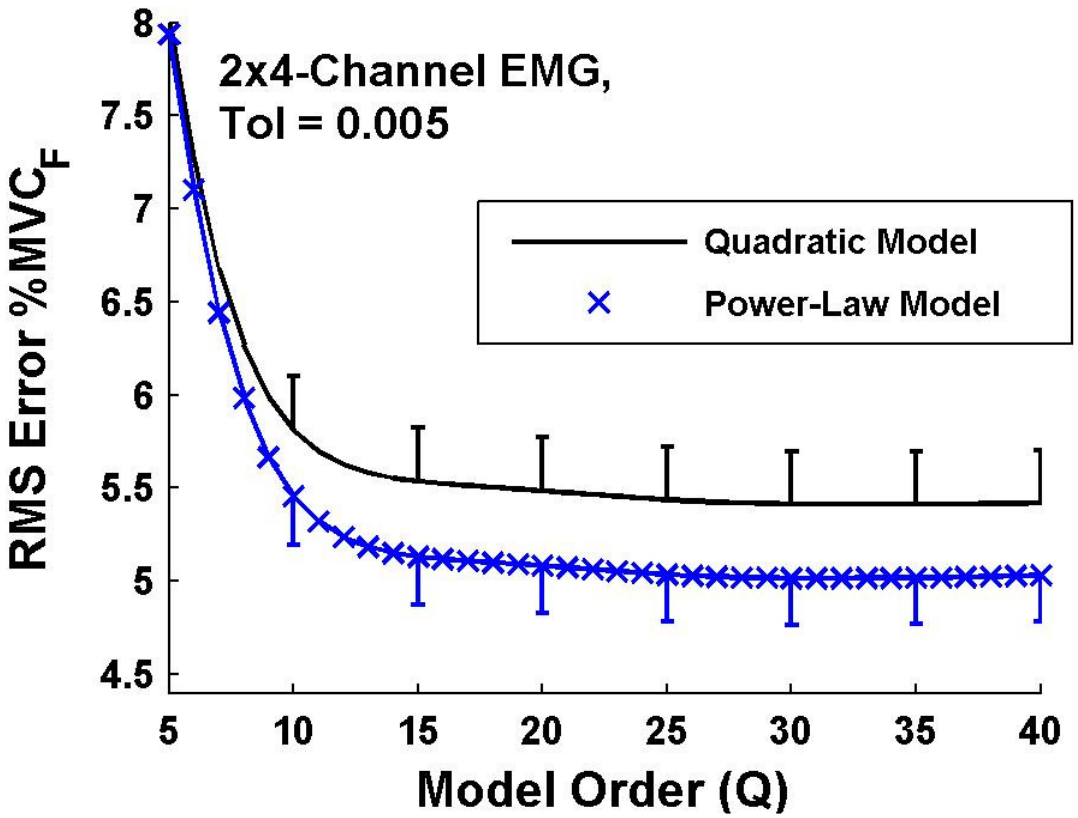

Fig. 5.8. Baseline Model vs. Power-Law Model: Average RMS errors from 65 subjects, EMGσ-only feature set. Results vs. model order (Q). Quadratic model used pseudo-inverse tolerance of Tol=0.005. Single-sided standard error bars shown for selected Q values.

6.4.2 One Improvement Technique vs. Two

We concluded from the above results that each of the three techniques improved EMG-torque performance *individually*. Thus we next evaluated *pairs* of techniques, comparing each pair to the individual improvements. For EMG feature sets, we only retained two options, EMGσ only and all features. The results above showed that the other feature set options had performance that fell between these two. Also, we eliminated the reporting of *post hoc* statistical evaluation for model order and tolerance, as their roles were well established by the results above and prior literature results [Clancy et al 2012]. Doing so placed our focus on the three improvement techniques.

<u>EMG Feature Set & EMG Channel Selection:</u> Above, Fig. 6.3 showed the error improvements from the baseline technique due to EMG feature set and Fig. 6.4 to EMG channel selection. Here, Fig. 6.6 repeats both of these individual results, then adds the results when these techniques are combined (quadratic model with all features and eight individual EMG channels). For the results

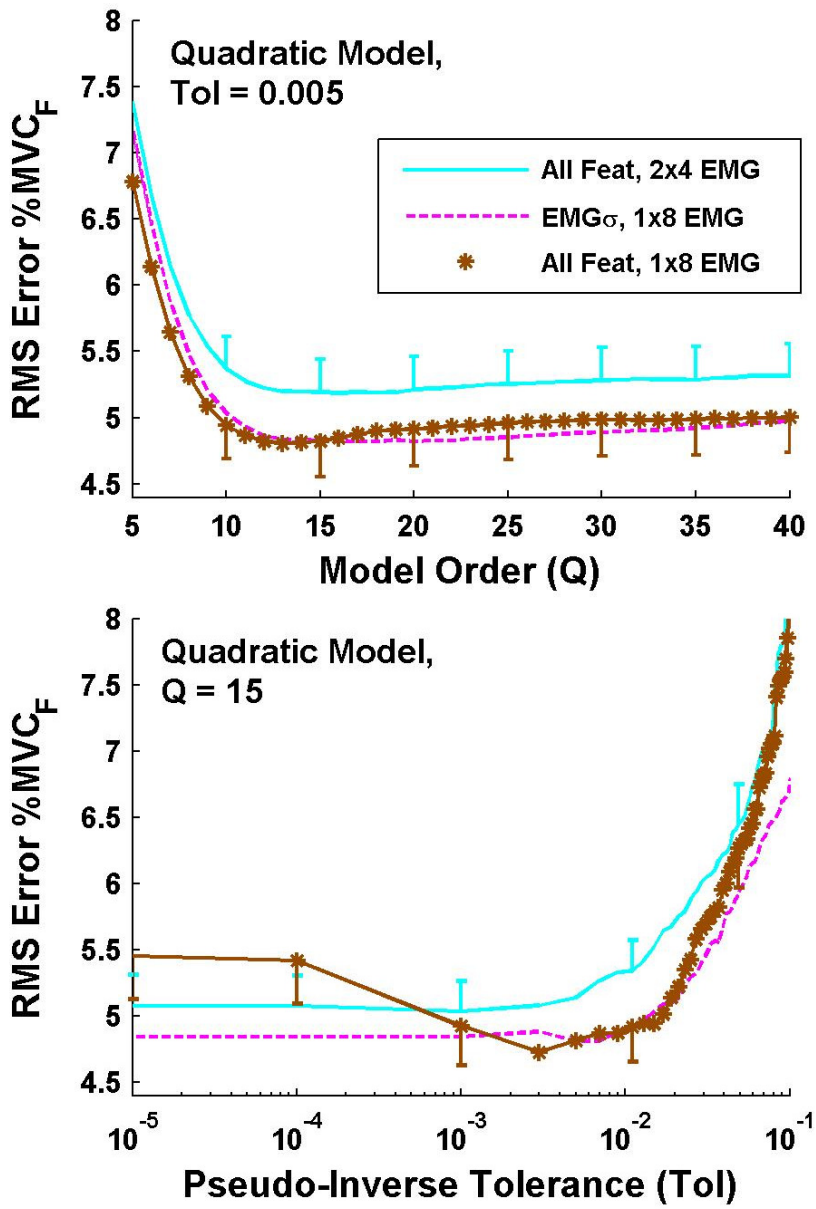

Fig. 5.9. Four-Channel EMG: All Features vs. Power-Law Model vs. Both. Average RMS errors from 65 subjects. Results vs. model order (Q). Quadratic model used pseudo-inverse tolerance of Tol=0.005. Single-sided standard error bars shown for two of three feature sets (standard errors were similar for the third feature set) for selected Q values.

shown in Fig. 6.6, top, a two-way ANOVA (Factors: model order, the three techniques) was significant for both main effects ($p<10^{-6}$), without interaction. *Post hoc* Tukey evaluation of technique found that using all EMG features with four-channel EMG had higher error than the other two techniques (EMGσ only, eight individual channels; all features, eight individual channels). At Q=15, the technique with all features and eight individual EMG channels had an

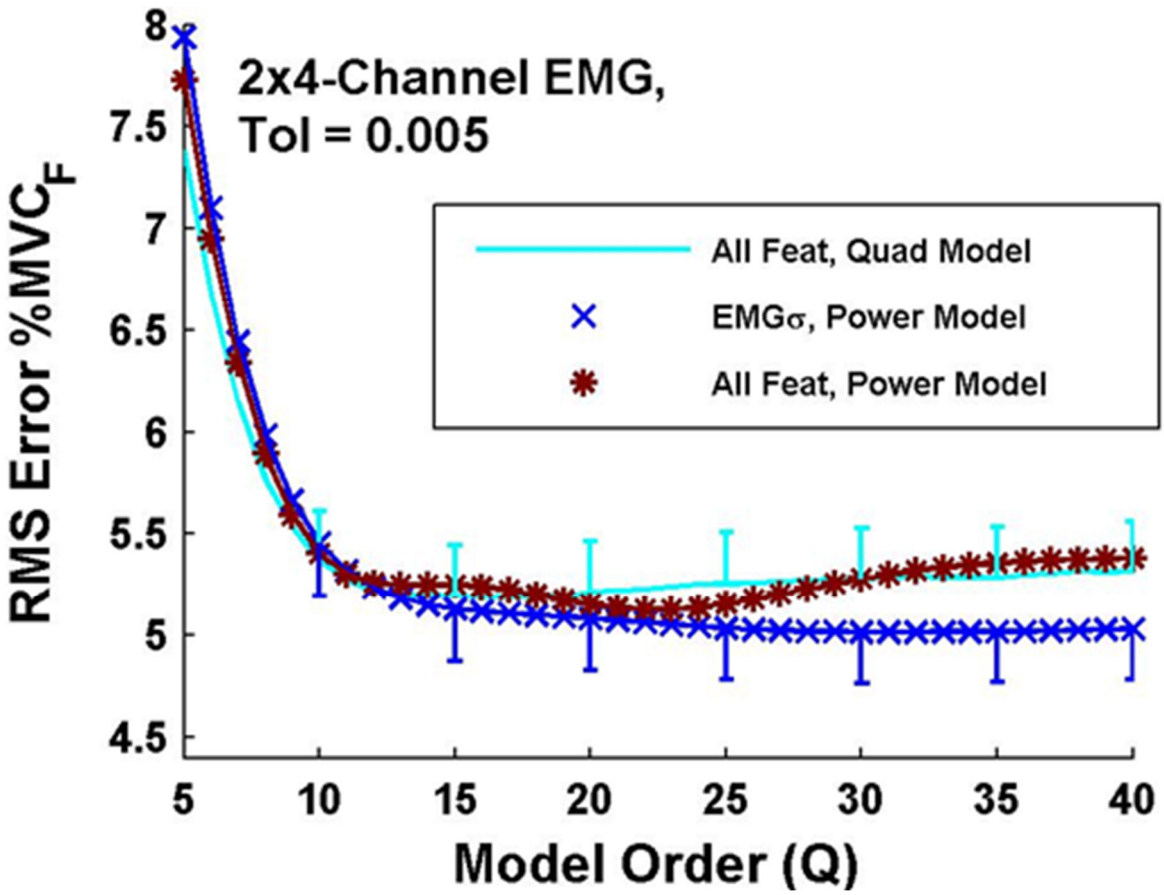

Fig. 5.10. EMGσ Feature: Eight Individual EMG vs. Power-Law Model vs. Both. Average RMS errors from 65 subjects. Results vs. model order (Q). Quadratic model used pseudo-inverse tolerance of Tol=0.005. Single-sided standard error bars shown for two of three feature sets (standard errors were similar for the third feature set) for selected Q values.

error mean ± std. of 4.8 ± 2.2 %MVC$_F$. The error results shown in Fig. 6.6, bottom, are high for all techniques for large tolerance values and climb when using all features and eight individual channels for tolerances $\leq 10^{-3}$. A two-way ANOVA (Factors: tolerance values ≤0.011, the three techniques) was only significant for technique (p=0.02, no interaction). *Post hoc* Tukey evaluation of technique found that using EMGσ only with eight individual channels exhibited lower error than the other two techniques. Nonetheless, Fig. 6.6 shows similar performance specifically in the region of the optimum tolerance value (e.g., $Tol = 0.005$), when comparing the technique of EMGσ only with eight individual channels to the technique of all features with eight individual channels..

<u>EMG Feature Set & Model Form:</u> Above, Fig. 6.3 showed the error improvements due to EMG feature set and Fig. 6.5 to model form. Here, Fig. 6.7 repeats both of these individual results, then adds the results when these techniques are combined (four-channel EMG with all features and the power-law model). A two-way ANOVA (Factors: model order, the three techniques) was

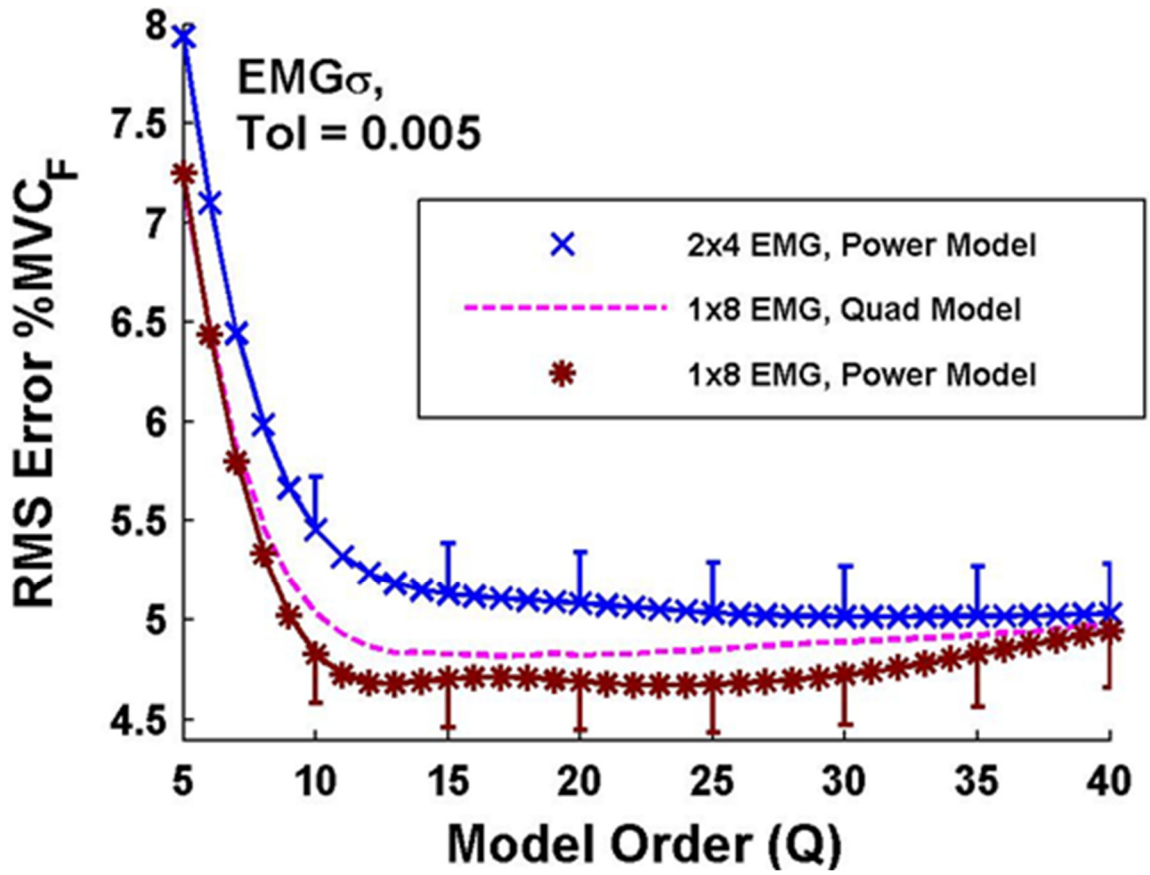

Fig. 5.11. Quadratic Model: All Features vs. Eight Individual EMG vs. Both. Average RMS errors from 65 subjects. Legend refers to both plots. Single-sided standard error bars shown for two of three feature sets (standard errors were similar for the third feature set) for selected *Q* values. Top: Results vs. quadratic model order (*Q*), using pseudo-inverse tolerance of *Tol*=0.005. Bottom: Results vs. pseudo-inverse tolerance, with quadratic model order *Q*=15.

significant for the main effect of model order ($p<10^{-6}$), but not significant for the main effect of technique (p=0.06), without interaction. Thus, this paired set of improvements did not reduce error beyond that found from each individual technique. At Q=15, each of the three techniques had an error mean ± std. of approximately 5.1 ± 2.1 %MVC_F.

<u>EMG Channel Selection & Model Form:</u> Above, Fig. 6.4 showed the error improvements due to eight individual EMG channels and Fig. 6.5 to model form. Here, Fig. 6.8 repeats both of these individual results, then adds the results when these techniques are combined (EMGσ-only feature with eight individual EMG channels and the power-law model). A two-way ANOVA (Factors: model order, the three techniques) was significant for both main effects ($p<10^{-6}$), without interaction. *Post hoc* Tukey evaluation of technique found that using four-channel EMG with the power-law model had higher error than the other two techniques. At Q=15, the technique with

eight individual EMG channels and the power-law model had an error mean ± std. of 4.7 ± 2.0 $\%MVC_F$.

6.5 Discussion

This study evaluated three techniques to reduce error in the EMG-torque relationship about the elbow—additional EMG features, EMG channel selection and EMG-force model form. Figs. 6.3–6.5 (and their associated statistical analyses) show that *each* of these techniques *individually* improved upon a "baseline" model that used only the EMGσ feature, four-channel EMG for each of the biceps and triceps, and the quadratic polynomial model. Note that this baseline model already optimizes several processing steps, including using EMG signal whitening, selecting the degree of the polynomial model and selecting the pseudo-inverse tolerance [Clancy et al. 1994, Clancy et al. 1995 , Clancy et al. 2012]. Whitening has previously been shown to reduce the variance of EMGσ estimates [Hogan and Mann 1980, Harba and Lynn 1981, Clancy et al. 1994, Clancy et al. 1995], e.g. providing an ≈63% improvement in SNR for constant-posture, constant-force elbow contractions when using a 245 ms smoothing window [Clancy et al. 1994]. EMG whitening leads to significant performance improvements in EMG-torque estimation [Potvin and Brown 2004, Clancy et al. 2012], e.g. a 14.1% reduction in RMS error during constant-posture, repetitive elbow exertions [Potvin and Brown 2004]. Whitening has also been shown to reduce the variance of WL and (to some extent) ZC estimates [Liu et al. 2013] (leading to performance improvements in multifunction prosthesis control [Liu et al. 2013]). The variance reduction is attributed to an increase in signal statistical bandwidth provided by whitening [Hogan and Mann 1980, Liu et al. 2013]. Therefore, we would expect similar variance reduction in whitened estimates of the SSC feature.

Of the three techniques, Figs. 6 and 8 show that using eight individual EMGs (as opposed to a four-channel EMG for each of the biceps and triceps) provides the clearest advantage. The concept of combining the information from multiple electrodes sited over a large muscle assumes that the spatially diverse information represents different statistical samples of the same underlying stochastic process [Hogan and Mann 1980]. The elbow contractions used herein were constrained to a single plane, reinforcing this assumption. Certainly, prior work has shown that four-channel EMG over the biceps and triceps leads to lower EMG-torque error than if only one biceps and one triceps EMG were used [Hogan and Mann 1980, Clancy et al. 2006, Clancy et al. 2012], attributed

largely to lower EMGσ variance [Hogan and Mann 1980, Clancy et al. 1994, Clancy et al. 1995, Potvin and Brown 2004]. However, our current results show that further error reduction is realized if the multiple EMG channels are used as separate inputs to the system identification model. Several concepts could explain this further improvement, all challenging the assumption that each electrode is stochastically sampling the same distribution. First, the individual electrodes could be sampling from distinct spatial regions with distinct neuromuscular control (i.e., neuromuscular compartments [English et al. 1993, Liu et al. 2014, Windhorst et al. 1989]). Second, we have anecdotally noticed that electrodes placed further from the muscle midline are more prone to crosstalk from the antagonist muscles, and that the EMG from such electrodes leads to a poorer EMG-torque estimate. The use of individual electrodes would permit the system identification model to de-emphasize those EMG channels that contribute less to reducing the EMG-torque error. Third, the quality of the EMG signal (e.g., signal to noise ratio) can vary electrode-to-electrode. When used as individual channels, the system identification model can de-emphasize the noisy electrodes; but when combined into a four-channel EMG, the emphasis of individual channels is purposely equalized [Hogan and Mann 1980, Clancy et al. 1995]. Future research should examine which EMG channels are more heavily weighted in these identified models.

Because the decrease in EMG-force error due to eight individual EMG channels was robust to model form, it may be especially applicable to other nonlinear models used in the literature, such as parallel-cascade models [Hashemi et al. 2012] and neural networks [Nielsen et al. 2011, Jiang et al. 2012, Ameri et al. 2014, Ameri et al. 2015, Muceli and Farina 2012]. All model forms, however, become increasingly ill-conditioned as more fit parameters are added, the relative importance of which may vary model form to model form.

Figs. 6–8 show that the remaining two improvement techniques (EMG feature sets and EMG-force model form) each provide approximately the same error reduction—Fig. 6.6, top, shows that all features, eight individual EMG channels and the quadratic model (Q=15, Tol=0.005) had an error mean ± std. of 4.8 ± 2.2 $\%MVC_F$.; while Fig. 6.8 shows that the EMGσ-only feature, eight individual EMG channels and the power-law model (Q=15) had an error mean ± std. of 4.7 ± 2.0 $\%MVC_F$. These error performances represent an ≈15% reduction in error compared to the baseline model error of 5.5 ± 2.3 $\%MVC_F$. The power-law model has the advantage of fulfilling the static EMG-force nonlinearity found by Vredenbregt and Rau [Vredenbregt and Rau 1973] with a single exponential parameter per EMG channel, but the disadvantage of requiring significantly more

computation time for determining fit coefficients via nonlinear least squares. A concern with using additional EMG features is their effect on the conditioning of the linear/nonlinear least squares fit, since conditioning is inversely related to the number of fit coefficients [Ljung 1999]. In particular, Fig. 6.6, bottom, shows error increasing for tolerances below 10^{-3} when all four features for each of eight individual channels are fit using the quadratic model (64 coefficients in total). Tolerances below 10^{-3} provide progressively less regularization, the opposite of what is needed when the number of fit coefficients grows. Hence, model error grows, likely due to overfitting. As a result, the range of tolerance values over which error is minimum shrinks, making the modeling less reliable.

Considering systematic errors in the EMG-torque techniques, the use of multiple features expands the model shapes that can be fit (i.e., beyond the shapes that can be accommodated when only using EMGσ as an input). The performance of EMG-torque models also suffer from random errors due to the stochastic nature of EMG. The uncorrelated components of the four EMG features would tend to average and reduce variance errors. (E.g., when one feature value is randomly above its "true" value, another feature might be below.) Hence, both systematic and stochastic improvements can result. Of course, a challenge is to improve EMG-torque performance due to these advantages, in spite of the detrimental effects of overfitting (due to the increased number of parameters) and feature correlation (which, combined with overfitting, degrade the conditioning of the least squares fit). Future modeling might consider a compromise approach that only utilizes a sub-set of the additional features.

For the quadratic polynomial model, we focused our attention on a model order of Q=15 and a tolerance of Tol=0.005. Our ANOVA results showed statistical differences (reductions) in error as model order increased from Q=5 to Q=7 or 8 (depending on the condition). Nonetheless, all of our graphical results show continuing decline in error up to about Q=15. Although we had a large sample size of 65 subjects, it is likely that statistical power limited our ability to find statistical differences for orders above 8. In particular, paired statistical tests can be more powerful when assessing different treatments (i.e., EMG-force techniques) applied to the same data. For example, consider the technique that demonstrated the lowest average error: EMGσ-only feature, eight individual channels and the power-law model (Fig. 6.8). If we successively compute paired sign tests [58] between adjacent model orders at/above Q=8, we find statistical differences (p<0.01) until comparing orders Q=12 to 13. Such comparisons support our choice of Q=15 (and are more

fully detailed in [Clancy et al. 2012]). A similar argument supports our use of *Tol*=0.005.

Within the literature, it is difficult to directly compare EMG-torque results between studies, since error is a function of many variables, including the experimental conditions (e.g., constant-posture vs. freely moving) and experimental tasks (e.g., random, broadband torques vs. sinusoidal). Further, several different error measures are used within the literature. However, relative changes in performance in the same dataset, evaluated with the same error measure, should be more robust when compared. To that end, we have studied sub-portions of this data set in several published studies. The highest error of 19.2 ± 11.2 $\%MVC_F$ was found when supplying single-channel, unwhitened EMGσ to a simple second-order Butterworth model, calibrated from 50% constant-force contractions [Clancy et al. 2012]. Our results herein reduced the error to 8.9 ± 3.0 $\%MVC_F$ when the single-channel, unwhitened EMGσ supplied to the Butterworth model was calibrated from two dynamic contractions. This error was reduced to 5.5 ± 2.3 $\%MVC_F$ with our "baseline" method that used four-channel, whitened EMG and a quadratic nonlinearity (and FIR linear model). Finally, error was reduced to 4.7 ± 2.0 $\%MVC_F$ (the primarily work reported herein) by substituting individual EMG channels (rather than grouping them, separately, from the biceps and triceps muscle groups) and the power-law model (or reduced to 4.8 ± 2.2 $\%MVC_F$ by substituting individual EMG channels and all features). Thus, dramatic reduction in EMG-torque error has been achieved overall. In many applications in clinical biomechanics and ergonomics assessment, electrodes would be mounted on a subject, calibration data recorded and then a clinical/experimental task completed in a single session. Since appropriate EMG-torque calibration data is required for these scenarios and computation is readily available, all of the performance gains realized by these modeling techniques could be utilized. For prosthesis control, however, there is some evidence that improved off-line classification results do not always translate into improved on-line classification performance when assessed on standard prosthesis tasks [Lock et al. 2005, Hargrove et al. 2007]. Although our research involved EMG-torque estimation and not EMG-based classification, similar concerns exist [Jiang et al. 2014].

We limited this work to constant-posture contractions in order to reduce the complexity of a problem that already considers many modeling variables. In so doing, our results are directly relevant to prosthesis control when EMG is observed over remnant muscles whose posture is constrained (e.g., secured at both ends to the same bone), and in clinical/ergonomic assessments in which such postural constraint is appropriate. But, when joint angle is varied, additional study

will be necessary. That said, the reduction in RMS error can be thought of as a reduction of two error components: a variance error and a bias error. Those processing techniques that generally reduce variance (e.g., whitening, averaging due to multiple EMG channels, averaging due to multiple EMG features) should reduce EMG-torque error regardless of the experimental conditions. Techniques that reduce bias would likely need to be substituted with appropriate posture-varying models. The relative magnitude of variance vs. bias error can also change in posture-varying contractions. Nonetheless, our results should be informative to future studies of the reduction of both components of the RMS error in posture-varying contractions.

6.6 Conclusion

Our baseline technique for relating EMG to torque—EMGσ feature only, four-channel EMG from each of the biceps and triceps and a dynamic, quadratic nonlinear model—produced an error mean ± std. on this dataset of 5.5 ± 2.3 $\%MVC_F$. This baseline technique already includes several technique optimizations, including EMG signal whitening, multi-site EMG and the use of the quadratic nonlinearity [Clancy et al. 2012]. Three technique improvements were individually applied. These improvements were: additional EMG features, the use of eight individual EMG channels and a power-law model. Each technique individually lowered EMG-torque fit error. Combining the techniques of additional features and individual channels reduced error to 4.8 ± 2.2 $\%MVC_F$, while combining individual channels with the power-law model reduced error to 4.7 ± 2.0 $\%MVC_F$. These error performances represent an ≈15% reduction in error compared to the baseline model. Hence, these combined techniques represent a substantial improvement in performance. These results should be informative to application areas, including prosthesis control, clinical biomechanics and ergonomics assessment.

REFERENCES

[1] J. Vredenbregt and G. Rau, "Surface electromyography in relation to force, muscle length and endurance," *New Developments Electromyogr. Clin. Neurophysiol.,* vol. 1, pp. 607–622, 1973.

[2] V. T. Inman, H. J. Ralston, J. B. Saunders, B. Feinstein, and E. W. Wright, "Relation of human electromyogram to musculuar tension," *EEG Clin. Neurophysiol.,* vol. 4, pp. 187–194, 1952.

[3] J. H. Lawrence and C. J. De Luca, "Myoelectric signal versus force relationship in different human muscles," *J. Appl. Physiol.: Respirat. Environ. Exercise Physiol.,* vol. 54, pp. 1653–1659, 1983.

[4] Z. Hasan and R. M. Enoka, "Isometric torque-angle relationship and movement-related activity of human elbow flexors: Implications for the equilibrium-point hypothesis," *Exp. Brain Res.,* vol. 59, pp. 441–450, 1985.

[5] C. W. Heckathorne and D. S. Childress, "Relationships of the surface electromyogram to the force, length, velocity, and contraction rate of the cineplastic human biceps," *Am. J. Phys. Med.,* vol. 60, pp. 1–19, 1981.

[6] D. Staudenmann, K. Roeleveld, D. F. Stegeman, and J. H. van Dieen, "Methodological aspects of EMG recordings for force estimation—A tutorial and review," *J Electromyogr Kinesiol,* vol. 20, pp. 375–387, 2010.

[7] R. H. Messier, J. Duffy, H. M. Litchman, P. R. Raslay, J. F. Soechting, and P. A. Stewart, "The electromyogram as a measure of tension in the human biceps and triceps muscles," *Int. J. Mech. Sci.,* vol. 13, pp. 585–598, 1971.

[8] K. N. An, W. P. Cooney, E. Y. Chao, L. J. Askew, and D. J. R., "Determination of forces in extensor pollicis longus and flexor pollicis longus of the thumb," *J Appl Physiol,* vol. 54, pp. 714–719, 1983.

[9] M. Solomonow, A. Guzzi, R. Baratta, H. Shoji, and R. D'Ambrosia, "EMG-force model of the elbows antagonistic muscle pair," *Am. J. Phys. Med.,* vol. 65, pp. 223–244, 1986.

[10] E. A. Clancy and N. Hogan, "Relating agonist-antagonist electromyograms to joint torque during isometric, quasi-isotonic, non-fatiguing contractions," *IEEE Trans. Biomed. Eng.,* vol. 44, pp. 1024–1028, 1997.

[11] D. G. Thelen, A. B. Schultz, S. D. Fassois, and J. A. Ashton-Miller, "Identification of dynamic myoelectric signal-to-force models during isometric lumber muscle contractions," *J. Biomech.,* vol. 27, pp. 907–919, 1994.

[12] N. Hogan and R. W. Mann, "Myoelectric signal processing: Optimal estimation applied to electromyography—Part I: Derivation of the optimal myoprocessor," *IEEE Trans. Biomed. Eng.,* vol. 27, pp. 382–395, 1980.

[13] N. Hogan and R. W. Mann, "Myoelectric signal processing: Optimal estimation applied to electromyography—Part II: Experimental demonstration of optimal myoprocessor performance," *IEEE Trans. Biomed. Eng.,* vol. 27, pp. 396–410, 1980.

[14] M. I. A. Harba and P. A. Lynn, "Optimizing the acquisition and processing of surface electromyographic signals," *J. Biomech. Eng.,* vol. 3, pp. 100–106, 1981.

[15] E. A. Clancy and N. Hogan, "Single site electromyograph amplitude estimation," *IEEE Trans. Biomed. Eng.,* vol. 41, pp. 159–167, 1994.

[16] E. A. Clancy and N. Hogan, "Multiple site electromyograph amplitude estimation," *IEEE Trans. Biomed. Eng.,* vol. 42, pp. 203–211, 1995.

[17] J. R. Potvin and S. H. M. Brown, "Less is more: High pass filtering, to remove up to 99% of the surface EMG signal power, improves EMG-based biceps brachii muscle force estimates," *J. Electromyo. Kinesiol.,* vol. 14, pp. 389–399, 2004.

[18] D. Staudenmann, I. Kingma, A. Daffertshofer, D. F. Stegeman, and J. H. van Dieen, "Heterogeneity of muscle activation in relation to force direction: A multi-channel surface electromyography study on the triceps surae muscle," *J. Electromyo. Kinesiol.,* vol. 19, pp. 882–895, 2009.

[19] J. Hashemi, E. Morin, P. Mousavi, and K. Hashtrudi-Zaad, "Enhanced dynamic EMG-force estimation through calibration and PCI modeling," *IEEE Trans. Neural Sys. Rehabil. Eng.,* vol. 23, pp. 41–50, 2015.

[20] D. Staudenmann, I. Kingma, A. Daffertshofer, D. F. Stegeman, and J. H. Van Dieen, "Improving EMG-based muscle force estimation by using a high-density EMG grid and principal component analysis," *IEEE Trans. Neural Sys. Rehabil. Eng.,* vol. 53, pp. 712–719, 2006.

[21] D. Staudenmann, I. Kingma, D. F. Stegeman, and J. H. van Dieen, "Towards optimal multi-channel EMG electrode configurations in muscle force estimation: A high density EMG study," *J. Electromyo. Kinesiol.,* vol. 15, pp. 1–11, 2005.

[22] G. L. Gottlieb and G. C. Agarwal, "Dynamic relationship between isometric muscle tension and the electromyogram in man," *J Appl Physiol,* vol. 30, pp. 345–351, 1971.

[23] T. D. Sanger, "Bayesian filtering of myoelectric signals," *J. Neurophysiol.,* vol. 97, pp. 1839–1845, 2007.

[24] J. Hashemi, E. Morin, P. Mousavi, K. Mountjoy, and K. Hashtrudi-Zaad, "EMG-force modeling using parallel cascade identification," *J Electromyogr Kinesiol,* vol. 22, pp. 469–477, 2012.

[25] A. L. Hof and J. Van den Berg, "EMG to force processing I: An electrical analogue of the Hill muscle model," *J. Biomech.,* vol. 14, pp. 747–758, 1981.

[26] E. P. Doheny, M. M. Lowery, D. P. FitzPatrick, and M. J. O'Malley, "Effect of elbow joint angle on force-EMG relationships in human elbow flexor and extensor muscles," *J Electromyogr Kinesiol,* vol. 18, pp. 760–770, 2008.

[27] J. Hashemi, E. Morin, P. Mousavi, and K. Hashtrudi-Zaad, "Surface EMG force modeling with joint angle based calibration," *J Electromyogr Kinesiol,* vol. 23, pp. 416–424, 2013.

[28] P. Liu, L. Liu, F. Martel, D. Rancourt, and E. A. Clancy, "Influence of joint angle on EMG-torque model during constant-posture quasi-constant-torque contractions," *J. Electromyo. Kinesiol.,* vol. 23, pp. 1020–1028, 2013.

[29] P. Liu, L. Liu, and E. A. Clancy, "Influence of joint angle on EMG-torque model during constant-posture, torque-varying contractions," *IEEE Trans. Neural Sys. Rehabil. Eng.,* vol. 23, pp. 1039–1046, 2015.

[30] E. A. Clancy, O. Bida, and D. Rancourt, "Influence of advanced electromyogram (EMG) amplitude processors on EMG-to-torque estimation during constant-posture, force-varying contractions," *J. Biomech.,* vol. 39, pp. 2690–2698, 2006.

[31] E. A. Clancy, L. Liu, P. Liu, and D. V. Moyer, "Identification of constant-posture EMG-torque relationship about the elbow using nonlinear dynamic models," *IEEE Trans. Biomed. Eng.,* vol. 59, pp. 205–212, 2012.

[32] R. W. Mann and S. D. Reimers, "Kinesthetic sensing for the EMG controlled "Boston Arm"," *IEEE Trans. Man-Mach. Sys.,* vol. 11, pp. 110–115, 1970.

[33] P. Parker, K. Englehart, and B. Hudgins, "Myoelectric signal processing for control of powered limb prostheses," *J. Electromyo. Kinesiol.,* vol. 16, pp. 541–548, 2006.

[34] C. A. M. Doorenbosch and J. Harlaar, "A clinically applicable EMG-force model to quantify active stabilization of the knee after a lesion of the anterior cruciate ligament," *Clin. Biomech.,* vol. 18, pp. 142–149, 2003.

[35] C. Disselhorst-Klug, T. Schmitz-Rode, and G. Rau, "Surface electromyography and muscle force: Limits in sEMG-force relationship and new approaches for applications," *Clin. Biomech.,* vol. 24, pp. 225–235, 2009.

[36] S. Kumar and A. Mital, *Electromyography in Ergonomics*. Briston, PA: Taylor & Francis, 1996.

[37] G. M. Hagg, B. Melin, and R. Kadefors, "Applications in ergonomics," in *Electromyography: Physiology, Engineering, and Noninvasive Applications*, R. Merletti and P. A. Parker, Eds., ed: IEEE Press/Wiley-Interscience, 2004, pp. 343–363.

[38] B. Hudgins, P. Parker, and R. N. Scott, "A new strategy for multifunction myoelectric control," *IEEE Trans. Biomed. Eng.,* vol. 40, pp. 82–94, 1993.

[39] S. Micera, J. Carpaneto, and S. Raspopovic, "Control of hand prostheses using peripheral information," *IEEE Rev. Biomed. Eng.,* vol. 3, pp. 48–68, 2010.

[40] J. L. Nielsen, S. Holmgaard, N. Jiang, K. B. Englehart, D. Farina, and P. Parker, "Simultaneous and proportional force estimation for multifunction myoelectric prostheses using mirrored bilateral training," *IEEE Trans. Biomed. Eng.,* vol. 58, pp. 681–688, 2011.

[41] E. N. Kamavuako, K. B. Englehart, W. Jensen, and D. Farina, "Simultaneous and proportional force estimation in multiple degrees of freedom from intramuscular EMG," *IEEE Trans. Biomed. Eng.,* vol. 59, pp. 1804–1807, 2012.

[42] N. Jiang, J. L. G. Vest-Nielsen, S. Muceli, and D. Farina, "EMG-based simultaneous and proportional estimation of wrist/hand kinematics in uni-lateral trans-radial amputees," *J. NeuroEng. Rehabil.,* vol. 9:42, 2012.

[43] N. Jiang, S. Muceli, B. Graimann, and D. Farina, "Effect of arm position on the prediction of kinematics from EMG in amputees," *Med. Biol. Eng. Comput.,* vol. 51, pp. 143–151, 2013.

[44] A. Ameri, E. J. Scheme, E. N. Kamavuako, K. B. Englehart, and P. A. Parker, "Real-time, simultaneous myoelectric control using force and position-based training paradigms," *IEEE Trans. Biomed. Eng.,* vol. 61, pp. 279–287, 2014.

[45] A. Ameri, E. N. Kamavuako, E. J. Scheme, K. B. Englehart, and P. Parker, "Support vector regression for improved real-time, simultaneous myoelectric control," *IEEE Trans. Neural Sys. Rehabil. Eng.,* vol. 22, pp. 1198–1209, 2014.

[46] A. W. English, S. L. Wolf, and R. L. Segal, "Compartmentalization of muscles and their motor nuclei: The partitioning hypothesis," *Phys. Ther.,* vol. 73, pp. 857–867, 1993.

[47] A.-T. Liu, B.-L. Liu, L.-X. Lu, G. Chen, D.-Z. Yu, L. Zhu*, et al.*, "Architectural properties of the neuromuscular compartments in selected forearm skeletal muscles," *J. Anat.,* vol. 225, pp. 12–18, 2014.

[48] U. Windhorst, T. M. Hamm, and D. G. Stuart, "On the function of muscle and reflex partitioning," *Behav. Brain Sci.,* vol. 12, pp. 629–645, 1989.

[49] L. Ljung, *System Identification: Theory for the User*. Upper Saddle River, NJ: Prentice-Hall, 1999, pp. 491–519.

[50] S. Muceli and D. Farina, "Simultaneous and proportional estimation of hand kinematics from EMG during mirrored movements at multiple degrees-of-freedom," *IEEE Trans. Neural Sys. Rehabil. Eng.,* vol. 20, pp. 371–378, 2012.

[51] E. A. Clancy, "Electromyogram amplitude estimation with adaptive smoothing window length," *IEEE Trans. Biomed. Eng.,* vol. 46, pp. 717–729, 1999.

[52] E. A. Clancy and K. A. Farry, "Adaptive whitening of the electromyogram to improve amplitude estimation," *IEEE Trans. Biomed. Eng.,* vol. 47, pp. 709–719, 2000.

[53] P. Prakash, C. A. Salini, J. A. Tranquilli, D. R. Brown, and E. A. Clancy, "Adaptive whitening in electromyogram amplitude estimation for epoch-based applications," *IEEE Trans. Biomed. Eng.,* vol. 52, pp. 331–334, 2005.

[54] J. S. Bendat and A. G. Piersol, *Random Data: Analysis and Measurement Procedures*. New York: John Wiley and Sons, Inc., 1971, pp. 277–281.

[55] L. Liu, P. Liu, E. A. Clancy, E. Scheme, and K. B. Englehart, "Electromyogram whitening for improved classification accuracy in upper limb prosthesis control," *IEEE Trans. Neural Sys. Rehabil. Eng.,* vol. 21, pp. 767–774, 2013.

[56] K. Koirala, M. Dasog, P. Liu, and E. A. Clancy, "Using the electromyogram to anticipate torques about the elbow," *IEEE Trans. Neural Sys. Rehabil. Eng.,* vol. 23, pp. 396–402, 2015.

[57] W. H. Press, B. P. Flannery, S. A. Teukolsky, and W. T. Vetterling, *Numerical Recipies in C*, 2nd ed. New York: Cambridge Univ. Press, 1994, pp. 671–681.

[58] I. Miller and J. E. Freund, in *Probability and Statistics for Engineers, 2nd edition*, ed: Prentice-Hall, Inc., 1977, pp. 272–275.

[59] B. A. Lock, K. Englehart, and B. Hudgins, "Real-time myoelectric control in a virtual environment to relate usability vs. accuracy," in *Myoelectric Controls/Powered Prosthetics Symposium*, New Brunswick, Canada, 2005.

[60] L. Hargrove, Y. Losier, B. Lock, K. Englehart, and B. Hudgins, "A real-time pattern recognition based myoelectric control usability study implemented in a virtual environment," in *29th IEEE Eng. Med. Biol. Conf.*, 2007.

[61] N. Jiang, I. Vujaklija, H. Rehbaum, B. Graimann, and D. Farina, "Is accurate mapping of EMG signals on kinematics needed for precise online myoelectric control?," *IEEE Trans. Neural Sys. Rehabil. Eng.,* vol. 22, pp. 549–558, 2014.

Appendix 1: Test Setup Validation

A-1.1 Electrode Amplifier

A briefer version of this appendix appeared as Appendix 2 in: Jennifer Keating, "Relating forearm muscle electrical activity to finger forces," M.S. thesis, Worcester Polytechnic Institute, Worcester, MA, May 2014, pp. 85-89

A-1.1.1 Executive Summary

The circuitry of the electrodes was tested at different stages during the manufacturing process: At the initial stage before soldering conductors, after soldering conductors, after pouring the epoxy, after connecting to male DB9 connectors, and after connecting male DB9 to female DB9-RJ45 assembly cable.

All signals were observed as expected, with no additive noise. The following sections detail the electrode design, the testing of the electrodes and the testing of the DB9 and RJ45 connector.

A-1.1.2 Electrode Design

Before describing the methodology used to validate test results, below is the circuit that the electrodes are made of.

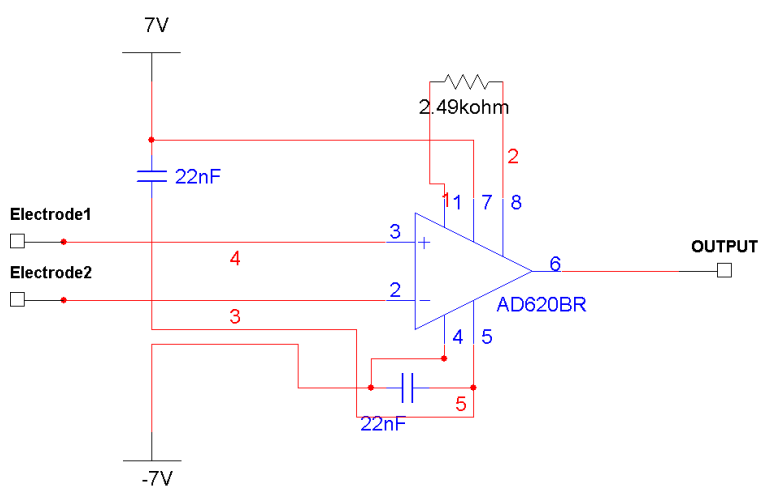

Fig. A-1. 1. Electrode circuitry

Fig. A-1.1 shows the electrical schematic for the electrode-amplifier. The circuit is built around an instrumentation amplifier, in this case the AD620 (Analog Devices, Norwood, MA). The 2.49 kOhm resistor sets the differential gain to 20. The two capacitors serve as decoupling capacitors for the IC voltage supply. As such, the capacitors should be placed as physically close to the IC as possible. Full discussion of the electrical schematic is available in MQP student project by Salini et al.2003]. Electrodes form the input to AD620 instrumentation amplifier with power-line decoupling capacitors. The circuit is supplied by +/- 7 V DC and the output is taken at terminal 6. Ultra-Flex wire is used to connect the circuit to DB9. These ultra-flex wire contains four different colored wires (Red, Green, White and Black), and 5 mils PVC insulated Ultraminiature conductors sandwiched inside a tinned copper braided shield. The whole assembly is covered with a flexible PVC jacket, as shown in Fig. A-1.2.

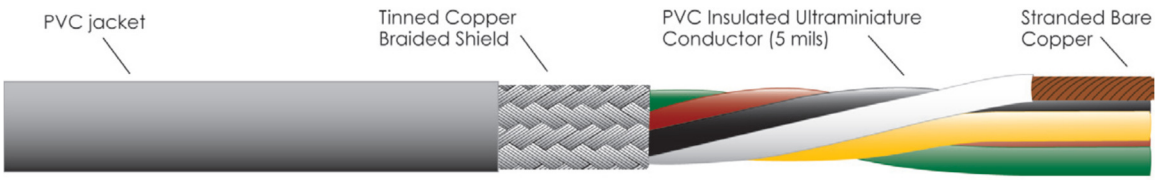

Fig. A-1. 2. Ultra-flex cable configuration

The red and green conductors are used for +7V and -7V, respectively, while the white and black conducts are for the output and ground, respectively.

The full assembly can be seen below in Fig. A-1.3.

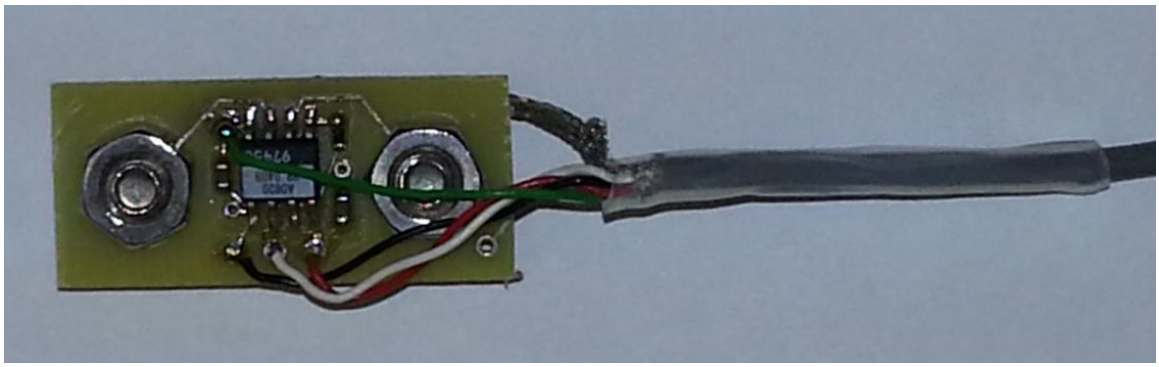

Fig. A-1. 3. PCB with electronic components, electrode assemblies, and ultra-flex cable

A-1.1.3 Electrode Manufacturing

Fig. A-1.4 shows the top and bottom layers of the PCB. The 8-pin AD620 IC is placed towards the center of the PCB, between the two electrode pads. The space shown in white inside the two electrode shells is a through hole in which the screw electrodes are passed. Incoming wire connections (positive voltage, negative voltage, reference voltage) and the outgoing wire connection (output signal) are soldered directly to the labeled pad. The bottom layer of the PCB much of it form a shield. The shield wire is soldered directly to the location specified.

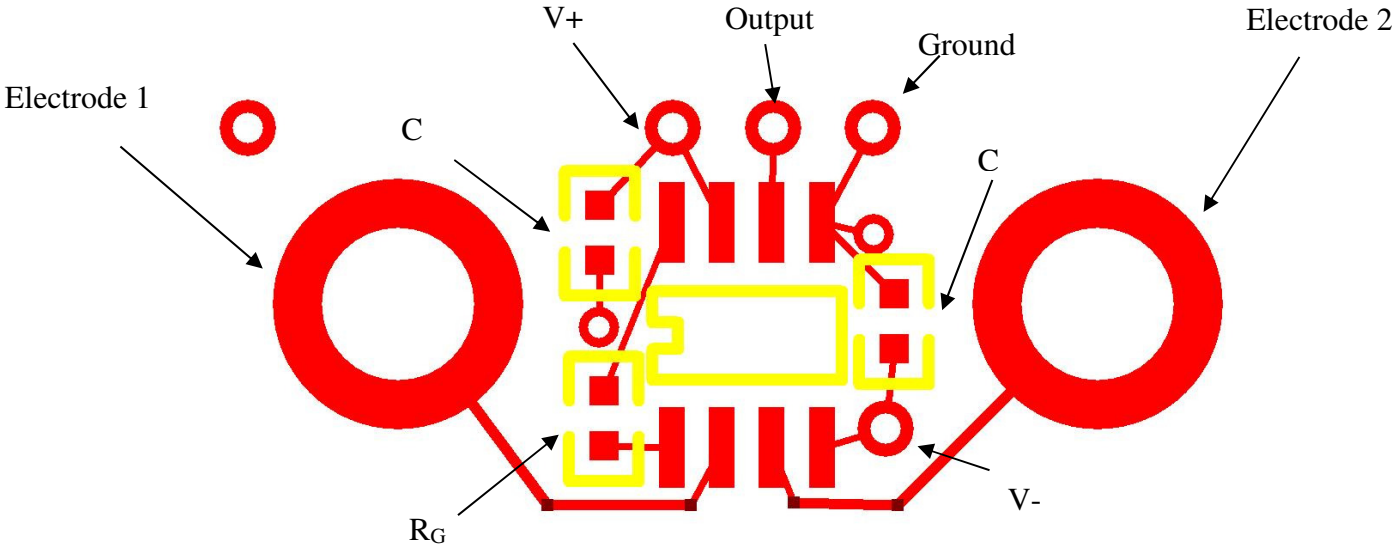

(a) Top

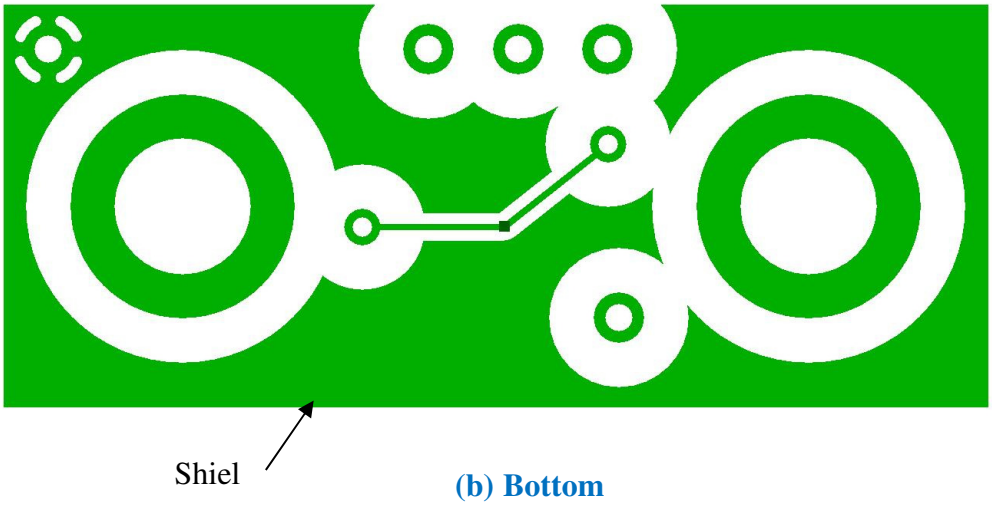

(b) Bottom

Fig. A-1. 4. PCB top and bottom copper layers

A-1.1.4 Materials:

- (2) Screws Stainless Steel M4x6MM (MX-M04/06P-C)

  Manufacturer: Small Parts Inc., www.smallparts.com

- (2) Hex nuts M4-.70 Stainless Steel (H#880794)

  Manufacturer: The Hillman Group Inc.., www.hillmangroupt.com

  Supplier: Lowes, www.lowes.com

- (2) Lock washers (#8 Stainless steel lock washer, internal tooth SAE)

  Manufacturer: Crown Bolt Inc., www.crownbolt.com

  Supplier: Home Depot, www.homedepot.com

- Printed circuit board

  Manufacturer: ExpressPCB, www.expresspcb.com

- 2.49kΩ resistor, ±1%, 1/16W, (ERJ-3EKF2491V)

  Manufacturer: Panasonic, www.panasonic.com

  Supplier: Digi-key, www.digi-key.com (P2.49KHCT-ND)

- (2) 2.2nF Capacitors, ±5%, (C1608C0G1H222J)

  Manufacturer: TDK Corporation, www.component.tdk.com

  Supplier: Digi-key, www.digi-key.com (445-1297-1-ND)

- AD620BR Instrumentation Amplifier

  Manufacturer: Analog Devices, www.analog.com

- 3 Feet of Ultra-flex cable (NMUF4/30-4046 SJ)

  Manufacturer: Cooner -Wire, Inc., www.coonerwire.com

- 2 cm of heat-shrink tubing (FP-301 1/8"CR500')

  Manufacturer: 3M/ESM, www.mmm.com/esm/

  Supplier: Digi-key, www.digi-key.com (FP018C-5-ND)

- (1/3) Package of Acrylic Epoxy (DP-460 Epoxy) or (DP-420 Epoxy), Duo-Pak Cartridge, Off-White

  Manufacturer: 3M, www.mmm.com

  Supplier: McMaster-Carr, www.mcmaster-carr.com (7467A26) or (7467A25)

- EPX Plus II Applicator Gun, 1.3 to 1.7 oz

  Manufacturer: 3M, www.mmm.com

  Supplier: McMaster-Carr, www.mcmaster-carr.com (7467A43)

- Mixer Nozzle for 1.3 to 1.7 oz 3M Adhesive Duo-Pak Cartridge, 2:1 Mix Ratio

  Manufacturer: 3M, www.mmm.com

Supplier: ***McMaster-Carr, www.mcmaster-carr.com (7467A12)***

- Metal Solder cup DB9 connector Male and Female

  Manufacturer: ***Jameco Valuepro, www.jameco.com***

  Supplier: ***Jameco, www.jameco.com (15748, 15771)***

- Hood, D-Sub Plastic, 9pin, Plastic Hood with Strain Relief (Gray)

  Manufacturer: ***Jameco Valuepro, www.jameco.com***

  Supplier: ***Jameco, www.jameco.com (15722)***

- Cat 5e Network Crossover Cable

  Manufacturer: ***Jameco Valuepro, www.jameco.com***

  Supplier: ***Jameco, www.jameco.com (302041)***

- Green Silicon Rubber Mold Making material, V-1065/Hi-Pro Green

  Manufacturer and Supplier: Freeman Manufacturing and Supply Co. , www.freemansupply.com (055211)

- Plywood

  Manufacturer and Supplier: Freeman Manufacturing and Supply Co. , www.freemansupply.com

A-1.1.5 Tools and Equipment:

- Soldering iron
- Solder
- Super glue
- Package molding
- Scotch Tape
- X-acto knife
- Wire Stripper
- Match
- Machine Saw
- Fine Sandpaper
- Tweezers
- Cutter
- Multi-position vise
- Heat gun
- Magnifier
- Vacuum Chamber

A-1.1.6 Work Instructions:

Step 1: Design PCB board using Express PCB software

Express PCB is free software that is available from www.expresspcb.com . It allows users to design their prototype, perform area optimization, estimate manufacturing cost and order online. After reading the Quick Start Guide from ExpressPCB software, design Fig. A-1.1 circuitry. See Fig. A-1.2 for final Layout. After completing the design, proceed with the order.

Step 2: Gather materials: Some materials may be unavailable thru the years. Use item's description to search for the correct product. For example, if screws are not available from the Smallparts, Inc. site, use their description to search the item in other sites such as McMaster carr.

Step 3: Solder components on PCB (Fig. A-1.5.)
After receiving the board and the materials, solder the AD620 amplifier on the PCB first. Then, proceed with soldering the capacitors (their orientation does not matter) and resistor. Use Fig. A-1.4. to assure components are soldered to the correct pads. Verify soldering quality under the magnifier. Re-solder as necessary. Pay close attention not to short certain paths or overheat the components, as doing so can cause circuit malfunction.

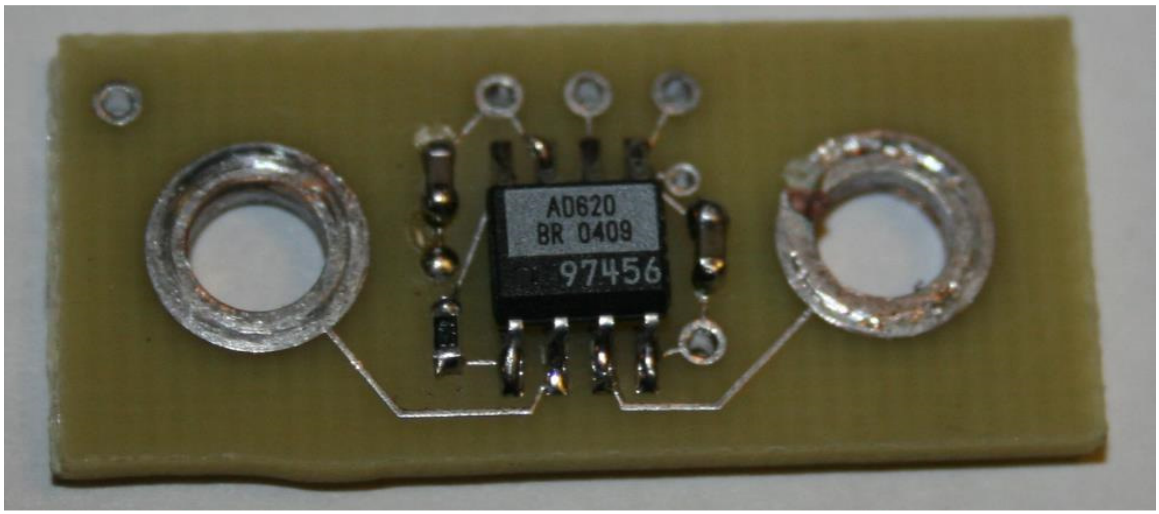

Fig. A-1. 5. PCB with resistor, capacitors and AD 620

Step 4: Place the washers on the screw shaft and screw them into the board. Screw on the nuts on the reverse side of the board. Be sure to have the connection as secure as possible by tightening the nut as much as possible. Also a tiny amount of super glue applied to where the screw shaft protrudes from the nut can help prevent the assembly from loosening. (Fig. A-1.6)

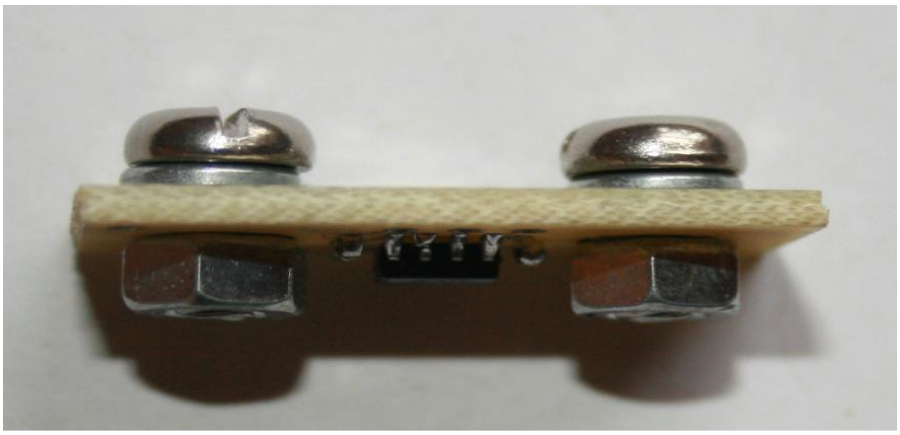

Fig. A-1. 6. PCB with electronics, screws, nuts, and washers (electronics on hidden surface)

Step 5: Manufacture the green rubber mold

Using plywood and following dimension from Fig. A-1.5, make the model. Then, assemble plywood blocks and the models as shown in Fig. A-1.7 (clamps excluded for clarity). Mix V-1065 and Hi-Pro Green using Freeman Manufacturing recommended ratio. De-air the mix in a vacuum chamber to remove any bubbles from the mix giving a nice and smooth finish for the mold. Pour the mix into the assembly and wait overnight. Fig. A-1.8 Shows the outcome of the green rubber mold.

Fig. A-1. 7. Model with plywood side walls

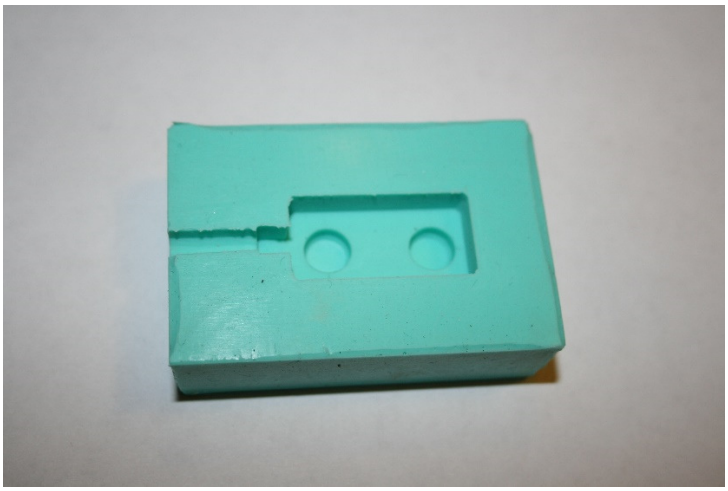

Fig. A-1. 8. Green Rubber Mold

Step 6: Obtain 5ft Ultra-Flex wire.

Ultra-Flex wires contain four different color (Red, Green, White and Black) 5 mils PVC insulated Ultraminiature conductors sandwiched inside a tinned copper braided shield and the whole assembly is covered with a flexible PVC jacket, as shown in Fig. A-1.10.

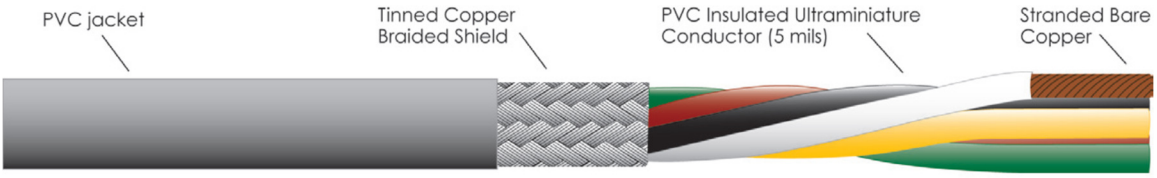

Fig. A-1. 9. Ultra-Flex wire

Step 7: From each edge of the cable mark 1”–1.5” . Remove the PVC jacket from this section using either a wire stripper or by heating with match fire and removing quickly by hand.

Step 8: Using a X-Acto knife, cut off a small area on the shield. Be careful not to cut so deep that you damage the Ultraminiature wires.

Step 9: Using sharp edge tweezers, extract each wire from the cut area. Pay close attention not to damage the shield or the wires.

Step 10: Strip 2 mm from the end of each Ultraminiature cable by pressing on the PVC insulation with a finger nail and pulling out.

Step 11: Solder the conductors of the Ultra-flex wire to the PCB. The green conductor is ground/reference, red is positive power, black is negative power, and white is output. Solder the tinned copper braided shield to the backside of the PCB. Place the wire-soldered assembly inside the rubber mold and check the position of the wires compared to the top part of the mold. Adjust the length of the conductors so that they sit tight inside the mold. Apply small amounts of super glue, as necessary, to adhere the wires to the PCB to relieve stress from the wires and hold them in place.

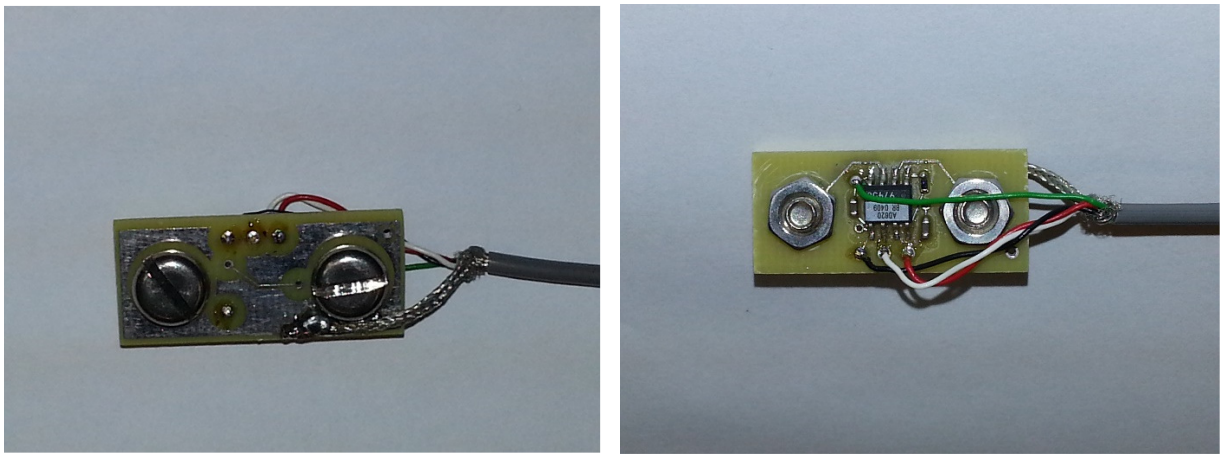

Fig. A-1. 10. PCB with electronic components, electrode assemblies, and ultra-flex cable Bottom (left) and Top (right) side view

Step 12: Slide approximately 2cm of heat-shrink tubing over the cable and shrink the tubing using a heat gun so it is tight to the cable as close to the PCB as possible (Fig. A-1.11)

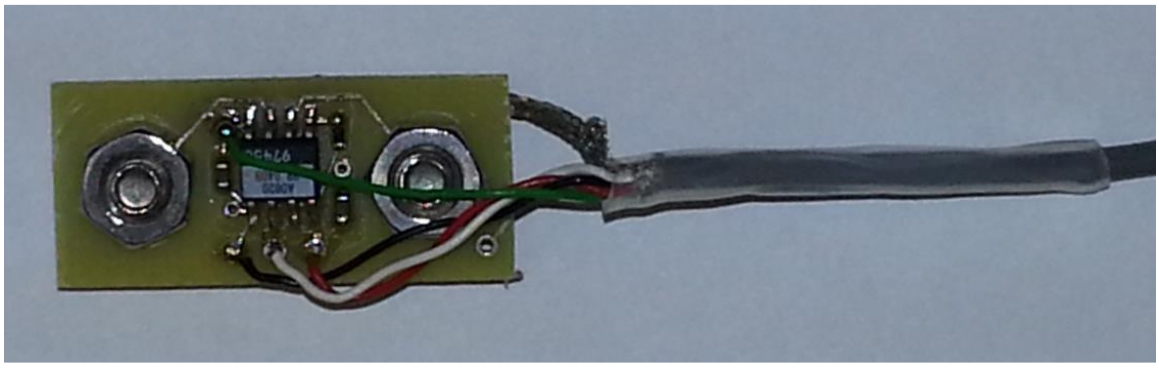

Fig. A-1. 11. Heat-shrink tubing added over cable

Step 13: Test the Soldered PCB

- Connect the red conductor on the other end of the cable (away from the PCB) to +7V DC
- Connect the green conductor on the other end of the cable to –7V DC
- Connect the white conductor to the oscilloscope.
- Use the signal generator to generate a sinusoid signal with 80 Hz and 150 mV_{PP}.
- Input the generated signal to the circuit by placing the probes on each of the tightened screws or nuts.
- Observe the output signal on the oscilloscope. You should expect to view magnified sinusoid signal with amplitude around 6 V_{PP} and the same frequency.
- Change the input signal amplitude and frequency and verify the response of the circuit.
- If the output signal is not magnified or results in different shapes, verify your work i.e. connectors, solder, components, wires.
- Fix as necessary until you get the desired response.

Step 14: Place the DP460 or DP420 cartridge inside the applicator gun as shown in Fig. A-1.12. Open the cartridge gap and engage the 2:1 mixer nozzle.

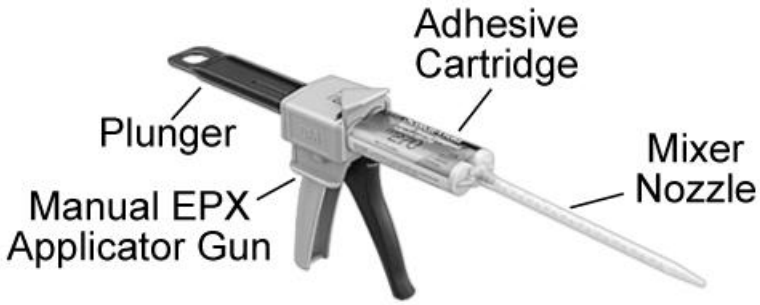

Fig. A-1. 12. DP460 or DP420 Applicator Gun

Step 15: Pour a thin layer of 3M DP-460 or DP-420 epoxy into the bottom of the mold (Fig. A-1.13)

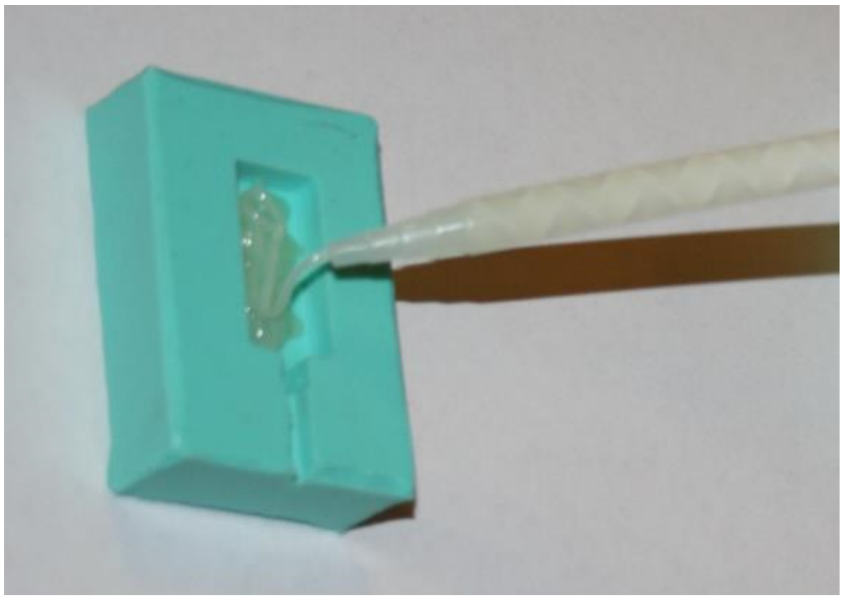

Fig. A-1. 13. Filling the base layer of epoxy in mold

Step 16: Immediately place the electrode amplifier assembly in the mold and press down gently so the screws fit into their holes. The cable should extend out of the mold resting in the slit cut inside the mold. Apply a thin piece of tape over the cable to close the slit so no epoxy can leak out during the curing process. (Fig. A-1.14)

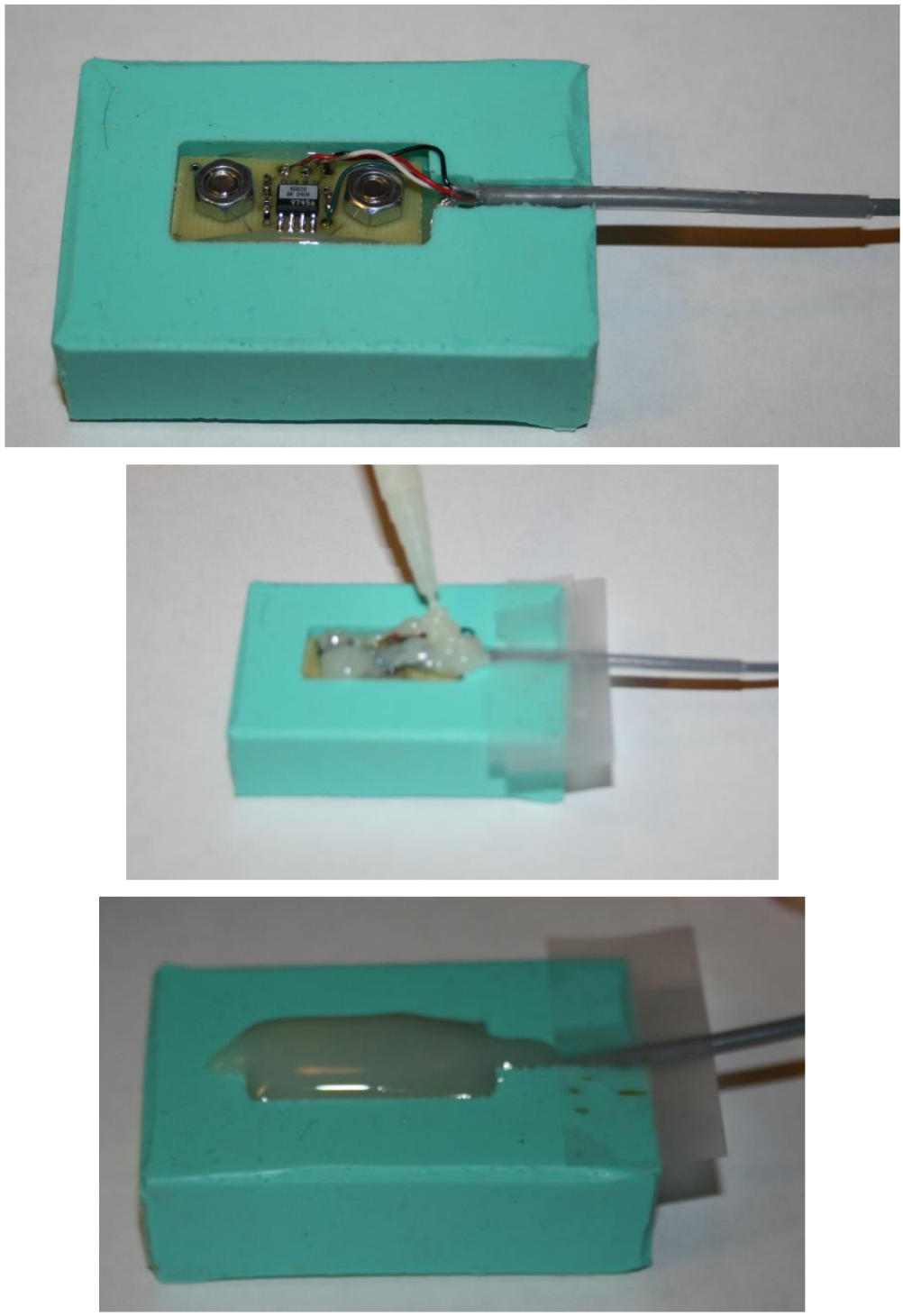

Fig. A-1. 14. Placing the PCB into the mold and pouring the epoxy

Step 17: Completely fill the mold with the remaining epoxy and allow at least 3 hours for curing.

Step 18: Remove the package from the mold. Sand the top of the package to achieve a perfectly flat surface. Lastly use a X-acto knife to remove any epoxy from the surface of the screws (Fig. A-1.15).

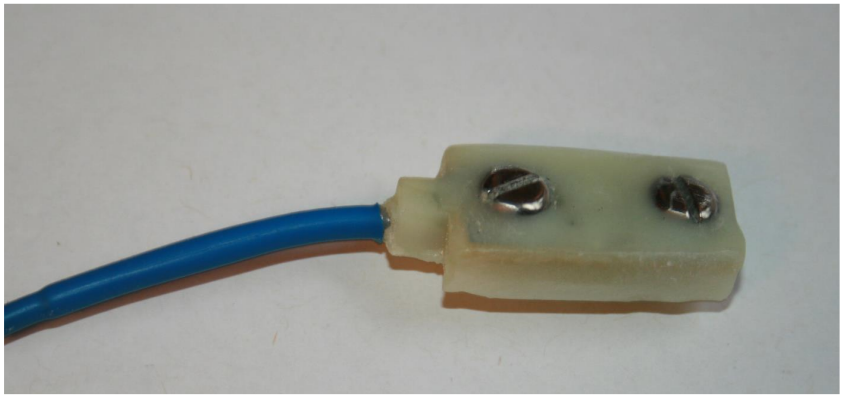

Fig. A-1. 15. Final product after sanding

Step 19: Apply any finishing required (such as spray paint or further sanding).

Step 20: Repeat step 13 and verify the result. If the response has changed, start all over from step 3.

Step 21: Slide approximately 2cm of heat-shrink tubing over each of the Ultraminiature conductors at the far end of the cable (away from the PCB). Solder the wires to a DB9 female connector following the diagram below (Fig. A-1.16). Slide the heat shrink tubing over the soldered junctions and shrink the tubing using a heat gun so that it is well insulated from the adjacent junctions. Secure all the wires in the plastic housing.

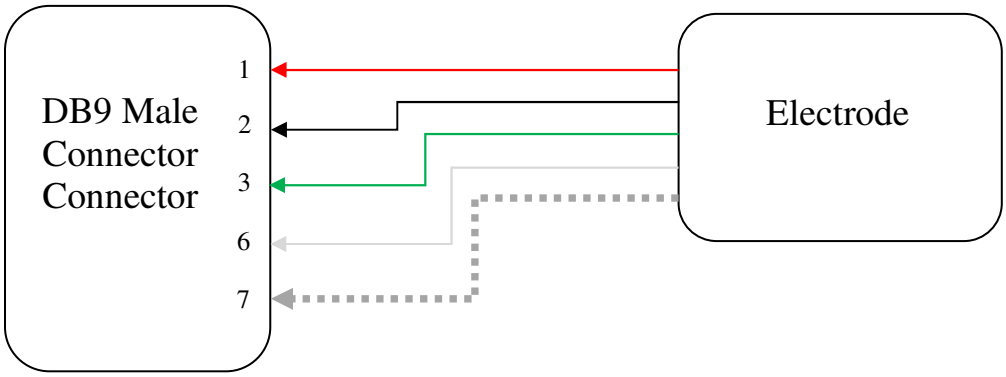

Fig. A-1. 16. Electrode-DB9 wiring diagram

A-1.1.7 Testing the Soldered PCB

The following steps were taken to test the soldered PCB before continuing with connecting the electrodes to the rest of the assembly.

- Connect the red conductor on the other end of the cable (away from the PCB) to +7V DC
- Connect the green conductor on the other end of the cable to –7V DC
- Connect the white conductor to the oscilloscope.
- Use the signal generator to generate a sinusoid signal with 80 Hz and 150 mV_{PP}.
- Input the generated signal to the circuit by placing the probes on each of the tightened screws or nuts.
- Observe the output signal on the oscilloscope.
    - The result should be a magnified sinusoid signal with amplitude around 6 V_{PP} and the same frequency as the input signal.
- Change the input signal amplitude and frequency and verify the response of the circuit.
- The output should be sinusoid signal as long the output V_{pp} is within the supply voltage range below +/- 7V and should get "chopped" signal when exceeds that range.

A-1.1.8 DB9 and RJ45 Connector Testing

Testing the circuit from DB9 and RJ45 connectors was completed by following the same test methodology described in *Section 5 – Testing the Soldered PCB* above. The only difference was that the oscilloscope connection was through the pins of DB9 and RJ45 instead of the ultra-flex wire conductors. These connections are shown in the wiring diagrams in Fig. A-1.17.

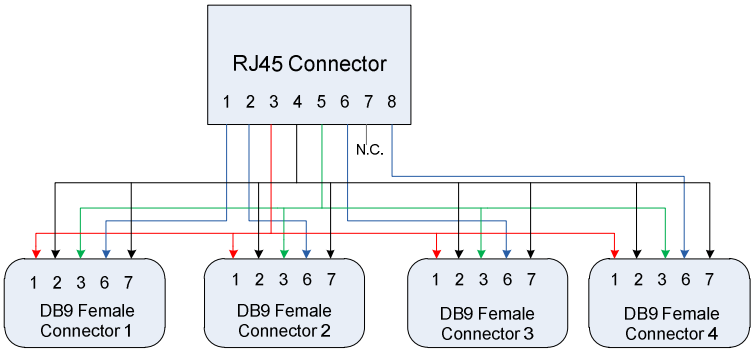

Fig. A-1.17. RJ45 to DB9 Female connector wiring Diagram

A-1.2 Bridge Amplifier

See: J. Keating and B. Bardizbanian, “Calibrating DMD-465WB Bridgesensor: AC Powered Signal Conditioner,” in Jennifer Keating, “Relating forearm muscle electrical activity to finger forces,” M.S. thesis, Worcester Polytechnic Institute, Worcester, MA, May 2014, pp. 103–121.

A-1.3 NI PCI 6229 DAQ Channels

See: Jennifer Keating, “Relating forearm muscle electrical activity to finger forces,” M.S. thesis, Worcester Polytechnic Institute, Worcester, MA, May 2014, pp. 109-121. My contributions to the NI PCI 6229 DAQ Channels appendix in Keating’s M.S. were: helping to understand the DAQ channels connections, the software and collecting all 32 waveform graphs.

A-1.4 Calibration for Finger and Grips LABVIEW VI

See: J. Keating and B. Bardizbanian, “Calibratiion (100%MVC) for Finger & Grips LabVIEW VI: Deseign & Troubleshooting Document,” in Jennifer Keating, “Relating forearm muscle electrical activity to finger forces,” M.S. thesis, Worcester Polytechnic Institute, Worcester, MA, May 2014, pp. 152–158.

An edited, reduced portion of this Appendix appears as Chapter 2. The full text is retained as this Appendix for future reference.

Appendix 2: Long-form EMG-finger paper

A-2.1 Introduction

Relating surface electromyogram (sEMG) activities of the forearm muscles to fingers have been the interest of many researchers. Existing commercially available myoelectric controlled prostheses provide extremely limited functionality to amputees, offering either discrete state recognition (open/close hand) or one degree of freedom of control and requiring multiple independent EMG control sites. [Parker et al., 2006]. Only a few studies of finger movement have begun to consider multi-finger proportional control via EMG-based estimation of finger forces [Castellini and van der Smagt, 2009; Smith et al., 2009].

Preliminary work by Liu et al. [P. Liu et al., 2011] showed promising results that electrical activity in the forearm may be used to estimate forces applied at the fingertips. Data were only successfully collected from four subjects and subjects only produced constant-posture, slowly force-varying contractions. It did not account for the influences of localized muscle fatigue, electrode movement and day-to-day variations. Spatial filters were used to derive EMG channels and an EMG-force model was generated to relate muscle activity to fingertip force via least squares estimation. The work indicated that multiple degrees of freedom of proportional control may be possible using EMG data collected from the forearm. Also, electrode arrays 64 channels were used. Some studies of finger movement have considered proportional control via EMG-based estimation of finger forces or joint angles.

Factors that influence the stability of EMG recordings include the presence of motor units/muscle tendons, the presence of other active muscles nearby, the distance

between the active muscle fiber and detection site, filtering properties of the electrode, and the location of innervation zones in relation to the recording electrodes. It is recommended that bipolar electrodes be positioned parallel to muscle fibers with a minimum spacing of 20 mm between centers of electrode poles. This placement is small enough to avoid most crosstalk, but large enough to allow selection from a pool of motor units.

Whitening of the sEMG using adaptive techniques has been shown to improve EMG amplitude estimation and to lower EMG-torque errors versus conventional whitening using linear filter. Clancy and al developed single site EMG model in additive noise and concluded the fact that increasing the additive noise level is one of the factors that diminishes the advantage of whiteninig. Also, suggested placing multiple electrodes on single muscle to increase quality of signal detection. Their study was manly implemented on bicep and tricep muscles and compared to theoretical models. Whitening on elbow and wrist hand studies were also implemented with varying degree of success. It is being used for elbow and multifinger studies. However, they were mainly used for constant posture limited number of electrodes and short duration.

The muscles of the forearm can be divided multiple groups including those responsible for moving the wrist, four fingers, and thumb, with the bulkiest portions of the muscles at the proximal forearm. These muscles are divided by fascia into the anterior flexors and posterior extensors, both of which have superficial and deep muscle layers. Most flexors are innervated by the median nerve while the extensors are innervated by the radial nerve. These muscles move fingers via their long tendons with the assistance of the small intrinsic muscles of the hand for more precise movement].

A study that mapped the innervation zones of forearm muscles demonstrated the difficulty of targeting electrode positions near innervation zones corresponding to specific muscles. Additionally, studies have shown that targeting specific muscles for pattern recognition control do not make improvements over evenly spacing electrodes around the forearm.

In this project A generalized electrode placement (equidistant spacing of electrodes mounted circumferentially) was used. Based on a conservative model of a female forearm, twelve surface EMG amplifiers were utilized on all subjects for consistency. Electrode 1 was always mounted on brachioradialis, followed by electrodes 2-6 mounted across the

anterior forearm muscles (flexor carpi ulnaris, flexor carpi digitorum superficialis) and electrodes 7-12 mounted across the posterior forearm muscles (extensor digitorum, extensor carpi radialis longus and brevis). System identification technique of regularizing the least squares fit (pseudoinverse approach) to improve the performance of EMG-torque modeling was studied for multi finger. In addition, three and four finger grip performance were analyzed. Finally, the pair of fingers with stable performance was suggested based on statistical modeling

A-2.2 Data Acquisition

A-2.2.1 EMG Signal

Fig. A-2.1 depicts the block diagram of EMG signal acquisition

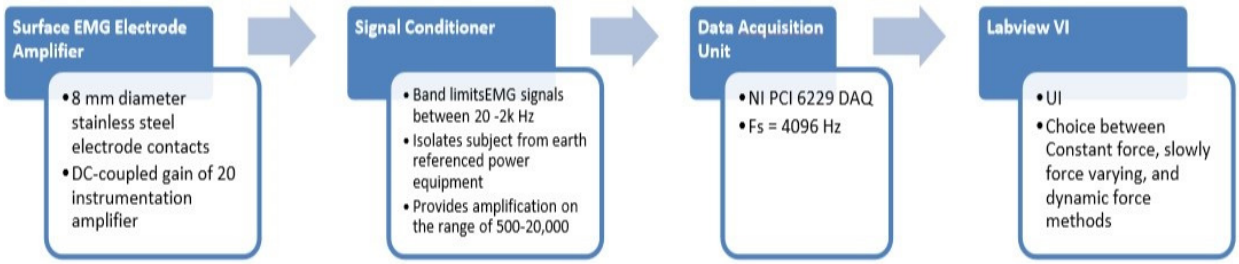

Fig. A-2. 1. EMG Signal Acquisition [Keating, 2014]

Bipolar three op amp instrumentation amplifiers 1.5 cm x 3 cm x 0.6 cm epoxy cast Stainless Steel electrodes (Fig. A-2.2) are used to acquire EMG signals from subject muscles. These electrodes are 8 mm in diameter and have Common Mode Rejection Ratio (CMRR) greater than 100 dB and gain of 20.

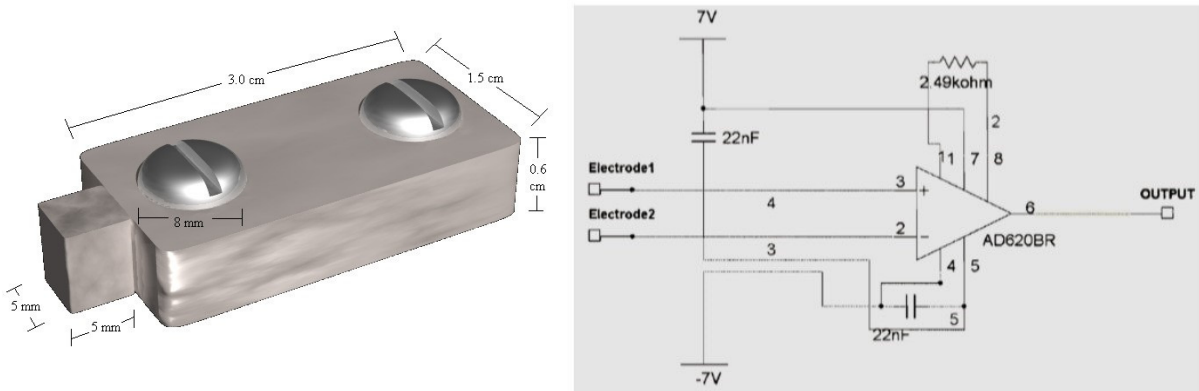

Fig. A-2. 2. Surface bipolar electrode-amplifier and its electrical circuit [Salini et al., 2003]

A signal conditioner then bandlimits the signals between 15 and 1800 Hz, isolates the subject from earth-referenced power, and amplifies EMG signals at gain from 200–25600. Shown below is the full signal conditioner circuit diagram (Fig. A-2.3).

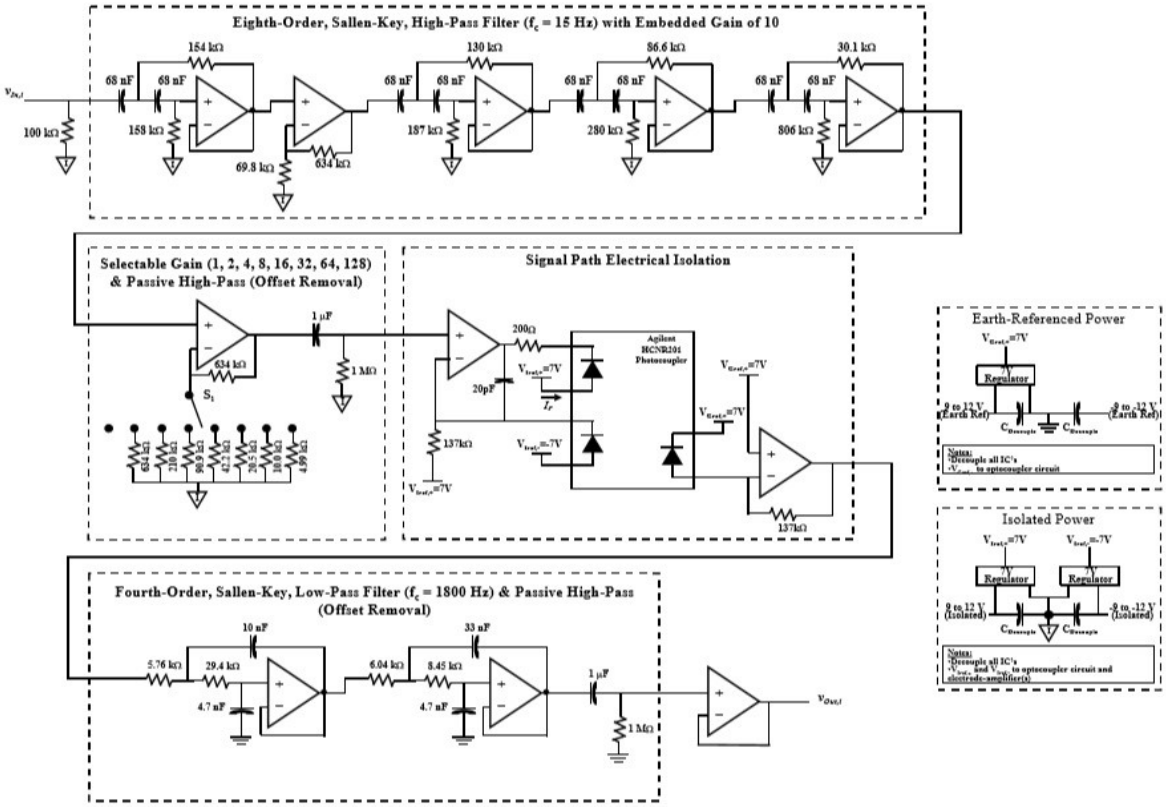

Fig. A-2. 3. Signal Conditioner circuit diagram [Clancy, 2013]

The raw EMG were then get digitized at 4096 Hz with 16-bit resolution (National Instruments NI-PCI 6229).

A-2.2.2 Force Signal

Fig. A-2.4 depicts the block diagram of Force signal acquisition

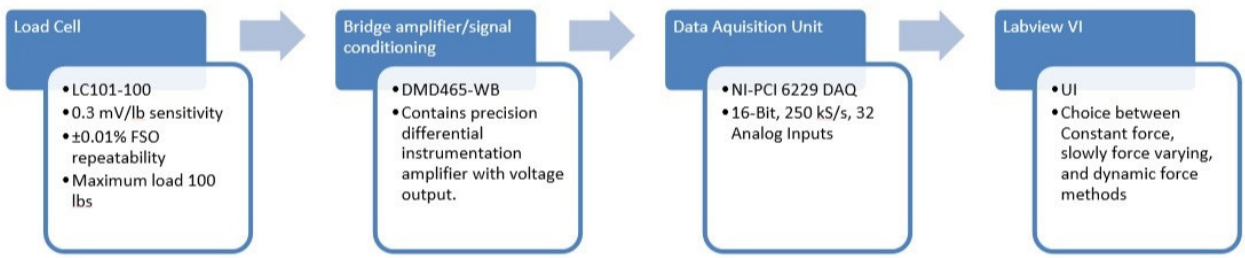

Fig. A-2. 4. Force Signal Acquisition [Keating, 2014]

A force transducer (LC101-100 load cell; Omega Engineering, Inc., Stamford, CT, USA) was used to obtain flexion and extension forces of the fingers and grips. The load cell produces output signals on a mV scale (0.3 mV/lb up to 30 mV maximum). A bridge amplifier/signal conditioner module (DMD465-WB; Omega Engineering, Inc., Stamford, CT, USA) (Fig. A-2.5) was used to amplify the signal to a +5 to -5 Volt scale and filter background noise. The force channel was acquired at a sampling rate of 4096 Hz (16-bit resolution) by the DAQ for various lengths of time (based on the test type) defined by the VI.

Fig. A-2. 5. Bridge Amplifier

A-2.3 Subject Interface

The overall subject interface for this study consisted of 12 surface EMG electrode amplifiers, a hand/finger restraint device, and various LabVIEW interfaces used for both collecting data and providing the user with an interface for each type of contraction trial conducted during testing (constant force, slowly force varying, and dynamic force varying muscular contractions). (Fig. A-2.6).

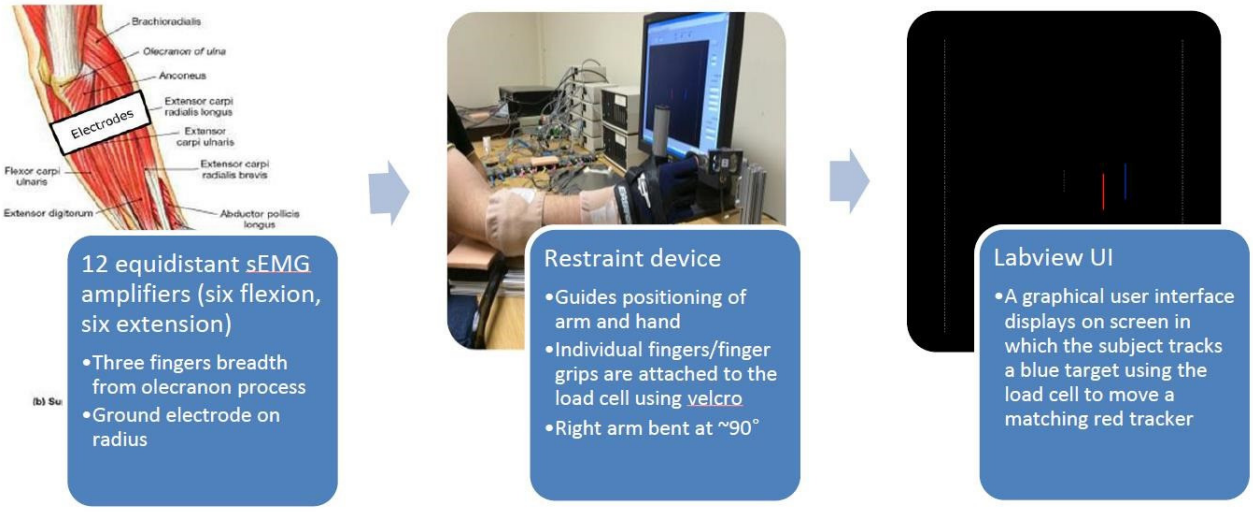

Fig. A-2. 6. Diagram of subject interface study [Keating, 2014]

A-2.3.1 Surface EMG Amplifier Placement

Based on a conservative model of a female forearm, twelve surface EMG amplifiers were used on all subjects for consistency. Electrode 1 was always mounted on brachioradialis, followed by electrodes 2-6 mounted across the anterior forearm muscles (flexor carpi ulnaris, flexor carpi digitorum superficialis) and electrodes 7-12 mounted across the posterior forearm muscles (extensor digitorum, extensor carpi radialis longus and brevis). First, each subject's wrist perimeter was measured. This distance was subtracted from (12x1.5) and then divided by 12 to calculate the distance between the electrodes. On a medical tape, the width and the calculated distance was marked and the 12 electrodes was adhered to the tape. To prepare the subject's forearm for electrode placement, it was first scrubbed with an alcohol wipe and then lubricated with conductive gel (Spectra 360 Electrode Gel; Parker Laboratories, Inc., Fairfield, NJ) so that it is absorbed into the stratum mucosum (germinativum) to make contact with derma(Fig. A-2.6-7), where it can serve to decrease the recording resistance through the skin. This is termed electrode-electrolyte interface. Then, the prepared surface EMG electrodes were mounted circumferentially around the forearm, parallel to muscle fibers (Fig. A-2.8). The proximal edge of each surface electrode was mounted three fingers breadth from the antecubital with a wrist-band reference electrode attached to the distal head of the radius [Perotto, 1994]. The minimum distance between the centers of the electrode contacts for the study was 2.66 cm. Electrodes were secured to the arm using ace bandages and medical tape. The outputs of each electrode amplifier were then further amplified and filtered between 15-1800 Hz.

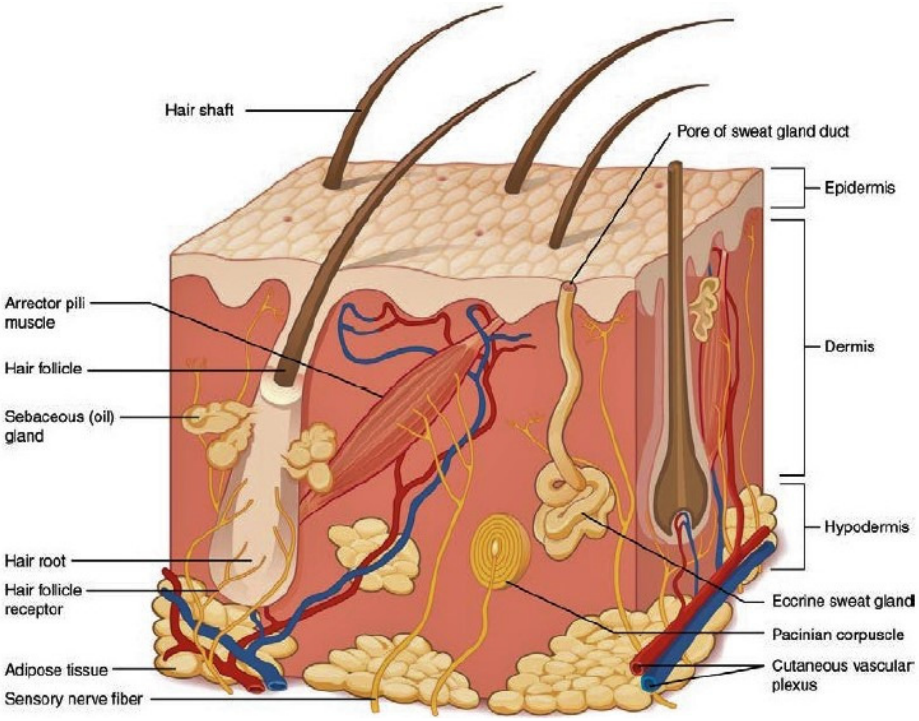

Fig. A-2. 7. Layers of Skin [Betts, 2017]

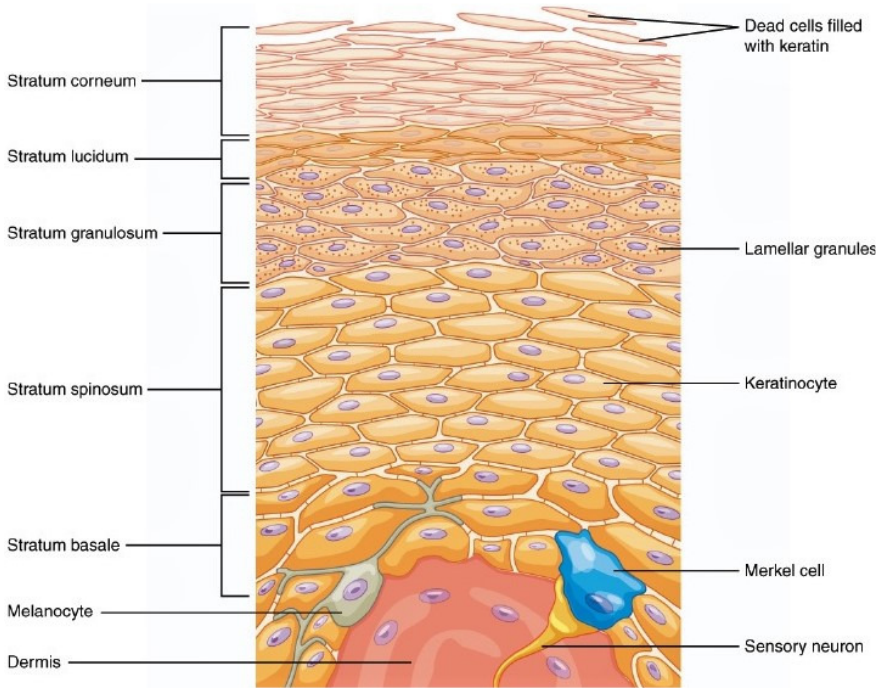

Fig. A-2. 8. Layers of Epidermis [Betts, 2017]

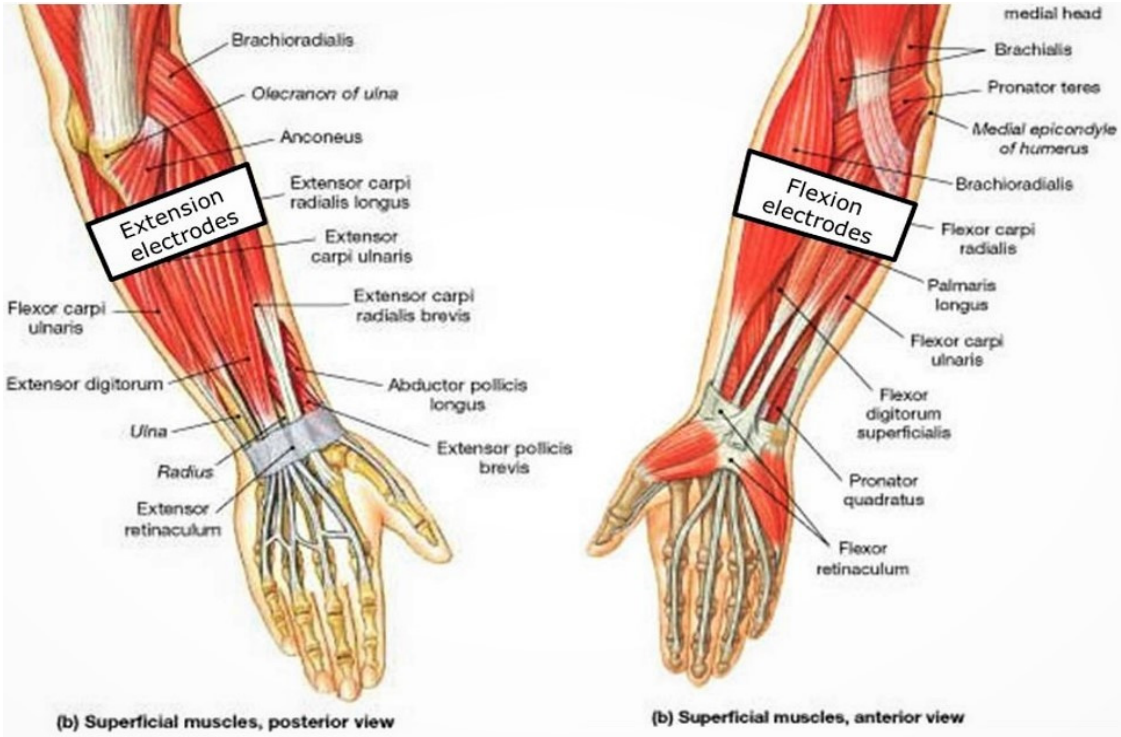

Fig. A-2. 9. Diagram of flexion and extension electrode placement with respect to forearm muscles [Marieb, 2013]

A-2.3.2 Finger Restraint Apparatus

To facilitate constant-posture finger flexion and extension trials a restraint device was used to ensure proper alignment and angular positioning of the subject's forearm throughout testing. This device was a modification of the restraint device used in previous testing by Liu et al. (2011).

The apparatus consisted of a rectangular base built using modular framing (10 Series Profiles, 80/20 Inc., Columbia City, IN, USA) in combination with a one degree of freedom LC101-1003 load cell (Omega Engineering, Inc., Stamford, CT, USA), and load cell attachments for use with individual fingers, four finger grip and three finger grip . Extensions from the rectangular based allowed the device to be rigidly clamped to the table. The gloved hand is attached to the upright pole using Velcro. Twelve surface EMG electrode amplifiers are wrapped around the circumference of the forearm, a ground/reference electrode is mounted on the radius at the wrist. As seen above, the hand was secured to an upright pole during data acquisition. A cushioned elbow rest plate was

mounted at the rear of the base for subject comfort. The height of this rest plate was adjusted for each finger to keep the long axis of the forearm parallel to the table. The subject was seated with their right arm bent at ~90 degrees for the duration of the study; the seat was adjusted to a comfortable height for the subject. Once mounted, the EMG electrodes were never in contact with the finger restraint setup. The force channel was digitized at the same sampling rate and resolution as sEMG signals. A similar grip restraint (Fig. A-2.10), but with a wider finger contact surface, was custom-built for simultaneous co-activation of three or four fingers, with net force measured by a single load cell.

Fig. A-2. 10. Finger and Grip Apparatus [Keating, 2014]

After donning a glove, the subject's palm was arranged perpendicular to the table and then secured to the front of a restraint using Velcro, to stabilize the hand during contraction trials. Next, subjects were instructed to support their forearm on the cushioned elbow rest plate via contact at the olecranon process, with their arm extending along the sagittal plane. For finger trials, each finger was individually fixed to the restraint (Fig. A-2.10); while for grip trials, four fingers (thumb excluded) were simultaneously fixed to the restraint.

A-2.3.3. Virtual Instruments

Fig. A-2.11 show the subject interaction screen. Using Clinical Procedures (Appendix 6) each subject was first informed to do 100% flexion and extension per each finger, three finger and four finger grips and the values were read from the screen below. Then, the 30% of the full calibration, were typed in into the designated area on the screen.

Subjects performed muscle contractions by interacting with a GUI designed in LabVIEW (National Instruments) and shown on a computer screen. On the GUI, a vertical blue line was displayed which represented a computer-controlled target that guided the subject to complete different experimental tasks by exerting force on the load cell. The subject's goal is to keep the red line in as close proximity as possible to the blue line throughout the entire test. A real-time feedback signal from the load cell was shown as a second red vertical line. Both lines were bounded within two fixed white vertical lines representing each subject's 30% maximum voluntary contraction (MVC). The x-axis location of each feedback line (positive and negative) corresponded to extension-flexion forces, respectively. Following the steps in the procedures, EMG and Force data were collected for each of the six cases mentioned above for constant force, slowly force varying, dynamic force varying.

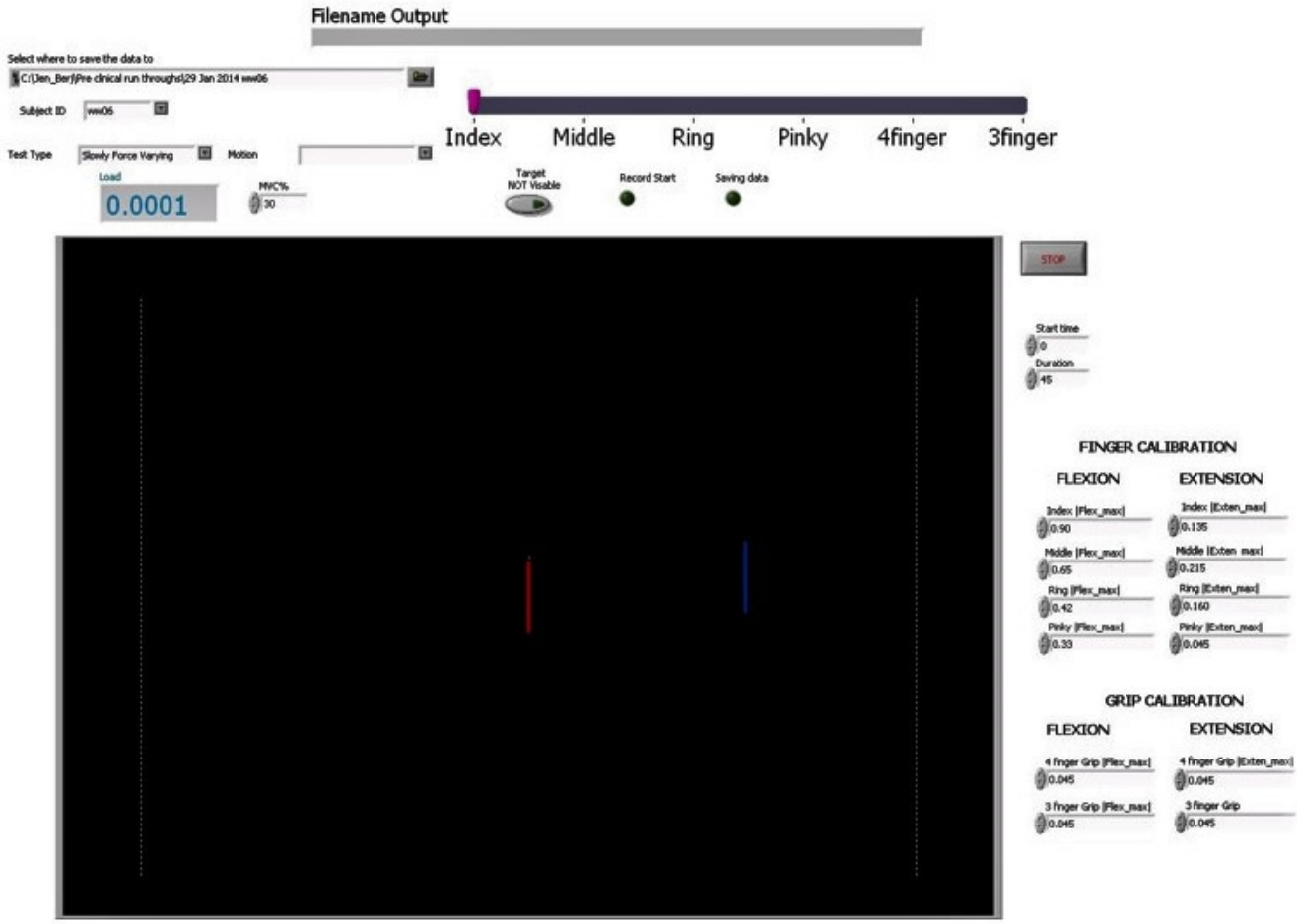

Fig. A-2. 11. Subject Interaction screen

A-2.3.4 Experimental Data Collection

Nineteen able-bodied human subjects (nine males, ten females; aged 23 to 62 years) each participated in one experiment. Subjects initially sat at the single-finger restraint and performed two 5-s 100% MVCs per finger, in each of flexion and extension, the average peaks of which were used as the subject's MVCs. Next, they performed a 0% MVC (rest contraction) and separate flexion and extension 30% MVCs (for each finger) for ten seconds each, utilizing force feedback on a computer screen. These contractions were used to calibrate the advanced EMG amplitude processors.

Subjects then performed three dynamic target tracking contractions per finger, each 45 s in duration. The random target was a 1 Hz band-limited, white and uniform random process and moved randomly between ±(|30 %MVC Ext| + |30 %MVC Flx|)/2, with subjects

tracking this movement by controlling the load cell force. A minimum two-minute rest interval was provided between each contraction to prevent muscle fatigue.

After completing the single-finger trials, the subject was arranged into the grip restraint in a similar manner. In four-finger grip trials, all four fingers (thumb excluded) were secured to the apparatus and for three-finger grip trials, only the middle, ring, and pinky fingers were secured to the apparatus. The same steps were followed to collect grip EMG and force data, for both three-finger and four-finger grips, as were followed for single-finger efforts.

A-2.3.5 Analysis—Signal Preprocessing

All signal processing was performed using MATLAB, with filtering applied in the forward, then reverse time directions, to achieve zero phase. To produce estimates of EMG standard deviation (EMGσ), the sampled EMG were highpass filtered (f_c=15 Hz, fifth-order Butterworth) and second-order IIR notch filtered (bandwidth 1 Hz) at the power line frequency and all harmonics (to attenuate power line interference). The narrow notch filter bandwidth eliminated the interference source with a limited decrease in overall statistical bandwidth of the signal. When desired, adaptive pre-whitening was applied to the EMG, since it is known to reduce the variance of the EMGσ estimate. This filtering was followed by a first order demodulator (i.e., rectifier). After demodulation, EMG signals were passed through a low pass 9th order Chebyshev Type 1 filter with an effective cutoff frequency of 16.8 Hz, and then decimated by a factor of 100, producing a resampled frequency of 40.96 Hz. This low pass filter served as the initial smoothing stage of the EMGσ processor. The original sampling rate of 4096 Hz is necessary for acquiring the raw EMG, but is not appropriate once EMGσ has been estimated [3, 4]. The force signal was similarly decimated, and then normalized to 100% MVC flexion to facilitate the reporting of error statistics across subjects.

A-2.3.6 Analysis— Models

EMGσ values were related to force output at the fingertips using both linear and nonlinear FIR dynamic EMGσ-force model structures for each EMG channel, as:

$$F[m] = \sum_{d=1}^{D} \sum_{q=0}^{Q} \sum_{c=1}^{12} f_{d,c} EMG\sigma_c^d\,[m-q] \qquad (1)$$

where *F[m]* is the force at decimated sample index *m*, *fd,c* are the fit parameters, *c* is the EMG channel, *d* is the degree of the polynomial nonlinearity, and parameter *q* sets the signal lags. For *D*=1, the model is linear, for *D* > 1 the model is nonlinear. Fit parameters were found via least squares, regularized via the pseudo-inverse approach, in which singular values of the design matrix were removed if the ratio of their magnitude to that of the largest singular value was less than an empirically defined tolerance *Tol*.

Six different EMG-force model sets (one, two, three, and four independent fingers; three finger grip; and four finger grip) were studied. Each model was studied for all combinations of polynomial nonlinearity (*D*=1, 2), system order (20≤*Q*≤40 samples, corresponding to 0.49–0.98 s), pseudo-inverse tolerance (0≤*Tol*≤0.1 in 0.0005 increments), and pre-whitening filter (used or unused). For all models, contraction Trials 1 and 2 were used for parameter training and Trial 3 for testing. Test error was the RMS difference between actual and EMGσ-estimated force, expressed in %MVC, ignoring the first 2 s of each trial (to account for filter start-up transients).

For one independent finger, separate EMGσ-force analysis was conducted for each of the four fingers (Index, Middle, Ring, Pinky), using only the single-finger contraction trials for each respective finger (12 EMGσ inputs, one force output). Twelve-input, one-output modeling was also performed using the three-finger grip data and, separately, the four-finger grip data. For two independent fingers, separate analysis was conducted for each of the six combinations of two fingers, using 12-input, two-output models (i.e., separate *fd,c* parameters per finger). Training trials from each of the two fingers were combined, with the unused "true" finger force assigned to zero. RMS error was assessed

on both testing trials (again assigning the "true" force of the unused finger to be zero), and then averaged. Similarly for three independent fingers, separate analysis was conducted for each of the four combinations of three fingers (12-input, three-output models), combining training and testing trials for the relevant fingers (assigning "true" forces in unused fingers to zero). Finally, only one combination of four independent fingers existed. This 12-input four-output model used all single-finger training and testing trials, assigning "true" forces in unused fingers to zero.

Next, the best combination of *D*, *Q*, *Tol*, and *filter* for each model was found using repeated measures analysis of variance (RANOVA). Additionally, RANOVA was conducted between the three finger (individual) and three finger grip model and the four finger (individual) and four finger grip models to identify the model with the lowest %MVC error. The latter comparison will help us to decide whether we should acquire grip data from subjects or the individual finger experiment is sufficient to predict all the different finger combinations. In the context of the physiology/health problem, if we can get an accurate measure from individual finger trials, we can use an orthotic/prosthetic that can carry out more degrees-of-freedom for the patient than in the grip case (a gripper is less useful than something with multiple fingers). These models are explained in detail in the following sections.

A-2.4 Statistical Methods

Differences in model performance were initially tested utilizing multivariate repeated measures analysis of variance (RANOVA) using SPSS version 25, assessing all possible interactions. Interactions were not significant, unless noted below. When degree of sphericity, ε, was <0.75, degrees of freedom were adjusted by the Greenhouse-Geisser method; for $0.75 \leq \varepsilon < 1$, the Huynh-Feldt method was used. For brevity, when related comparisons are summarized, degrees of freedom are reported without adjustment, since the adjusted values vary within each comparison. Post hoc pair-wise comparisons were conducted using paired t-tests with Bonferroni correction. A significance level of $p = 0.05$ was used.

A-2.5 Results and Discussion

A-2.5.1 One-Finger Models

Fig. A-2.12 show plots of the average errors per index finger presented in average MVC% across the study for each model, Q and filter versus tolerance. Similar plots are presented in Appendix A for Middle, Ring, Pinky fingers. All models experienced unstable error values in the range less than 0.01 and relatively increasing error values as tolerance increases greater than 0.01.

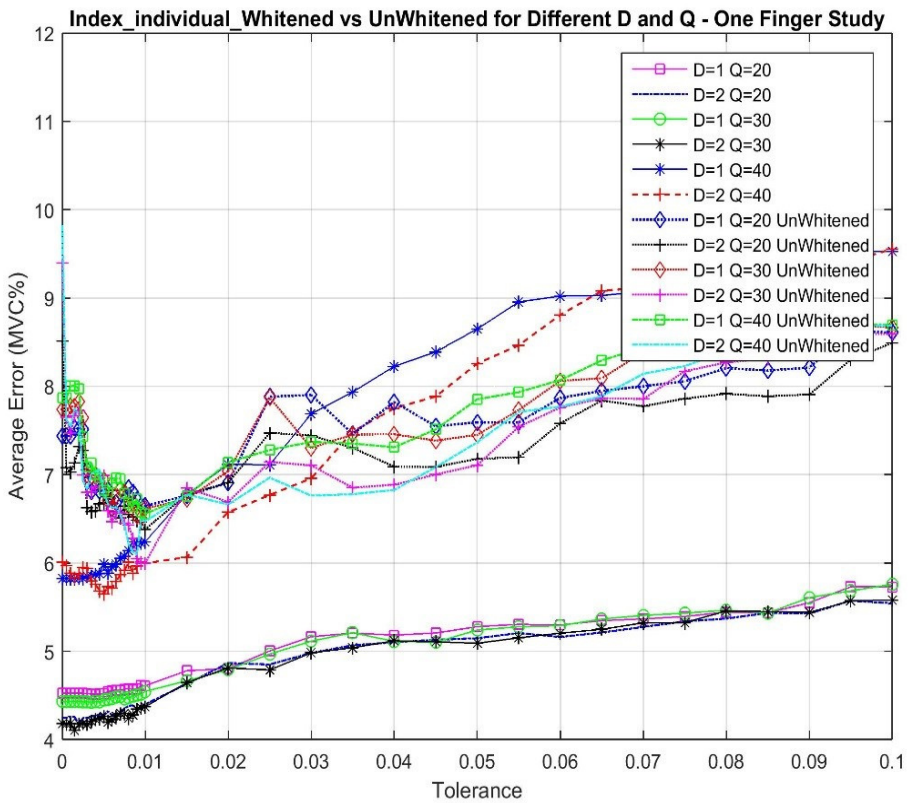

Fig. A-2. 12. Mean Error in MVC% for Index Finger across the study for each model, Q and whitened/unwhitened

Fig A-2.13 shows sample results of the actual versus estimated force for one – finger study case with close to ideal tracking and lower estimation error. However, the intent of the study is to reflect practical cases, i.e. all fingers. When one fingertip was exerting force on the load cell, the force for the remaining unmeasured fingertips was set to zero.

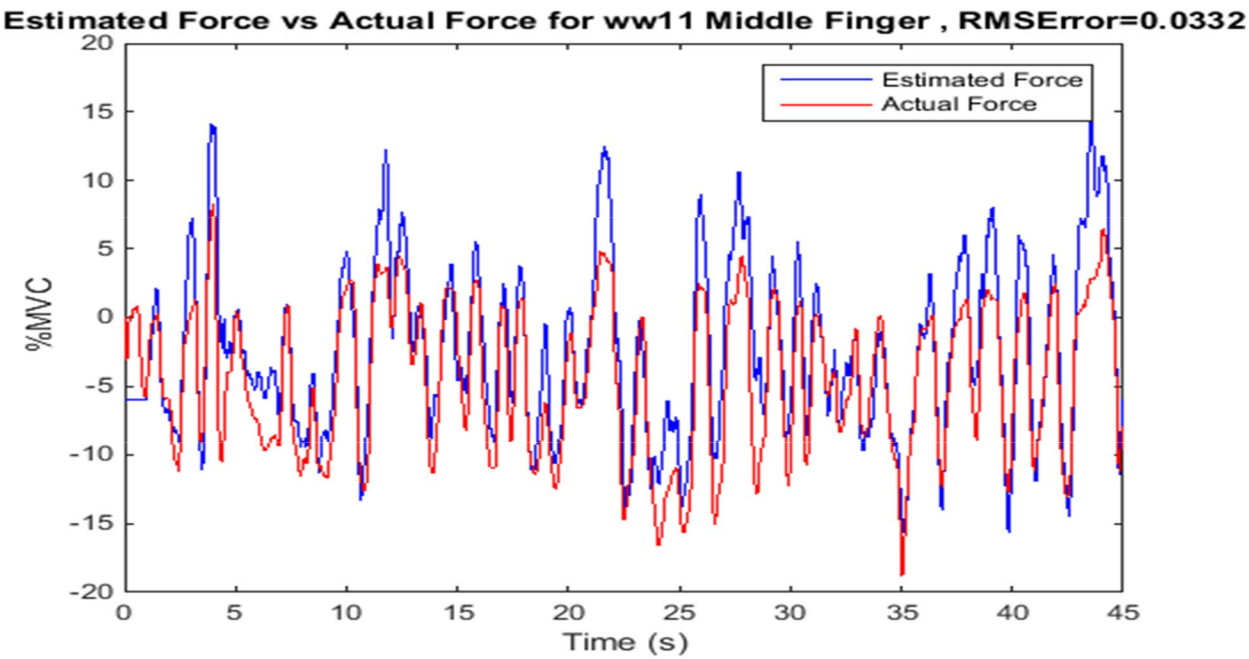

Fig. A-2. 13. . Estimated Force versus Actual Force for subject ww11 Middle Finger.

Using all the results of one-finger models, a five-way RANOVA was computed [factors: finger (index, middle, ring, pinky), tolerance (0.01:0.01:0.1), polynomial degree (1, 2), order (20, 30, 40) and filter (whitened, unwhitened)]. Since there was a significant two way interaction term involving polynomial degree and system order [F(1, 18.005) = 18.837, p_{GG}=0.0001] four way RANOVA's were implemented fixing polynomial degree. Since there was still two way interaction terms involving finger and tolerance [F(3.136, 56.444) = 7.716, p_{GG}=0.0001] and tolerance and system order [F(1.342, 24.147) = 18.462, p_{GG}=0.0001] three way RANOVA's were implemented fixing polynomial degree and system order. Summarizing these six RANOVA's, the main effects of tolerance [F(9,162)>11.04, $p \leq 0.002$] and finger (except Q=20) [F(3,54)>7.88, $p \leq 0.002$] were significant, however the filter was not [F(1,18)<.2, p>0.51]. Tukey *post hoc* comparisons

were computed for all six three-way RANOVA's. When comparing the one-finger models, tolerance value of 0.02 exhibits the lowest %MVC error for each model and significantly different from the rest of tolerance values. Also, there is a significant difference between the pinky finger and the rest and exhibits the lowest %MVC error.

A-2.5.2 Two-Finger Models

Fig. A-2.14 show plots of the average errors per Ring-Pinky finger presented in average MVC% across the study for each model, Q and filter versus tolerance. Similar plots are presented in Appendix A for all six combinations of the two-finger models. As in the case of one-finger, all models experienced unstable error values in the range less than 0.01 and relatively increasing error values as tolerance increases greater than 0.01.

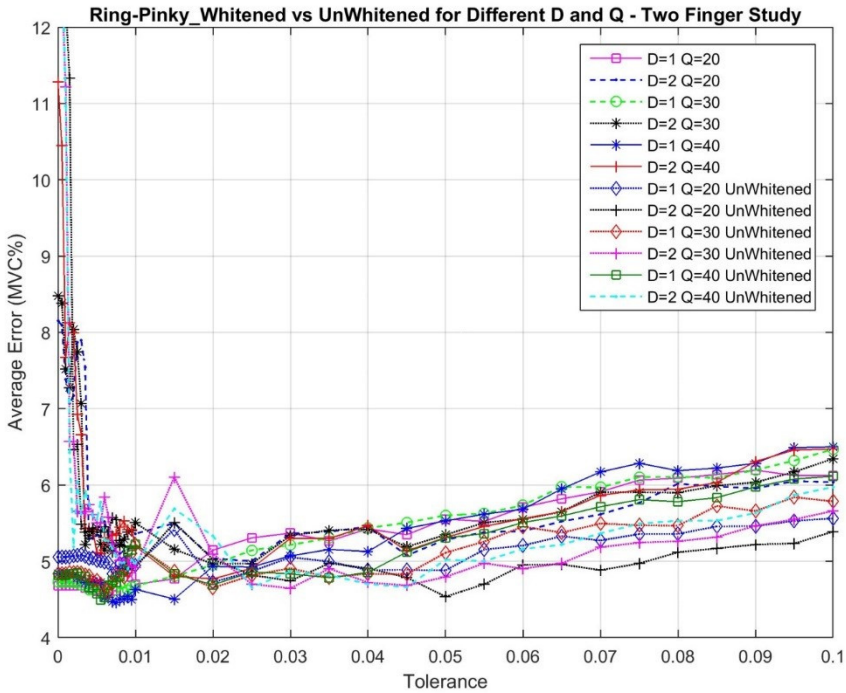

Fig. A-2. 14. . Mean Error in MVC% for Ring-Pinky Finger across the study for each model, Q and whitened/unwhitened

Fig A-2.15 shows sample results of the actual versus estimated force for two –finger study case. As seen in the images, the model estimates "noisy" signals in the period where the

second finger is not active and tracks the actual signal in a close manner. So, when Ring-Pinky finger model was studied, by assuming zero-force first on the Pinky finger then on the Ring finger, it is assumed that there is no co-contraction between the two fingers. So, our intention in the two-finger modeling is to assume that an independent two-finger force is applied and RMS error between the estimated and measured two-finger torques is studied

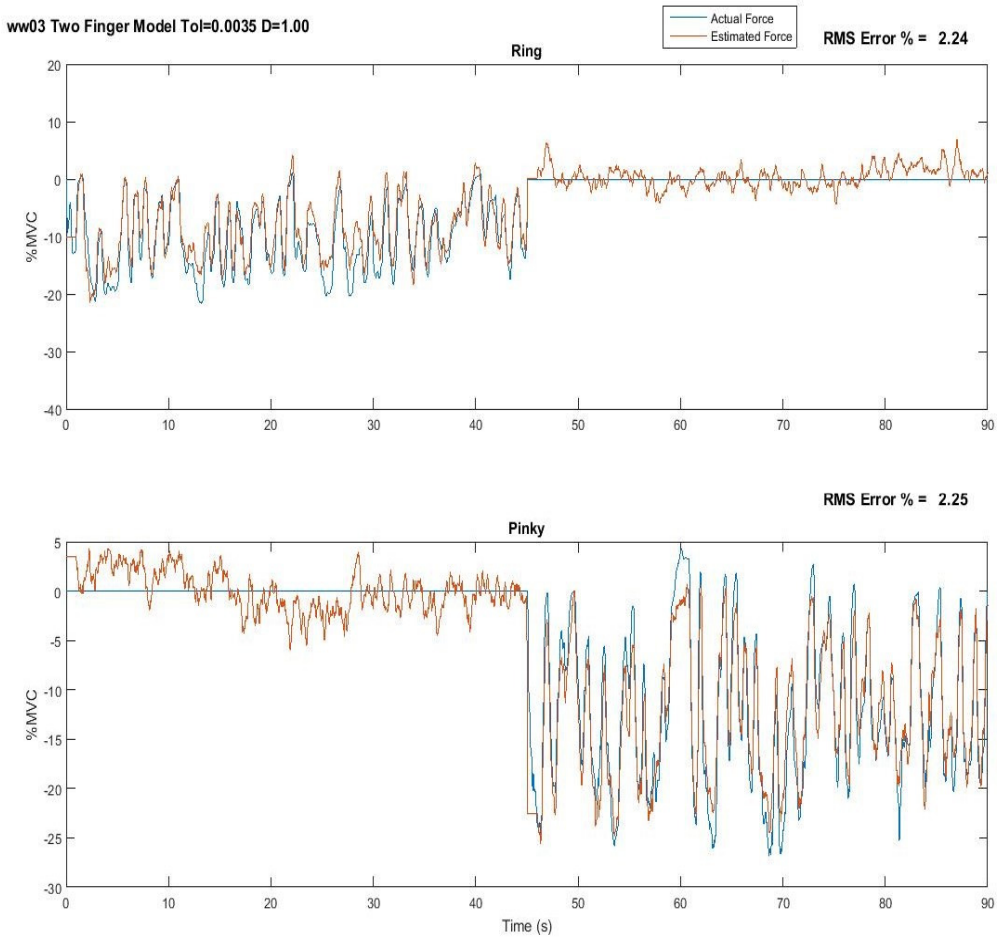

Fig. A-2. 15. Estimated Force versus Actual Force for subject ww03 two finger study Ring-Pinky.

Using all the results of two-finger models, a five-way RANOVA was computed [factors: finger (index-middle, index-ring, index-pinky, middle-ring, middle-pinky, ring-pinky), tolerance (0.01:0.01:0.1), polynomial degree (1, 2), system order (20, 30, 40) and filter (whitened, unwhitened)]. Since there was a significant two way interaction term

involving finger and tolerance [F(5.262, 94.728) = 3.053, p_{GG}=0.012],tolerance and polynomial degree [F(1.273, 22.915) = 4.959, p_{GG}=0.029] and polynomial degree and system order [F(1.894, 34.092) = 3.738, p_{GG}=0.036] four way RANOVA's were implemented fixing polynomial degree. Since there was still two way interaction terms involving finger and tolerance [F(4.237,76.267) = 3.566, p_{GG}=0.009] three way RANOVA's were implemented fixing polynomial degree and system order. Summarizing these six RANOVA's, the main effects of filter [F(1,18)>.75, p>0.12] is not significant. The effect of finger [F(5,90)>1.1, p>0.2] for Q=20 is not significant. filter[F(1,18)>1.2, p>0.12] and tolerance [F(9,162)>.9, p>0.3] were not significant for both Q=20 and 30. However, there was a significant differences between the fingers and tolerances for Q=40. Tukey *post hoc* comparisons were computed for Q=40. When comparing the two-finger models, Ring-Pinky and tolerance value of 0.08 exhibit the lowest %MVC error for each model and significantly different from the rest of tolerance values and two-finger combinations. Even though five out of six two-finger models show the tolerance with the minimum % MVC error close to .01.02 range, the Index-Ring combination appear to affect the output result.

A-2.5.3 Three-Finger Models

Fig. A-2.16 show plots of the average errors per Middle-Ring-Pinky finger presented in average MVC% across the study for each model, Q and filter versus tolerance. Fig 8 shows sample results of the actual versus estimated force for three –finger study case.

Similar plots are presented in Appendix A for all four combinations of the three-finger models. Similar to the two-finger concept, a zero force was assumed for the remaining fingers. In general, all models experienced unstable error values in the range less than 0.01 and relatively increasing error values as tolerance increases greater than 0.01.

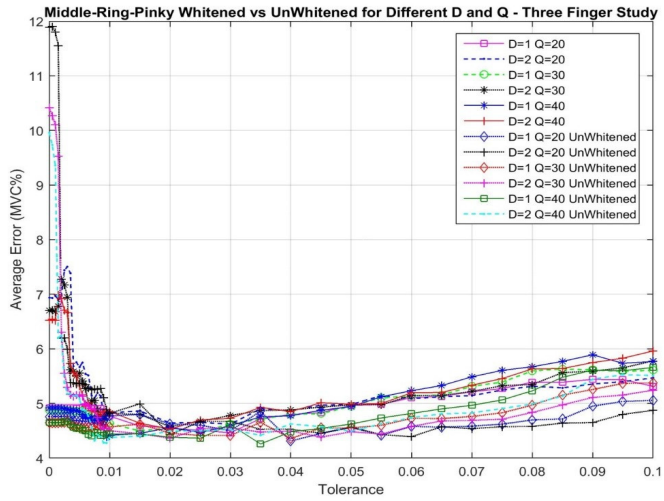

Fig. A-2. 16. Mean Error in MVC% for Middle-Ring-Pinky Finger across the study for each model, Q and whitened/unwhitened.

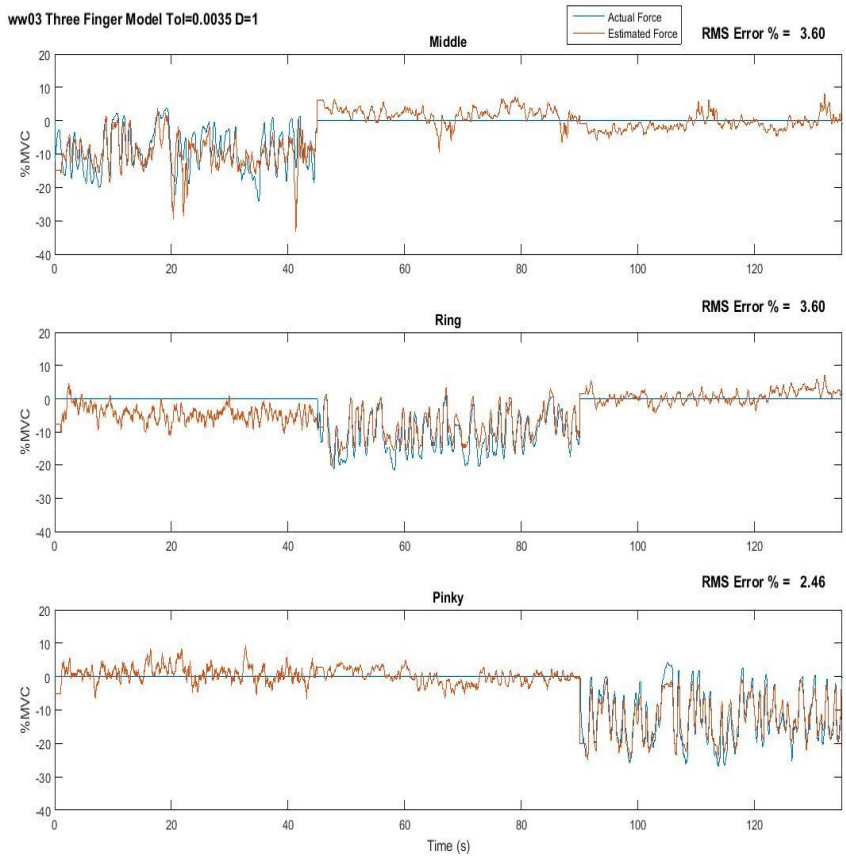

Fig. A-2. 17. Estimated Force versus Actual Force for subject ww03 three finger study Middle-Ring-Pinky.

Using all the results of three-finger models, a five-way RANOVA was computed [factors: finger (index-middle-ring, index-middle-pinky, index-ring-pinky, middle-ring-pinky), tolerance (0.01:0.01:0.1), polynomial degree (1, 2), system order (20, 30, 40) and filter (whitened, unwhitened)]. Since there was a significant two way interaction term involving tolerance and polynomial degree [F(2.051,36.925) = 4.991, p_{GG}=0.012] and tolerance and system order [F(2.716,48.896) = 4.43, p_{GG}=0.010] four way RANOVA's were implemented fixing polynomial degree. Since there was still two way interaction terms involving finger and tolerance [F(2.744,49.388) = 8.497, $p_{GG}=10^{-4}$] and three way interactions involving finger, tolerance and system order [F(1.795,32.304) = 3.648, p_{GG}=.042], three way RANOVA's were implemented fixing polynomial degree and system order. Summarizing these six RANOVA's, the main effects of filter [F(1,18)>0, p>0.77] is not significant. The effect of finger [F(5,90)>4.5, $p<.009$] and tolerance [F(9,162)>.2.3, p<0.05] were significant except for D=2,Q=20 which were not significant. Tukey *post hoc* comparisons were computed for all six RANOVA's. When comparing the three-finger models, Index-Ring-Pinky and tolerance value of 0.02 exhibit the lowest %MVC error for each model and significantly different from the rest of tolerance values and three-finger combinations.

A-2.5.4 Four-Finger Models

Fig. A-2.18 show plots of the average errors per Index-Middle-Ring-Pinky finger presented in average MVC% across the study for each model, Q and filter versus tolerance. This model assumes that the four fingers simultaneously applied a force to an object, assuming that their co-contraction is negligible. EMG to force is related and RMS error is calculated. Fig A-2.19 shows sample results of the actual versus estimated force for four –finger study case. In general, all models experienced unstable error values in the range 0-0.1.

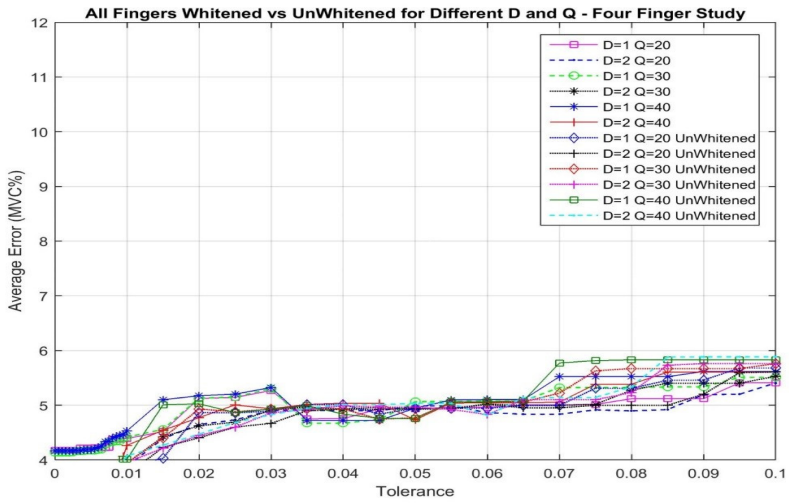

Fig. A-2. 18. Mean Error in MVC% for Four Finger across the study for each model, Q and whitened/unwhitened.

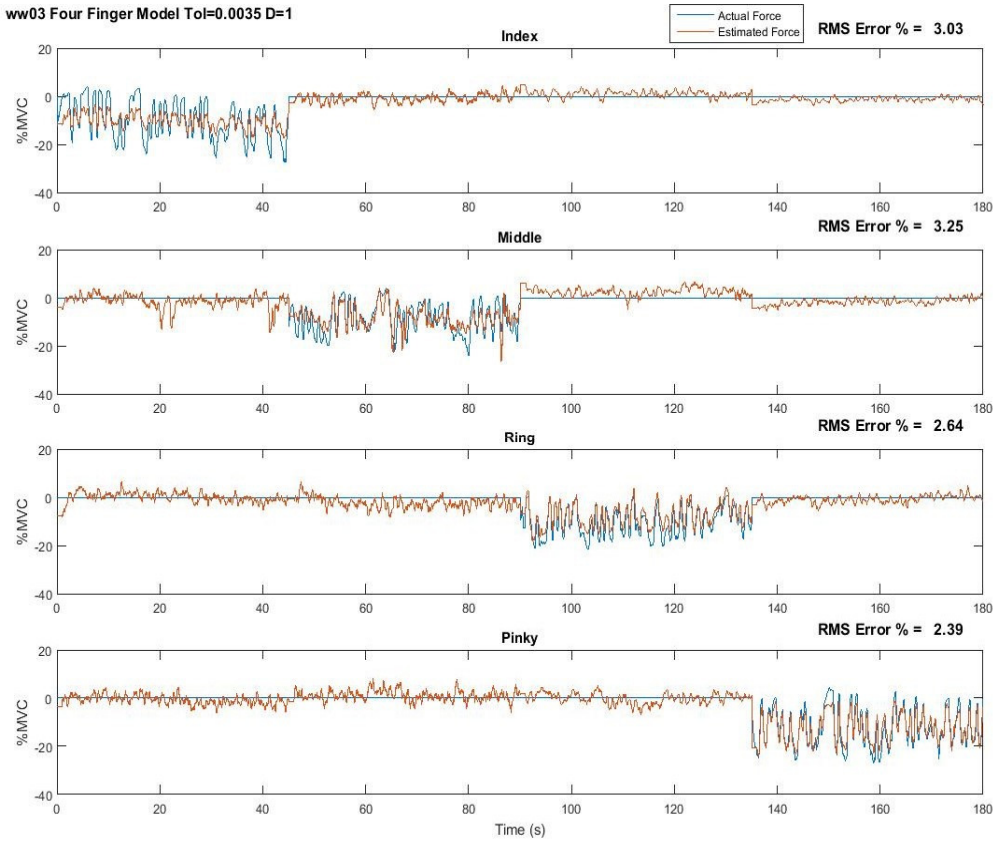

Fig. A-2. 19. Estimated Force versus Actual Force for subject ww03 Four Finger Study.

Using all the results of four-finger models, a four-way RANOVA was computed [factors: tolerance (0.01:0.01:0.1), polynomial degree (1, 2), system order (20, 30, 40) and filter (whitened, unwhitened)]. Since there was a significant two way interaction term involving tolerance and polynomial degree [F(2.199,39.582) = 5.488, p_{GG}=0.006] and tolerance and system order [F(2.731,49.155) = 3.719, p_{GG}=0.020] tolerance and filter [F(2.083,37.5) = 4.708, p_{GG}=0.014] and three way interactions involving tolerance,polynomial degree and system order [F(2.211,39.783) = 5.295, p_{GG}=0.007], three way RANOVA's were implemented fixing polynomial degree. Since there was still two way interaction terms involving tolerance and system order [F(2.893,51.895) = 8.021, $p_{GG}=10^{-4}$], tolerance and filter [F(3.34,60.118) = 6.972, $p_{GG}=10^{-4}$], and system order and filter [F(1.897,34.147) = 4.713, p_{GG}=.017], and three way interactions including tolerance, system order and filter [F(2.545,.504) = 5.052, p_{GG}=.002], two way RANOVA's were implemented fixing polynomial degree and system order. Summarizing these six RANOVA's, the main effects of filter [F(1,18)>7.4, $p<.015$] is significant. For D=2 and Q(20,30) the tolerance is not significant [F(9,162)>1.7, $p>.050$], but for the other combination it is significant [F(9,162)>3.2, $p<.010$]. Tukey *post hoc* comparisons were computed for all six RANOVA's. When comparing the four finger models, tolerance values of 0.01 and 0.02 had the lowest mean and significantly different from the rest . Unwhitened filter exhibited lower %MVC error and significantly different from the whitened filter.

A-2.5.5 Three-Finger Grip Models

This case is a special case of the above mentioned three-finger model. In this case, three fingers were simultaneously active through use of the grip-based setup Fig. A-2.20 show plots of the average errors per Middle-Ring-Pinky Grip presented in average MVC% across the study for each model, Q and filter versus tolerance.

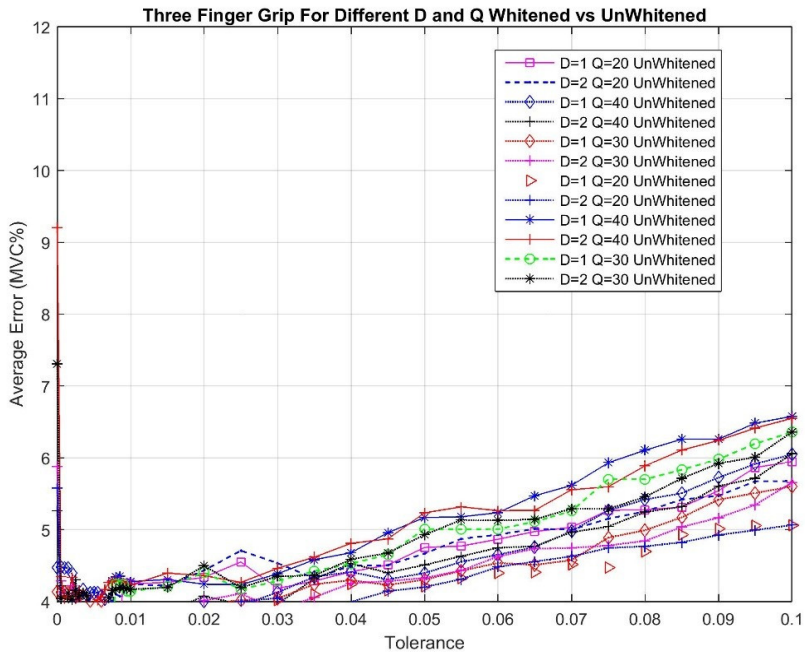

Fig. A-2. 20. Mean Error in MVC% for Three Finger Grip across the study for each model, Q and whitened/unwhitened.

Using all the results of three finger Grip models, a four-way RANOVA was computed [factors: tolerance (0.01:0.01:0.1), polynomial degree (1, 2), system order (20, 30, 40) and filter (whitened, unwhitened)]. Since there was a significant three way interaction term involving tolerance,polynomial degreeand system order [F(1.814,32.649) = 5.926, p_{GG}=0.008] , three way RANOVA's were implemented fixing polynomial degree. Since there was still two way interaction terms involving tolerance and system order [F(1.741,31.341) = 5.517, p_{GG}=*.011*], two way RANOVA's were implemented fixing polynomial degree and system order. Summarizing these six RANOVA's, the main effects of filter [F(1,18)>2.8, *p<.03*] and tolerance [F(9,162)>3.3, *p<.035*] were significant. Tukey *post hoc* comparisons were computed for all six RANOVA's. When comparing the three finger grip models, tolerance values of 0.01,.02,.03 were not significant from each other but .01 had the lowest mean. Similarly to the case of four finger models Unwhitened filter exhibited lower %MVC error and significantly different from the whitened filter.

A-2.5.6 Four-Finger Grip Models

This model used the actual collected data from the experiment. Subject applied one force using all the fingers simultaneously. So, similar to the three finger grip model, there is no assumption of excluding the co-contraction._Fig. A-2.21 show plots of the average errors per IndexMiddle-Ring-Pinky Grip presented in average MVC% across the study for each model, Q and filter versus tolerance.

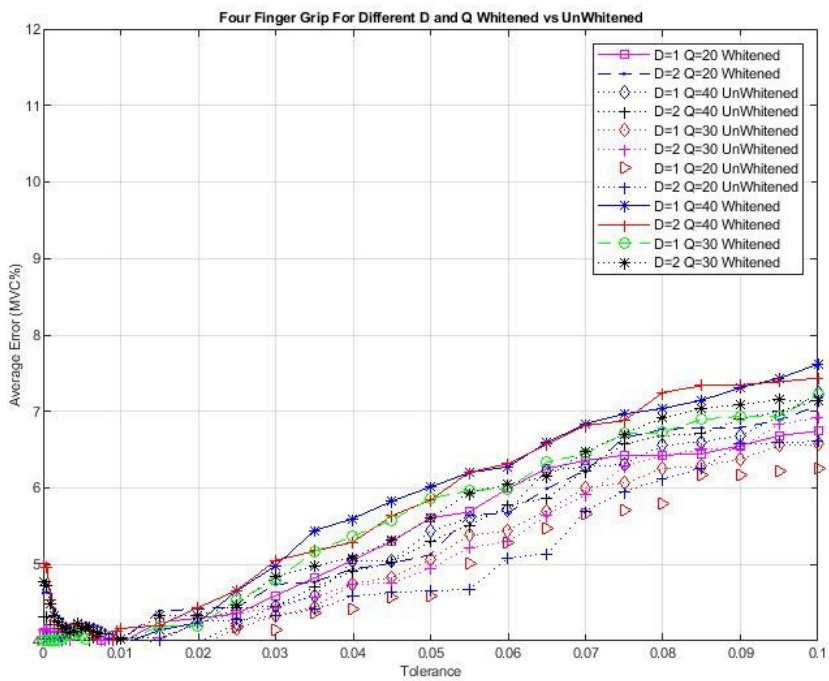

Fig. A-2. 21. Mean Error in MVC% for Four Finger Grip across the study for each model, Q and whitened/unwhitened.

Using all the results of three finger Grip models, a four-way RANOVA was computed [factors: tolerance (0.01:0.01:0.1), polynomial degree (1, 2), system order (20, 30, 40) and filter (whitened, unwhitened)]. Since there was a significant two way interaction term involving tolerance, polynomial degree [F(2.359,42.437) = 30.459, $p_{GG}=10^{-4}$] , tolerance system order [F(4.115,74.072) = 27.237, $p_{GG}=10^{-4}$] three way interaction term involving tolerance, polynomial degree and system order [F(2.791,50.244) =24.922, $p_{GG}=10^{-4}$] three

way RANOVA's were implemented fixing polynomial degree. Since there was still two way interaction terms involving tolerance and system order [F(3.217,57.907) = 22.308, $p_{GG=}10^{-4}$], system order and filter [F(1.506,27.109) = 3.850, $p_{GG=}.045$],two way RANOVA's were implemented fixing polynomial degree and system order. Summarizing these six RANOVA's, the main effects of filter [F(1,18)>26.5, $p<.001$] and tolerance [F(9,162)>18.05, $p<.001$] were significant. Tukey *post hoc* comparisons were computed for all six RANOVA's. When comparing the three four finger grip models, tolerance value of 0.01 is significantly different from greater than .01 and had the lowest mean. Similarly, to the case of three finger grip models Unwhitened filter exhibited lower %MVC error and significantly different from the whitened filter.

REFERENCES

Castellini C. and van der Smagt P. "Surface EMG in Advanced Hand Prosthetics," Bio. Cyber, vol. 100, pp. 35-47, 2009.

Clancy EA. "Design of a High–Resolution, Monopolar, Surface Electromyogram (EMG) Array Electrode–Amplifier and Its Associated Signal Conditioning Circuit." TS. Worcester Polytechnic Institute, Worcester, MA.2003

Keating J, "Relating forearm muscle electrical activity to finger forces," M.S. thesis, Worcester Polytechnic Institute, Worcester, MA, May 2014, pp. 19-25.

Liu P., Brown DR., Martel F., Rancourt D. and Clancy EA "EMG-to-force Modeling for Multiple Fingers," in Proc. of Bioengineering Conference (NEBEC), 2011 IEEE 37th Annual Northeast, New York, Troy.

Marieb EN., Hoehn K. Anatomy & Physiology. 5th ed, Boston, Pearson, pp. 281-290, 2013.

Parker P., Englehart K., and Hudgins B. "Myoelectric signal processing for control of powered limb prostheses," J. Electromyo. Kinesiol., vol. 16, pp. 541–548, 2006.

Perotto AO, Anatomical Guide for the Electromyographer, 3 ed., Springfield, IL: Charles C Thomas, 1994, pp. 30-73.

Smith RJ, Huberdeau D., Tenore F. and Thakor NV. "Real-Time Myoelectric Decoding of Individual Finger Movements for a Virtual Target Task," Proc. 31st Ann. Int. Conf. IEEE EMBS, pp. 2376-2379, 2009.

Appendix 3: Long-form EMG-Finger Paper Figures

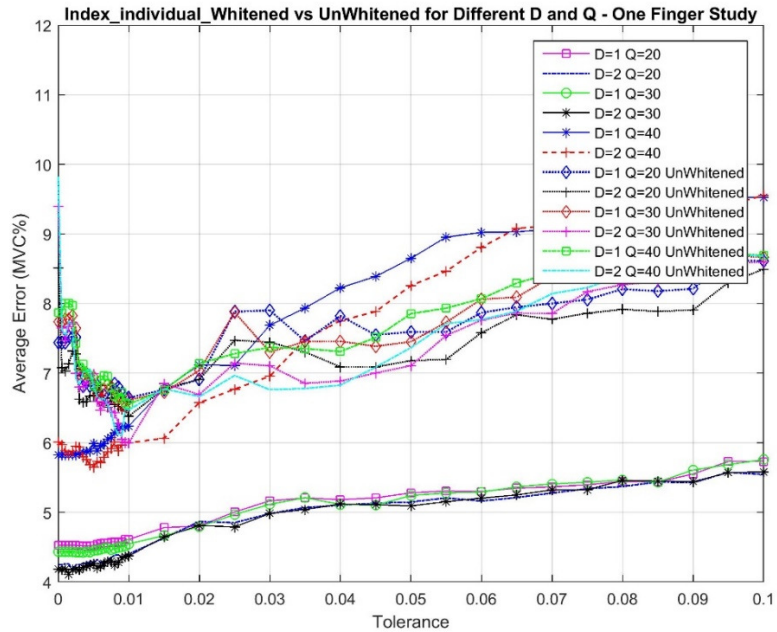

Fig. A-3. 1. Mean Error in MVC% for Index Finger across the study for each model, Q and whitened/unwhitened

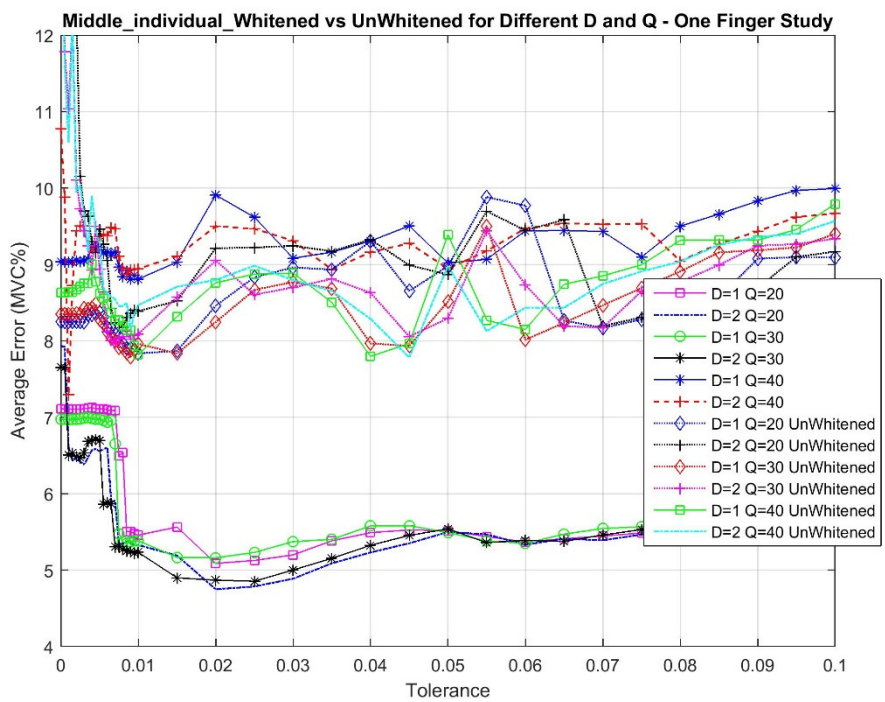

Fig. A-3. 2. Mean Error in MVC% for Middle Finger across the study for each model, Q and whitened/unwhitened

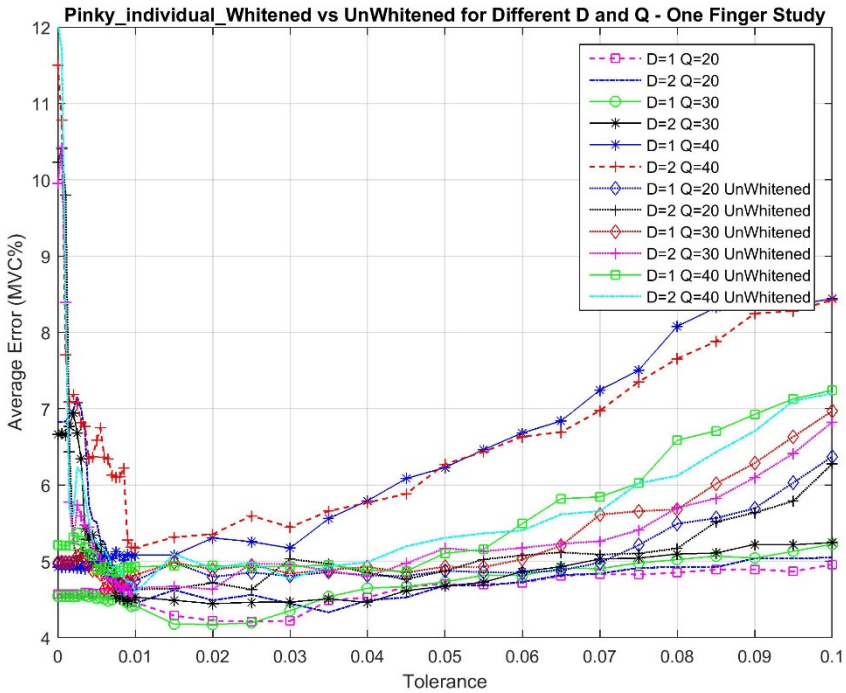

Fig. A-3. 3. Mean Error in MVC% for Pinky Finger across the study for each model, Q and whitened/unwhitened

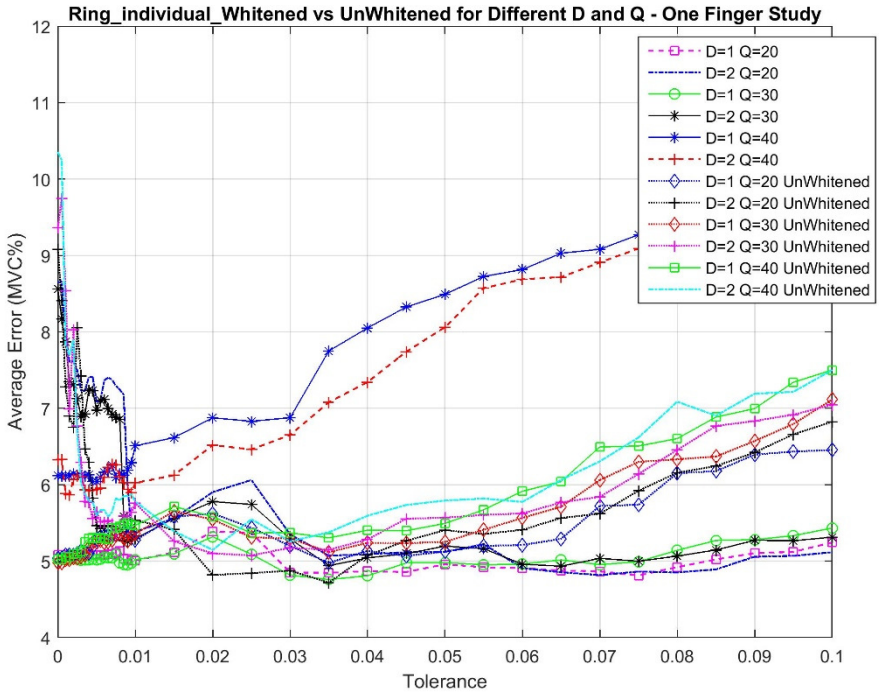

Fig. A-3. 4. Mean Error in MVC% for Ring Finger across the study for each model, Q and whitened/unwhitened

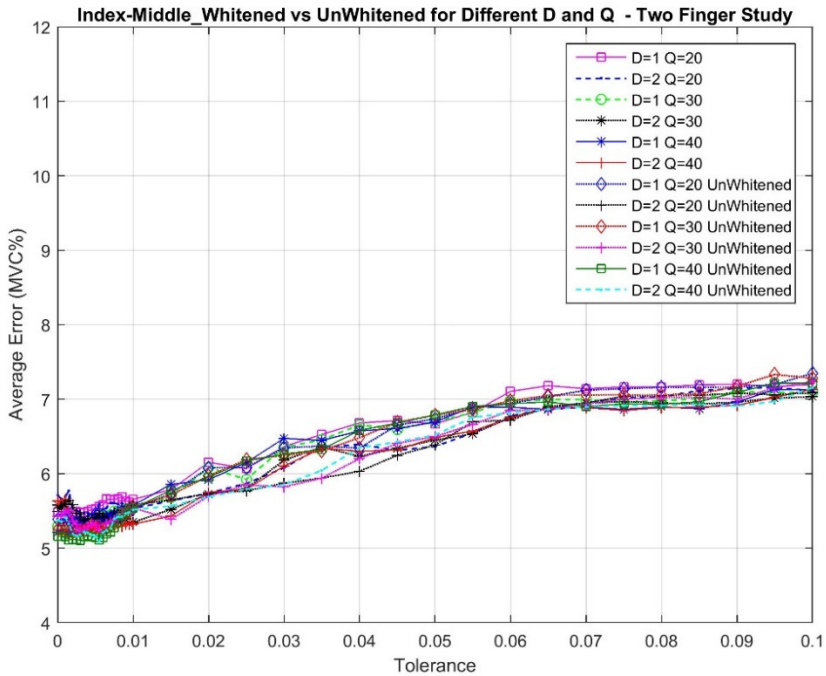

Fig. A-3. 5. Mean Error in MVC% for Index-Middle Finger across the study for each model, Q and whitened/unwhitened

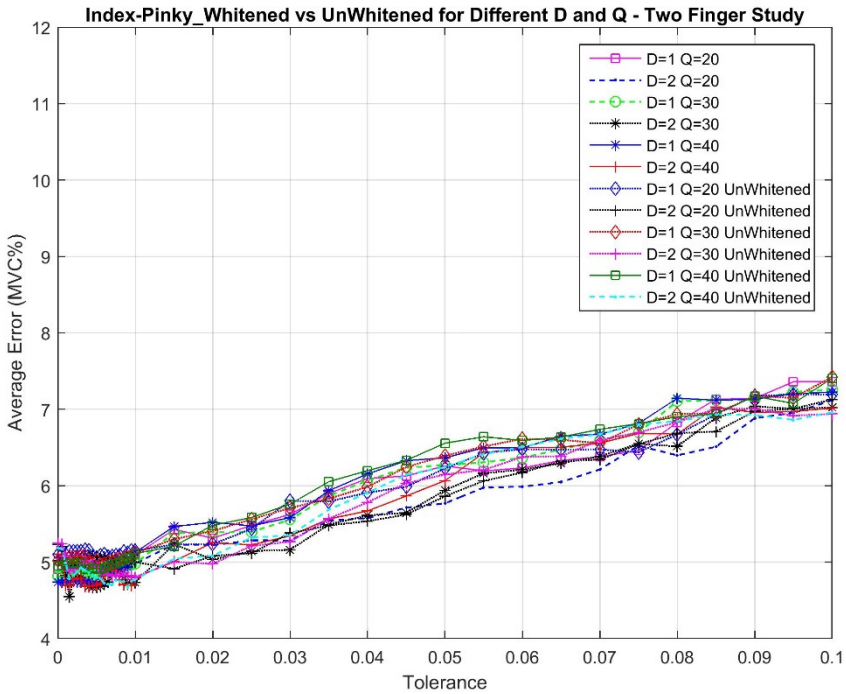

Fig. A-3. 6.Mean Error in MVC% for Index-Pinky Finger across the study for each model, Q and whitened/unwhitened

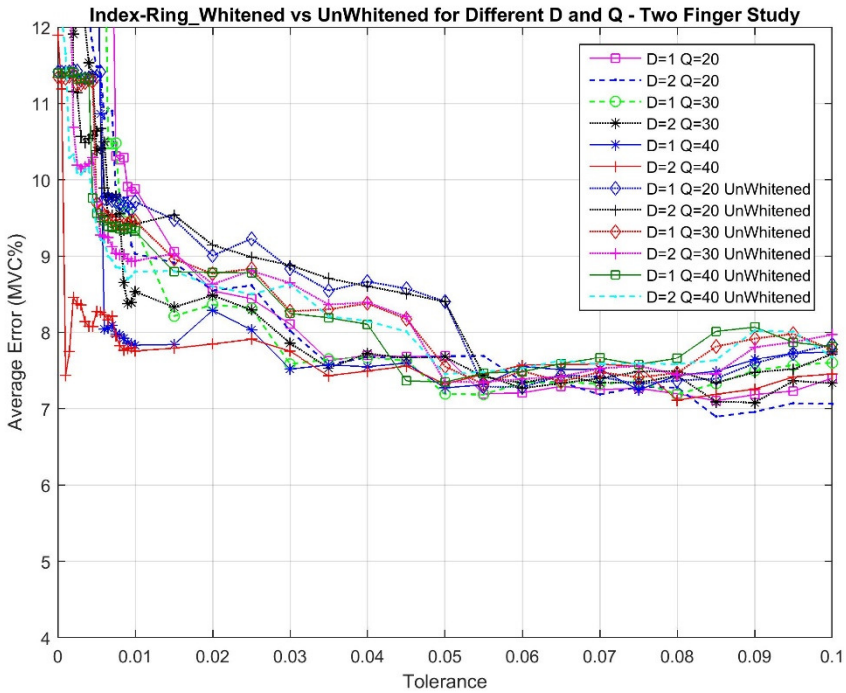

Fig. A-3. 7. Mean Error in MVC% for Index-Ring Finger across the study for each model, Q and whitened/unwhitened

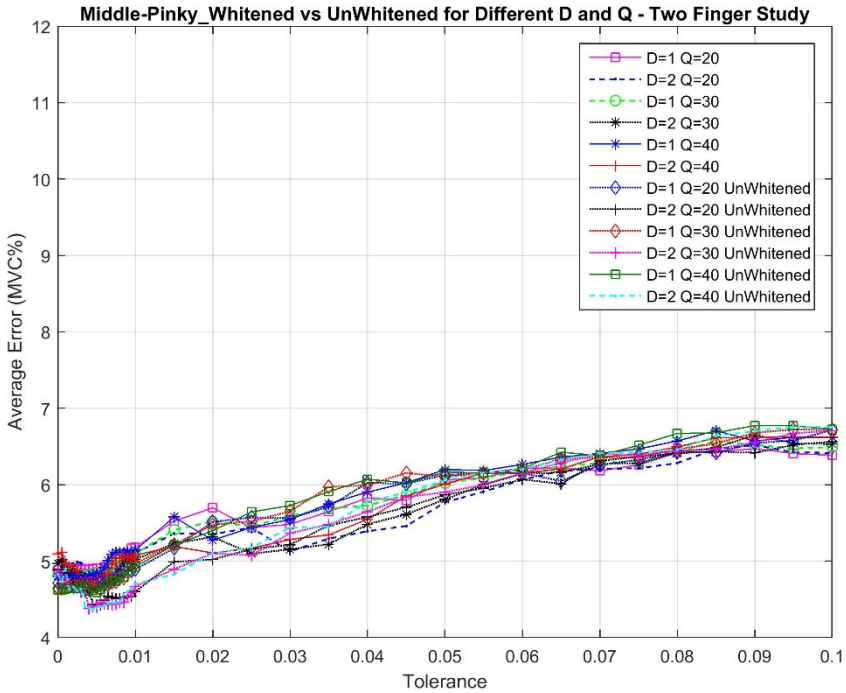

Fig. A-3. 8. Mean Error in MVC% for Middle-Pinky Finger across the study for each model, Q and whitened/unwhitened

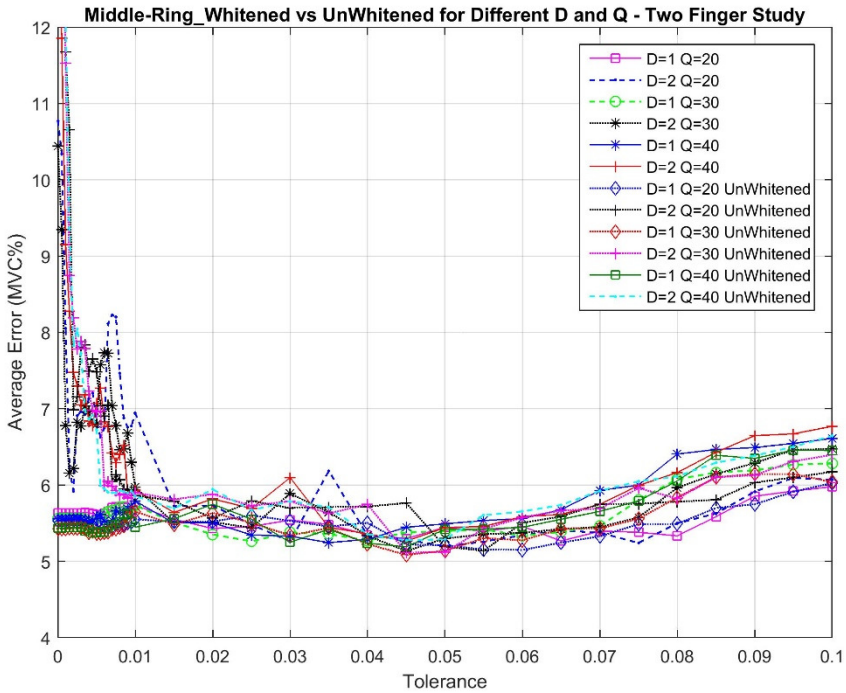

Fig. A-3. 9. Mean Error in MVC% for Middle-Ring Finger across the study for each model, Q and whitened/unwhitened

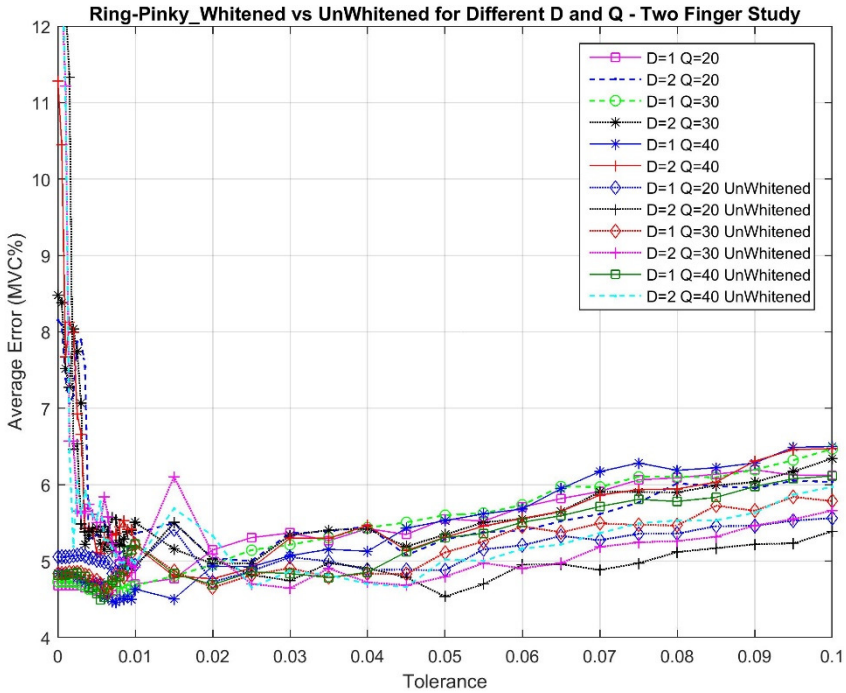

Fig. A-3. 10. Mean Error in MVC% for Ring-Pinky Finger across the study for each model, Q and whitened/unwhitened

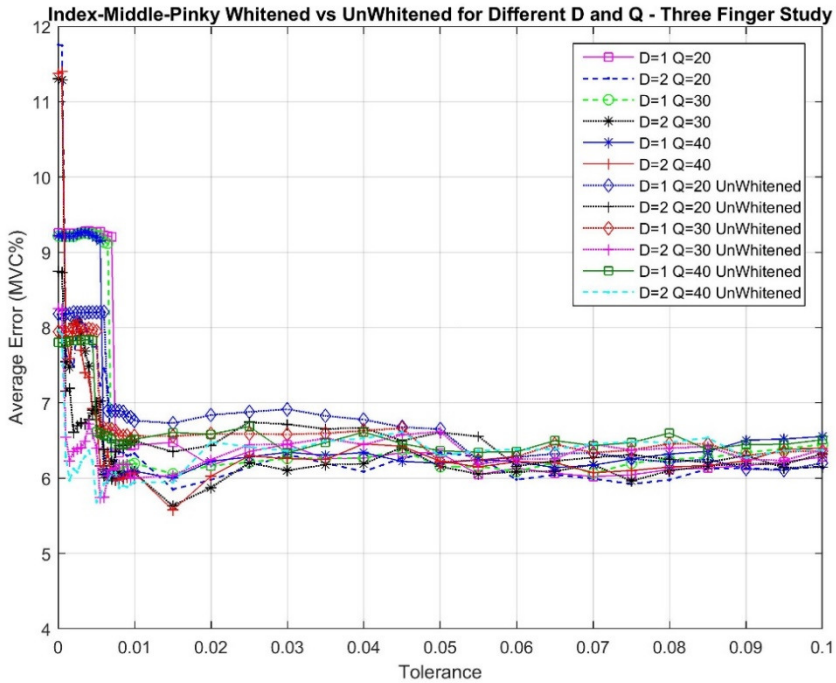

Fig. A-3. 11. Mean Error in MVC% for Index-Middle-Pinky Finger across the study for each model, Q and whitened/unwhitened

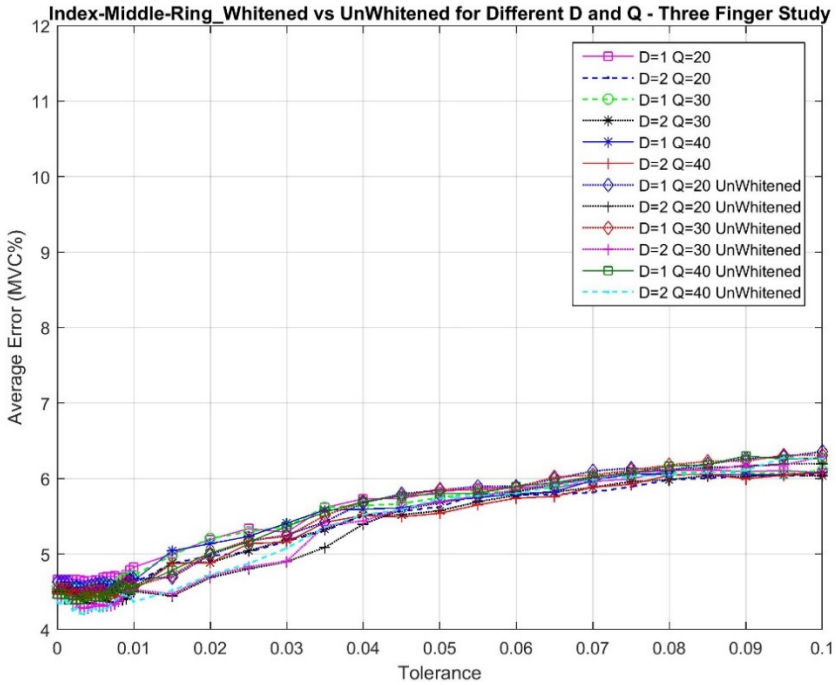

Fig. A-3. 12. Mean Error in MVC% for Index-Middle-Ring Finger across the study for each model, Q and whitened/unwhitened

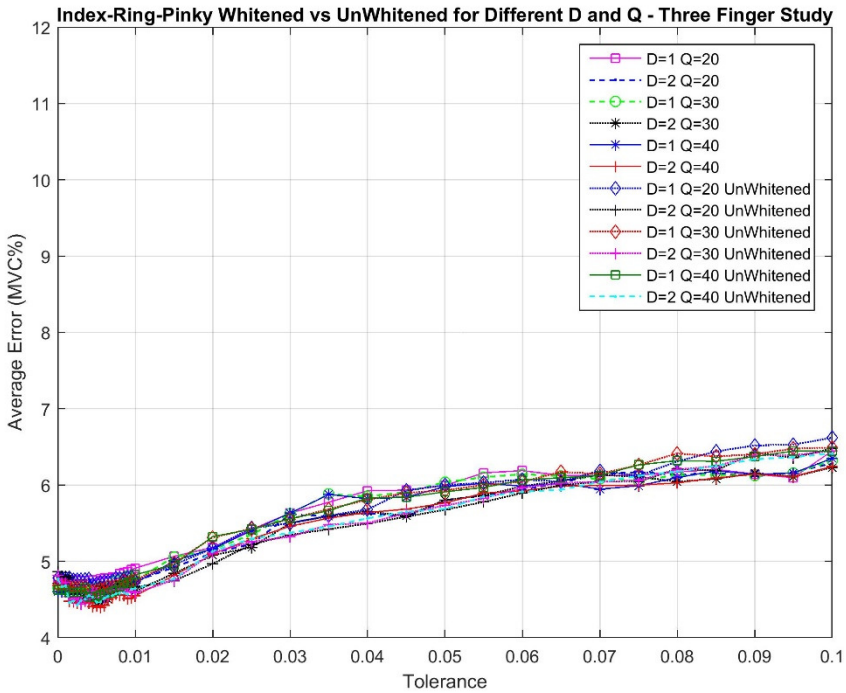

Fig. A-3. 13. Mean Error in MVC% for Index-Ring-Pinky Finger across the study for each model, Q and whitened/unwhitened

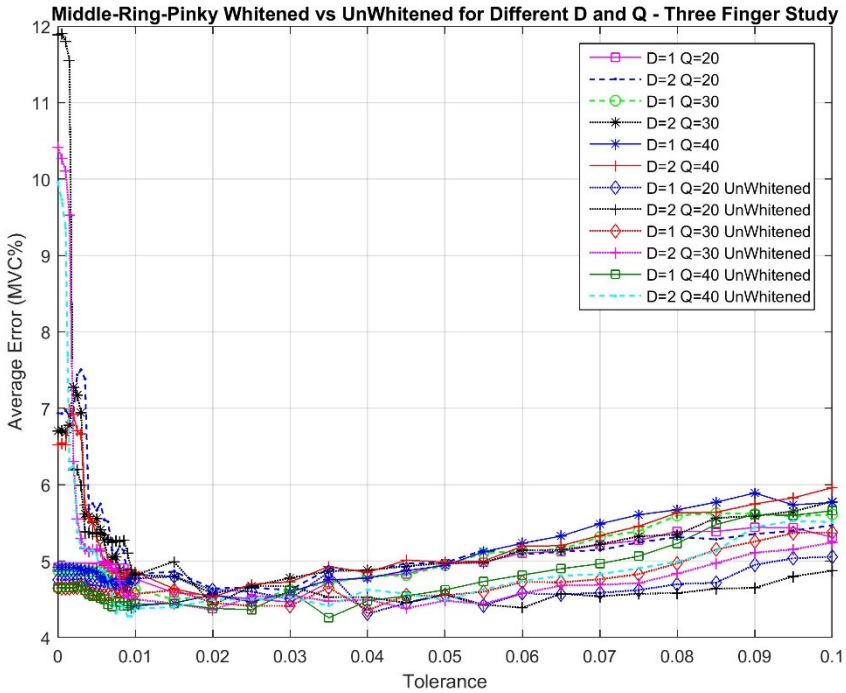

Fig. A-3. 14. Mean Error in MVC% for Middle-Ring-Pinky Finger across the study for each model, Q and whitened/unwhitened

Portions of this Appendix appear in the conference papers provided in Chapters 3,4 and 5. The full text is retained as this Appendix for future reference.

Appendix 4: Long-form Hand-Wrist paper

A-4.1 Methods

A-4.1.1 Experimental Data and Apparatus

Data Collection—Setup: The Institutional Review Board of Worcester Polytechnic Institute approved reprocessing of previously acquired experimental data from nine able-bodied subjects (five males, four females; aged 27±9.7 years). See [1] for full experimental details. Briefly, subjects sat at the experimental apparatus with their dominant hand cuffed to a six-DoF load cell, to measure wrist force/torque. Separately, open-close (Opn-Cls) grip force was measured by a single-axis load cell by securing the thumb to one side of the cell via a rigid tube and using Velcro to secure the proximal aspects of the four fingers to the opposite side of the cell (see Fig. A-4.1). The shoulder was flexed 45° forward from the anatomical position along the sagittal plane, the wrist was relaxed in a neutral position with respect to the hand and the palm of the hand was perpendicular with the plane of the floor. The elbow was supported.

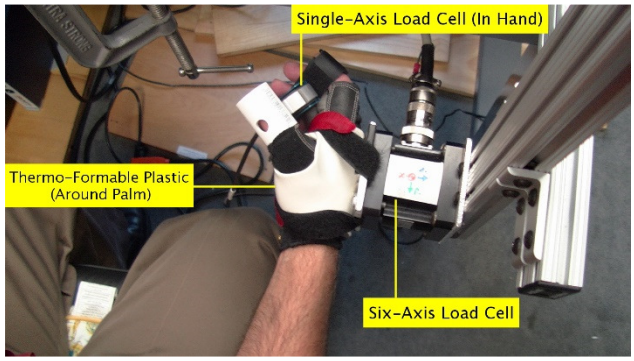

Fig. A-4. 1. Force/moment measurement apparatus (viewed from above). Dominant hand was secured via thermo-formable plastic and Velcro to six-axis load cell. Fingers were secured to a single-axis load cell (thumb on one side, remaining digits on the other).

The skin about the forearm was scrubbed with an alcohol wipe and electrode gel was applied. Sixteen bipolar EMG electrodes were applied equidistant and circumferentially about the forearm, with their mid-point located 5 cm distal to the elbow crease. Bipolar electrodes were 5 mm diameter, stainless steel, hemispherical contacts separated 1 cm edge-to-edge, oriented along the forearm's long axis. A gelled reference electrode was secured immediately distal on the ventral forearm. Each bipolar EMG signal was differentially amplified (30–500 Hz pass band, CMRR > 100 dB over the pass band), with selectable gain applied. A real-time feedback signal from the load cells was displayed as a blue arrowhead on a computer screen (see [1], Fig. 3). The arrowhead displayed four different DoFs—*x*-axis location for extension-flexion (Ext-Flx) force, *y*-axis location for radial-ulnar (Rad-Uln) force, rotation for pronation-supination (Pro-Sup) moment, and size for hand Opn-Cls. A second red arrowhead displayed a computer-controlled target to guide the subject to complete different experimental tasks. Four load cell signals and 16 EMG channels were each sampled at 2048 Hz with 16-bit resolution.

Data Collection—Contractions: All contractions were constant-posture, with at least a two-minute rest interval to prevent muscle fatigue. After warming-up, maximum voluntary contraction (MVC) was measured separately for both directions (e.g., radial, ulnar) for each of the four DoFs. Next, subjects produced 5 s constant-force 50% MVC contractions for each of the 4 DoFs (for each direction within a DoF).

Then, subjects completed 1-DoF *dynamic* tracking trials, separately for each of the four DoFs. Subject feedback only displayed changes in the specified DoF. For Rad-Uln, the target moved randomly between $\pm(|30\ \%\text{MVC Rad}| + |30\ \%\text{MVC Uln}|)/2$, with subjects tracking this movement by controlling the load cell force. The random target was a 0.75 Hz band-limited, white and uniform random process. Four trials of 40 s duration each were completed. The equivalent trial was completed for the three remaining DoFs (16 trials total); except that the maximum force was reduced to 15 %MVC for Opn-Cls due to excessive hand open fatigue found during preliminary testing. The order of presentation of the DoFs was randomized.

Lastly, subjects tracked *dynamic* 2-DoF targets comprised of hand Opn-Cls combined with one of the three wrist DOFs (Ext-Flx, Rad-Uln or Pro-Sup) representative of command hand-wrist tasks. The same random target style was used, but with independent random instances per DoF. Four trials of 40 s duration were completed for each hand-wrist combination (12 trials total).

A-4.1.2 Analysis—Signal Preprocessing

Data analysis was performed offline in MATLAB. EMG standard deviation (EMGσ) was estimated for each channel. Raw EMG were highpass filtered (5th -order Butterworth, fc=15 Hz), notch filtered to attenuate power-line interference with little loss of signal power (2nd-order IIR filter at 60 Hz, notch bandwidth of 1Hz), rectified, lowpass filtered at 16 Hz (Chebyshev Type 1 filter, 9th-order, 0.05 dB peak-to-peak passband ripple), and downsampled from 2048 Hz to 40.96 Hz [2, 3]. Note that further lowpass filtering is inherently provided by subsequent dynamic EMG-force modeling [4]. Each force/moment signal was normalized by its corresponding MVC level pair. For example, Rad-Uln was normalized by: $\left(\left|MVC_{Rad}\right|+\left|MVC_{U\ln}\right|\right)/2$.

A-4.1.3 Analysis—One-DoF Models

<u>1) Subject-Specific, Full-Duration Model:</u> EMGσ values were initially related to force/moment—separately for each DoF—via the 1-DoF linear dynamic model:

$$T[m]=\sum_{q=0}^{Q}\sum_{e=1}^{E}c_{e,q}\,EMG\sigma_e[m-q], \qquad (1)$$

where T was hand/wrist force/moment, m was the decimated discrete-time sample index, Q=20 was the order of the linear dynamic model [5], E was the number of electrodes used in the fit (initially set to 16), and $c_{e,q}$ were the fit coefficients. Model training used the least squares pseudo-inverse method [6], with singular values of the design matrix removed if the ratio of their magnitude to that of the largest singular value was less than 0.01 [5]. Trials 1 & 2 were used for training, and Trials 3 & 4 for testing (RMS error between the estimated and measured torques, expressed in %MVC, after discarding the first 2 s of each 40 s trial to account for start-up transients). Backward stepwise selection (using training data only) [1, 7] was used to progressively reduce the number of retained electrodes from 16 down to 2, with RMS test error assessed at each step. Training and testing trials were then exchanged (two-fold cross-validation), with the average of these two folds reported. Two-fold cross validation is computationally efficient, and the remaining folds are correlated (i.e., statistically less efficient).

2) Subject-Specific, Reduced-Duration Model: Separately for each DoF, the above procedure was repeated while varying the time duration used for training. For training durations of 14, 22, 30 and 38 s, only the necessary initial portion of the first training trial was used. For training durations of 44, 52, 60, 68 and 76 s, equal durations of both training trials were used (e.g., the first 22 s of each trial were used when evaluating 44s for training). As above, model testing used both full testing trials, with the two-fold cross-validation results averaged.

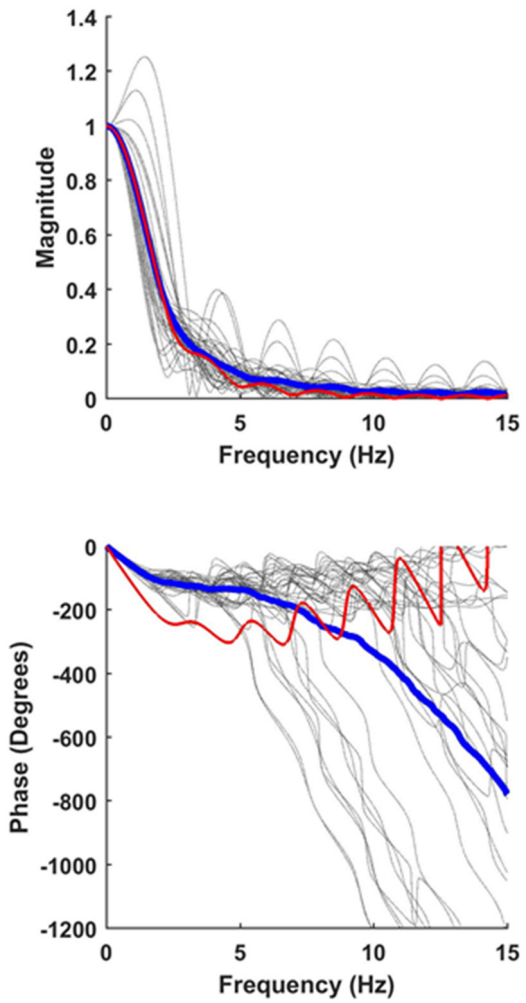

Fig. A-4. 2. Each of 144 magnitude (top) and phase (bottom) responses of the 1-DoF models is shown in grey (nine subjects, selection of two EMG channels per subject, two cross-validations and four DoFs). Thick blue lines are the averages and thin red lines are the universal FIR filter fit to these responses.

3) DoF-Specific Model: Combined full Trials 1 & 3 were used to fit the subject-specific, full-duration models and backward stepwise selected down to two EMG channels (as explained above). For each of the two retained EMG channels (representing channels preferred for EMG-force estimation), the fit coefficients define a FIR filter, which is inherently lowpass in shape [4, 8-12]. These filters were each normalized to a gain of one at 0 Hz—expressing the EMGσ-force dynamics, absent of the gains for each EMG channel. A total of 36 gain-normalized filters were formed per DoF (nine subjects, two EMG channels per subject, two cross-validations). The ensemble mean coefficient values of these filters (one filter per DoF) were computed.

This DoF-specific filter was used, respectively, in place of the dynamics provided by the subject-specific, EMG channel-specific filters of the previous analysis, by appending the DoF-specific filter to the EMG pre-processing (after the decimation step). This evaluation assessed if subject-specific, EMG channel-specific calibration of dynamics could be replaced with one dynamic filter per DoF. Once the DoF-specific filters were formed, Trials 1 & 3 were used to calibrate *only* the gains of each EMG channel [equation (1) with Q=0 (gain-only)]. Testing was performed on full Trials 2 & 4. Backward stepwise selection from 16 down to 2 electrodes was performed, with only results for two EMG channels reported (with cross-validation). This analysis was completed for each of the DoFs and training durations.

4) Universal Model: This analysis was similar to the prior analysis, except that the DoF-specific filter coefficients were ensemble averaged into one "universal" filter to assess if one filter shape could capture all dynamics for all DoFs. This universal filter (Fig. 2) was derived from $36 \cdot 4 = 144$ individual gain-normalized filters. Again, analysis was completed for all training durations and only the results for two EMG channels are reported.

5) Eight Pre-Selected Electrode Locations: We compared eight pre-selected electrode sites to backward stepwise selection of eight (out of 16) electrode sites, to evaluate the need for stepwise selection. For pre-selection, every other electrode was automatically included in a model, aligned with the most dorsal electrode. Only subject-specific models were investigated, as a function of training duration, for each DoF (using two-fold cross-validation).

A-4.1.4 Analysis—Two-DoF Models

Similar 2-DoF EMG-force models were evaluated (with backward stepwise selection of EMG channels and two-fold cross-validation) for each of Opn-Cls paired with one wrist DoF, always estimating two DoFs simultaneously. Each EMG channel contributed to both DoFs. All six combinations of three different training paradigms and two testing paradigms were performed to evaluate the best modeling strategy. The training paradigms were: training with 1-DoF trials, with 2-DoF trials, or with both 1- and 2-DoF trials. The testing paradigms were: testing on 1-DoF trials or on 2-DoF trials. When testing 2-DoF models using 1-DoF tasks, the unused dimension remained near a value of zero. These 1-DoF tests were intended to determine if 2-DoF models could still perform well when encountering 1-DoF tasks. Two DoF models with eight backward selected electrodes also compared to models with the eight pre-selected electrodes. Again, only subject-specific models were studied using pre-selection, as a function of training duration, for each DoF pair (using two-fold cross-validation).

A-4.2 Statistics

Performance differences were tested statistically with SPSS 25 using multivariate repeated measures analysis of variance (RANOVA), assessing all possible interactions. Interactions were not significant, unless noted. When degree of sphericity ε was <0.75, degrees of freedom was adjusted by the method of Greenhouse-Geisser; and when $0.75 \leq \varepsilon < 1$, it was adjusted by the method of Huynh-Feldt [13]. For brevity, when multiple comparisons are summarized, degrees of freedom are reported without adjustment, since the adjusted values vary within each comparison. *Post hoc* pair-wise comparisons were conducted using paired *t*-tests with Bonferroni correction for multiple comparisons. A significance level of $p = 0.05$ was used.

A-4.3 Results

A-4.3.1 One-DoF Models, Backward Selected Locations

Figs. A-4.3–5 show summary test error results after calibrating subject-specific, DoF-specific and universal models, respectively, plotted separately for each of the four DoFs, as a function of training duration for each number of backward selected electrodes. All models experienced lower mean error as training duration increased from 14 seconds, with less improvement as training duration grew.

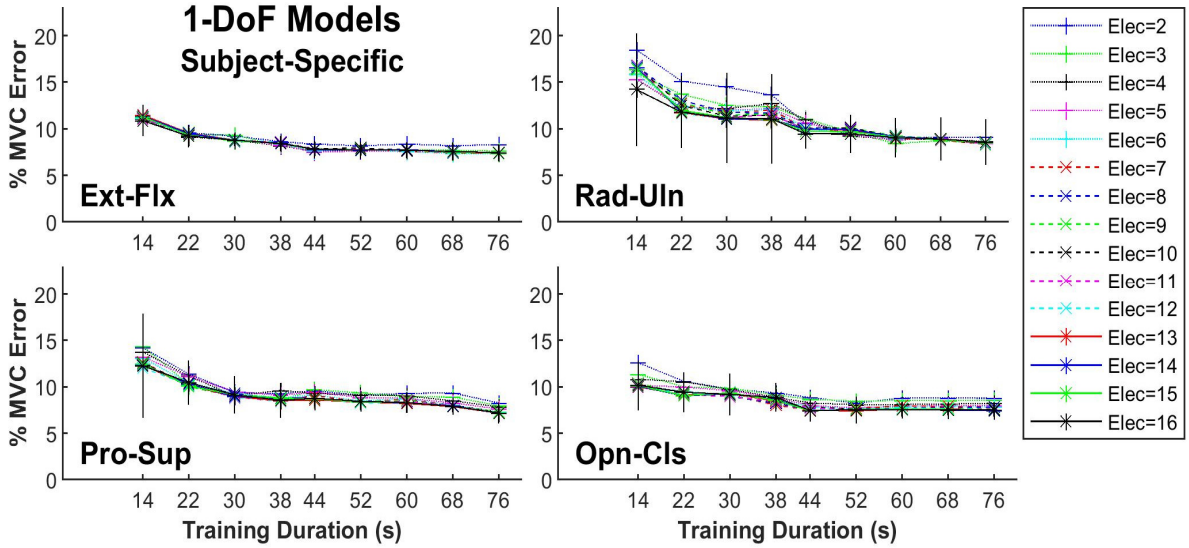

Fig. A-4. 3. One-DoF summary error results after calibrating dynamic models to each subject, presented separately for each DoF as a function of training duration for each number of backward selected electrodes. Mean values shown by markers. Vertical lines show standard deviations only for the 16-electrode models. Standard deviations for other numbers of electrodes were similar.

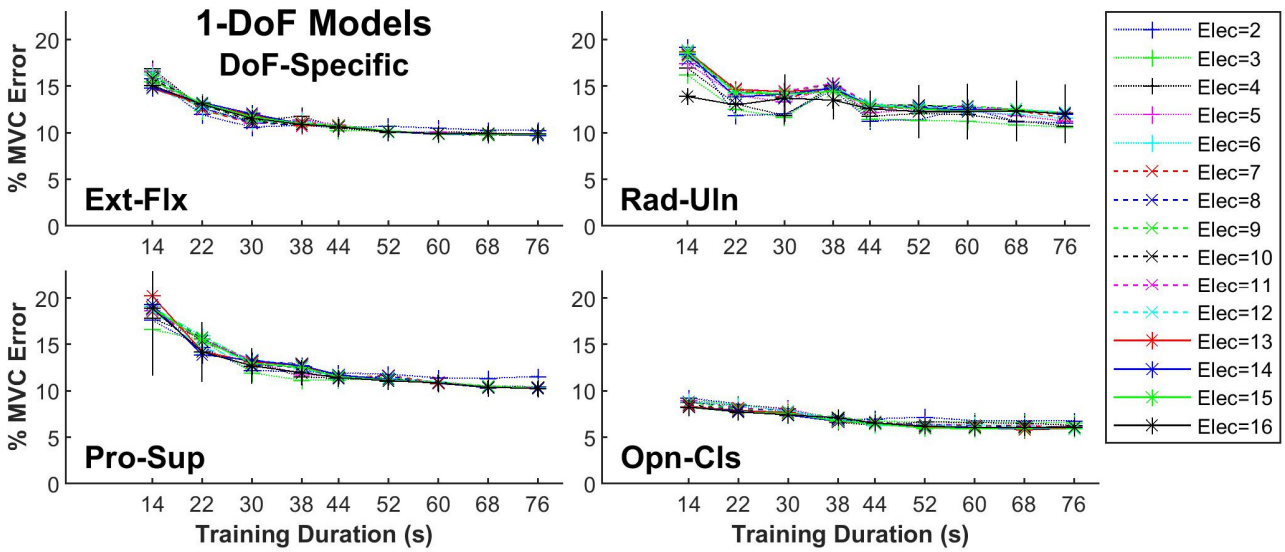

Fig. A-4. 4. One-DoF summary error results after calibrating dynamic models to each DoF, presented separately for each DoF as a function of training duration for each number of backward selected electrodes. Mean values shown by markers. Vertical lines show standard deviations only for the 16-electrode models. Standard deviations for other numbers of electrodes were similar.

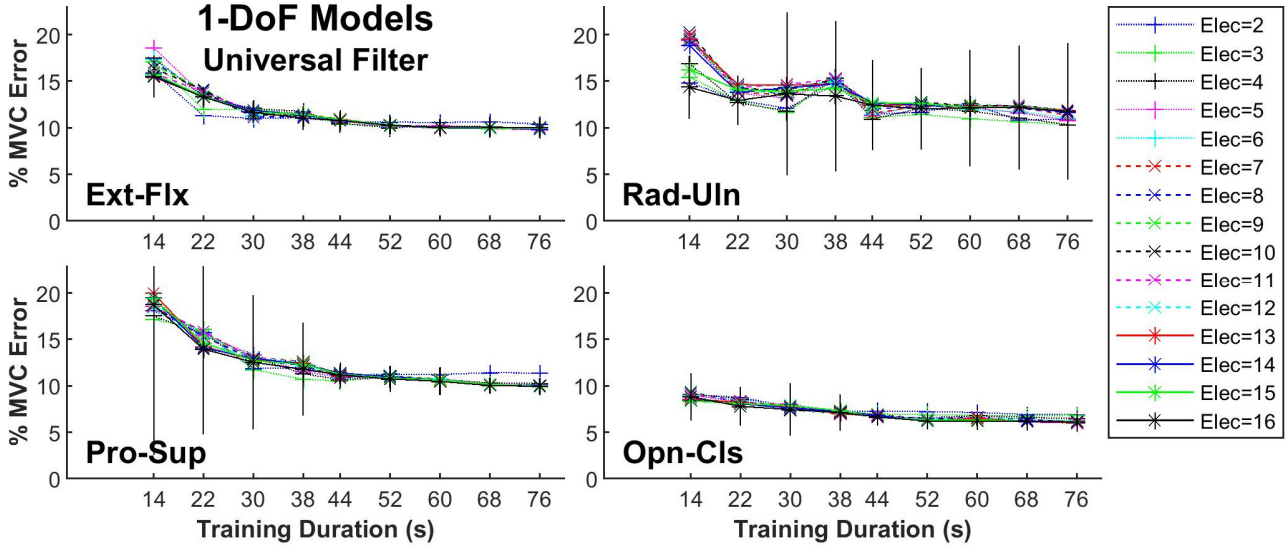

Fig. A-4. 5. One-DoF summary error results after calibrating dynamic models to universal filter, presented separately for each DoF as a function of training duration for each number of backward selected electrodes. Mean values shown by markers. Vertical lines show standard deviations only for the 16-electrode models. Standard deviations for other numbers of electrodes were similar.

Using all the results of 1-DoF models, a four-way RANOVA was computed [factors: model (subject-specific, DoF-specific, universal), number of electrodes (2–16), duration (14, 22, 30, 38, 44, 52, 60, 68, 76 s) and DoF (Flx-Ext, Rad-Uln, Pro-Sup, Opn-Cls)]. Since there was a significant

two way interaction term involving model and DoF [F(2.696, 21.569) = 6.822, p_{GG}=0.003] three way RANOVA's were implemented fixing each DoF. DoF was fixed because we wanted to study the effect of the model, electrode and duration for each of the different motions. Summarizing these four RANOVA's, the main effects of model [F(2,16)>6.9, $p \leq 0.03$] and duration [F(8,64)>5, $p \leq 0.04$] were significant, however the number of electrodes was not [F(14,112)<3.5, p>0.07]. Tukey *post hoc* comparisons were computed for all four three-way RANOVA's. When comparing the 1-DoF models, Fig. A-4.6 summarizes the rank order of the %MVC errors for each DoF, as well as the significant differences. The trends were mixed, with the subject-specific model having significantly lower error for three of the four DoFs. Fig. A-4.7 depicts the significant differences between durations. There was a general trend for higher %MVC errors at shorter training durations versus longer durations. For example, training with 14 s always exhibited higher error than ≥ 30s and training with 22 s always exhibited higher error than ≥ 68s.

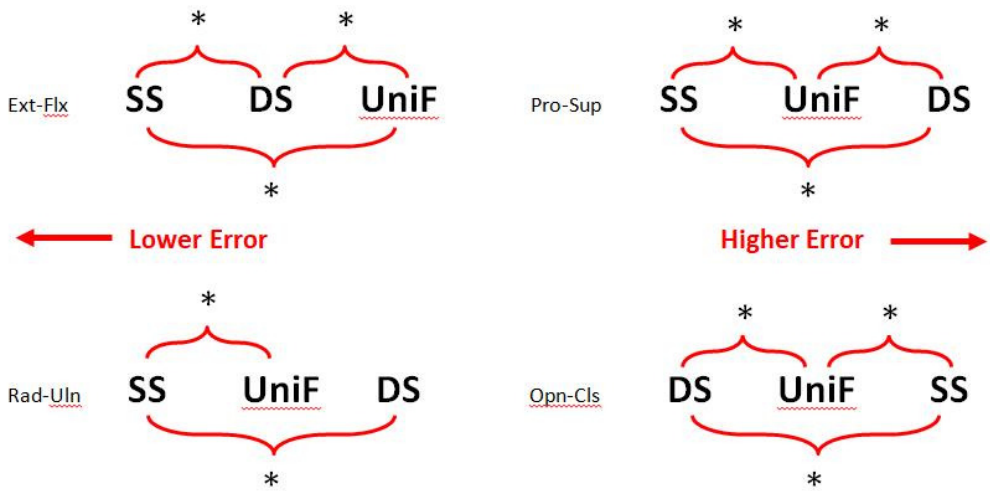

Fig. A-4. 6. Rank order of errors (left ➔ lower error) for different models and DoFs. Star indicates statistically significant difference. SS= Subject-Specific, DS = DoF Specific, UniF = Universal Filter.

	14s	22s	30s	38s	44s	52s	60s	68s
22s	*							
30s	*	*						
38s	*	*						
44s	*	*						
52s	*	*	*		*			
60s	*	*	*	*	*	*		
68s	*	*	*	*	*	*		
76s	*	*	*	*	*	*		

ExtFlx

	14s	22s	30s	38s	44s	52s	60s	68s
22s	*							
30s	*							
38s	*							
44s	*	*						
52s	*	*						
60s	*	*						
68s	*	*						
76s	*	*	*					

RadUln

	14s	22s	30s	38s	44s	52s	60s	68s
22s	*							
30s	*	*						
38s	*	*						
44s	*							
52s	*							
60s	*				*			
68s	*	*			*	*	*	
76s	*	*			*	*	*	

ProSup

	14s	22s	30s	38s	44s	52s	60s	68s
22s								
30s	*	*						
38s	*	*						
44s	*	*	*					
52s	*	*	*		*			
60s	*	*	*		*			
68s	*	*	*					
76s	*	*	*		*	*		

OpnCls

Fig. A-4. 7. Statistical differences between durations. Star indicates that the difference is significant while blank cell indicates that the difference is not. When significant, the shorter duration always had higher error.

A-4.3.2. One-DoF Models, Eight Pre-Selected Locations

When using the eight pre-selected locations, Fig. A-4.8 shows summary test error results for only subject-specific models, plotted separately for each of the four DoFs, as a function of training duration. All models experienced lower mean error as training duration increased from 14 seconds, with less improvement as training duration grew. Using all the results of the *preselected* eight electrodes versus eight *backward stepwise selected* electrodes, a three way RANOVA was computed [factors: site selection (pre-selected, backward selected), duration (14, 22, 30, 38, 44, 52, 60, 68, 76 s) and DoF (Ext-Flx, Rad-Uln, Pro-Sup, Opn-Cls)]. The main effects of site selection [$F(1,7) = 9.499$, $p=0.018$], duration [$F(8,56) = 51$, $p=0.0001$] and DoF [$F(3,21)=2.6$, $p=0.014$] were significant.

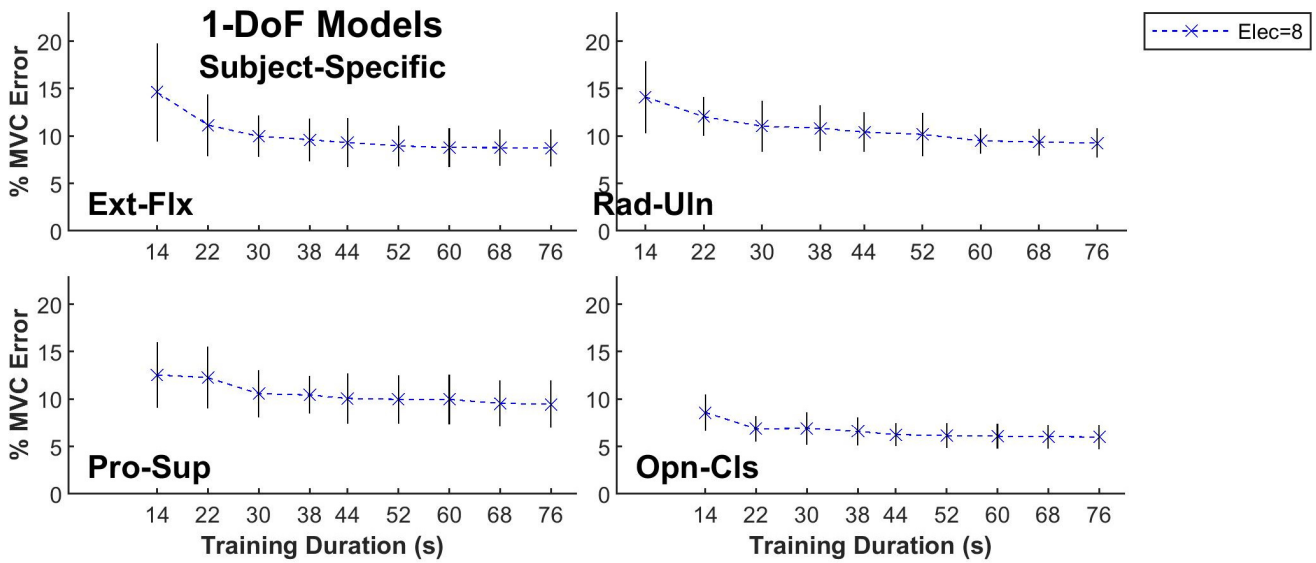

Fig. A-4. 8. One-DoF summary error results for preselected eight electrodes versus duration, presented separately for each DoF as a function of training duration. Mean values shown by markers. Vertical lines show standard deviation.

Tukey post hoc comparison for site selection was not necessary, since only two methods were tested and found to be statistically different. Eight preselected sites had a mean error of 9.02 %MVC, while backward selected sites had a mean error of 10.15 %MVC.. Post hoc evaluations for duration and DoF are not reported since our primary interest in this sub-analysis was in the site selection techniques (and because the results are similar to above).

A-4.3.3. Two-DoF Models, Backward Selected Locations

Figs. A-4.9–11 show summary test error results after calibrating subject-specific, DoF-specific and universal models, respectively, plotted separately for each of the three DoF pairs, as a function of training duration for each number of backward selected electrodes. All models experienced generally lower error as training duration increased from 14 seconds, with less improvement as training duration grew.

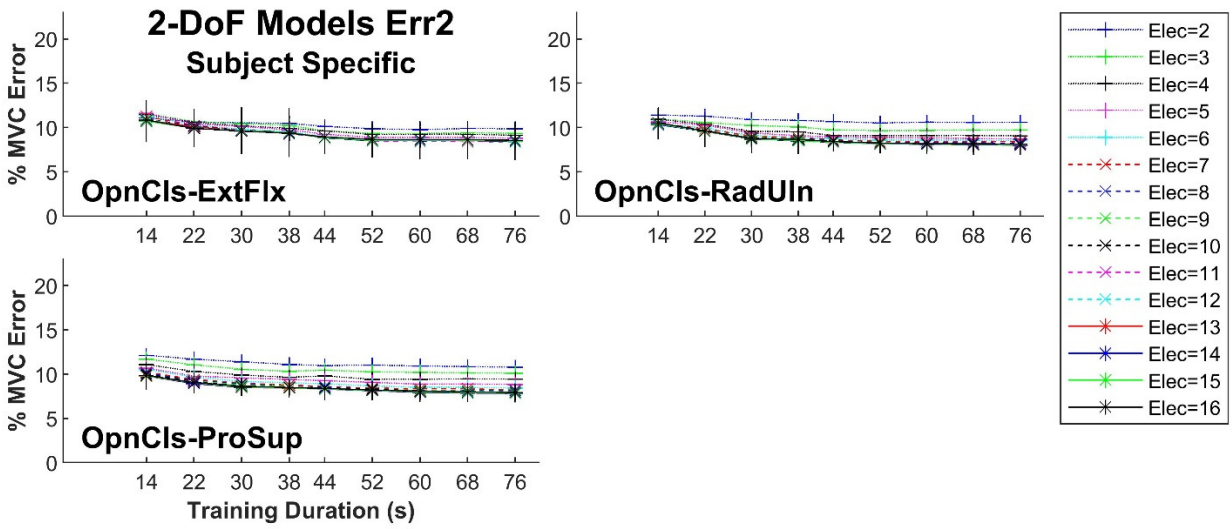

Fig. A-4. 9. Two-DoF summary error results after calibrating dynamic models to each subject, presented separately for each DoF pair as a function of training duration for each number of backward selected electrodes. Mean values shown by markers. Vertical lines show standard deviations only for the 16-electrode models. Standard deviations for other numbers of electrodes were similar.

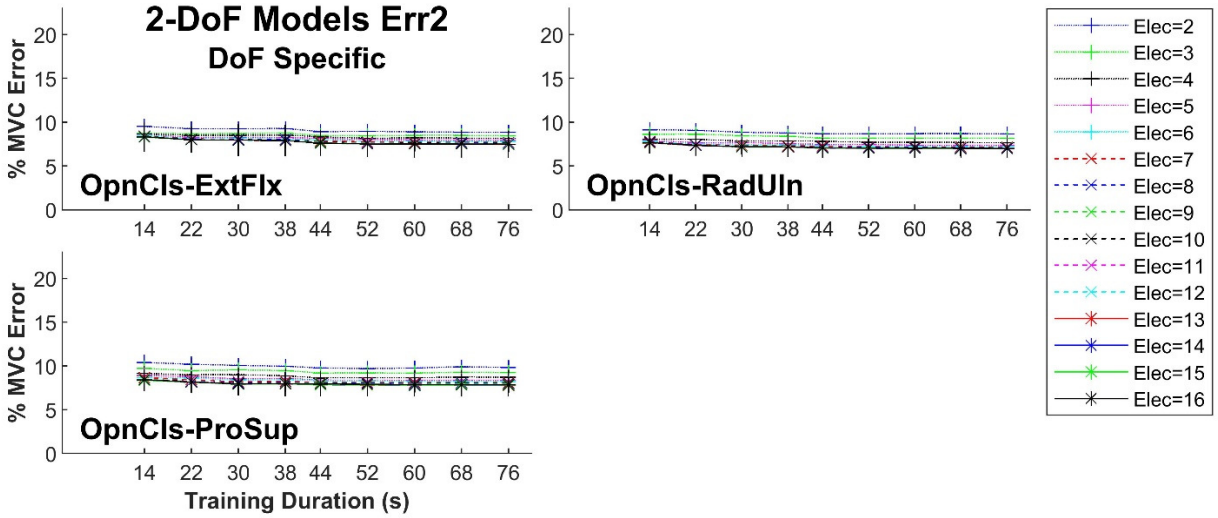

Fig. A-4. 10. Two-DoF summary error results after calibrating dynamic models to each DoF pair, presented separately for each DoF pair as a function of training duration for each number of backward selected electrodes. Mean values shown by markers. Vertical lines show standard deviations only for the 16-electrode models. Standard deviations for other numbers of electrodes were similar.

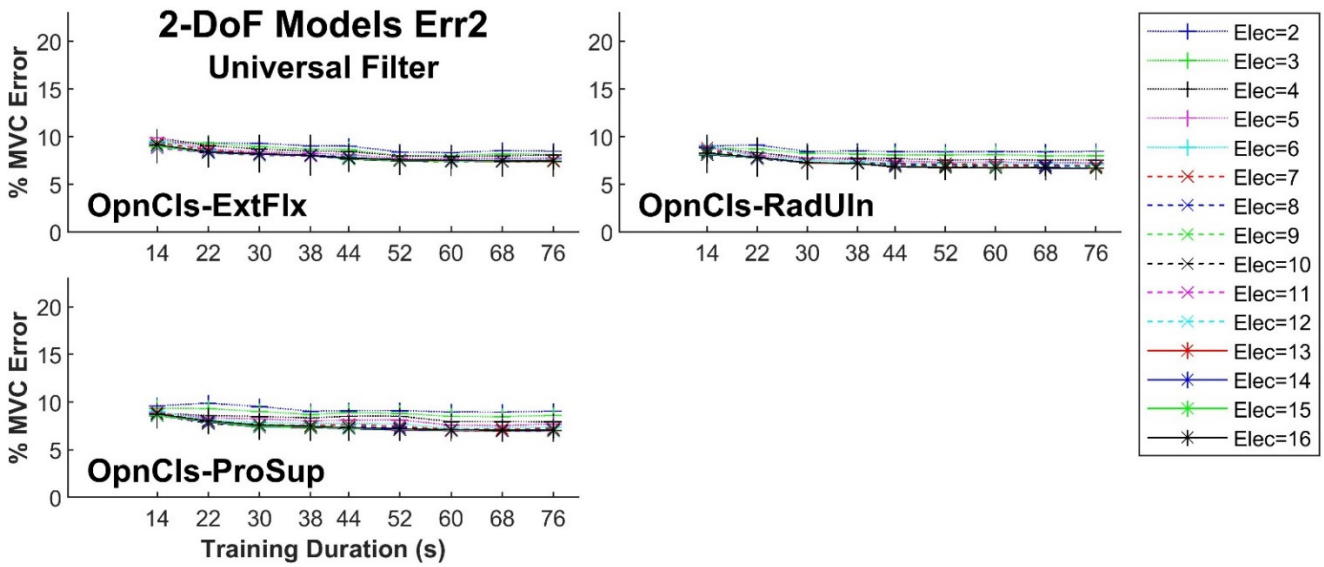

Fig. A-4. 11. Two-DoF summary error results after calibrating dynamic models to universal filter, presented separately for each DoF pair as a function of training duration for each number of backward selected electrodes. Mean values shown by markers. Vertical lines show standard deviations only for the 16-electrode models. Standard deviations for other numbers of electrodes were similar.

Using all the results of 2-DoF models, a four-way RANOVA was computed [factors: model (subject-specific, DoF-specific, universal), number of electrodes (2–16), duration (14, 22, 30, 38, 44, 52, 60, 68, 76 s) and DoF pair (OpnCls with Flx-Ext, OpnCls with Rad-Uln, OpnCls with Pro-Sup). There were significant interactions involving all factors. Thus, three way RANOVA's were implemented fixing each DoF pair. Summarizing these three RANOVA's, the main effects of model for ExtFlx-OpnCls and RadUln-OpnCls [$F(2,16)>6.38$, $p\leq0.04$] electrode [$F(14,112)>13.5$ $p\leq0.001$] and duration [$F(8,64)>7.89$, $p_{GG}\leq0.001$] were significant; however, model for ProSup-OpnCls was not [$F(2,16)=4.26$ $p=0.058$]

Tukey *post hoc* comparisons were computed for all significant differences. When comparing the 2-DoF models, the DOF-specific models always had the lowest error, followed by the Subject-Specific models, followed by the Universal Filter models. When comparing the 2-DoF number of electrodes, Fig. A-4.12 summarizes the significant differences. The trend was for higher error at smaller numbers of electrodes, with 2, 3 and 4 electrodes always having more error than when compared to more electrodes. Further, for all models there were no significant differences when comparing 10 electrodes to more than 10. When comparing durations, Fig. A-4.13 depicts the significant differences. There was a general trend for higher errors at shorter training durations

versus longer durations. For example, training with 14 s always exhibited higher error than ≥ 30s and training with 22 s always exhibited higher error than ≥ 44s. There was no significant RMS error difference for durations of ≥44 s for Opn-Cls with Flx-Ext, ≥52 s for Opn-Cls with Rad-Uln, and ≥60 s for Opn-Cls with Pro-Sup.

	E2	E3	E4	E5	E6	E7	E8	E9	E10	E11	E12	E13	E14	E15
E3														
E4	*													
E5	*	*	*											
E6	*	*	*	*										
E7	*	*	*	*										
E8	*	*	*	*	*									
E9	*	*	*	*										
E10	*	*	*	*										
E11	*	*	*	*										
E12	*	*	*											
E13	*	*	*											
E14	*	*	*											
E15	*	*	*											
E16	*	*	*											

ExtFlx-OpnCls

	E2	E3	E4	E5	E6	E7	E8	E9	E10	E11	E12	E13	E14	E15
E3	*													
E4	*	*												
E5	*	*	*											
E6	*	*	*	*										
E7	*	*	*	*	*									
E8	*	*	*	*	*	*								
E9	*	*	*	*	*	*								
E10	*	*	*	*	*	*								
E11	*	*	*	*	*	*								
E12	*	*	*	*	*	*								
E13	*	*	*	*	*	*								
E14	*	*	*	*	*	*								
E15	*	*	*	*	*	*								
E16	*	*	*	*	*	*								

ProSup-OpnCls

	E2	E3	E4	E5	E6	E7	E8	E9	E10	E11	E12	E13	E14	E15
E3	*													
E4	*	*												
E5	*	*	*											
E6	*	*	*	*										
E7	*	*	*	*										
E8	*	*	*	*										
E9	*	*	*	*	*									
E10	*	*	*	*	*	*	*	*						
E11	*	*	*	*	*	*	*	*						
E12	*	*	*	*	*	*	*	*						
E13	*	*	*	*	*	*	*	*						
E14	*	*	*	*	*	*	*	*						
E15	*	*	*	*	*	*	*							
E16	*	*	*	*	*	*	*							

RadUln-OpnCls

Fig. A-4. 12. Statistical differences between number of electrodes. Star indicates that the difference is significant while blank cell indicates that the difference is not. When significant, the smaller number of electrodes always had higher error.

	14s	22s	30s	38s	44s	52s	60s	68s
22s	*							
30s	*							
38s	*							
44s	*	*						
52s	*	*	*					
60s	*	*	*	*				
68s	*	*	*	*				
76s	*	*	*	*				

ExtFlx-OpnCls

	14s	22s	30s	38s	44s	52s	60s	68s
22s	*							
30s	*	*						
38s	*	*						
44s	*	*						
52s	*	*		*				
60s	*	*	*	*	*			
68s	*	*	*	*	*			
76s	*	*	*	*	*	*		

ProSup-OpnCls

	14s	22s	30s	38s	44s	52s	60s	68s
22s	*							
30s	*	*						
38s	*	*						
44s	*	*						
52s	*	*	*		*			
60s	*	*	*	*	*			
68s	*	*	*	*	*			
76s	*	*	*	*	*			

RadUln-OpnCls

Fig. A-4. 13. Statistical differences between durations Star indicates that the difference is significant while blank cell indicates that the difference is not. When significant, the shorter duration always had higher error.

A-4.3.4 Two-DoF Models, Eight Pre-Selected Locations

When using the eight pre-selected locations, Fig. A-4.14 shows summary test error results for only subject-specific models, plotted separately for each of the three DoF pairs, as a function of training duration. All models experienced lower mean error as training duration increased from 14 seconds, with less improvement as training duration grew. Using all the results of the *preselected* eight electrodes versus eight *backward stepwise selected* electrodes, a three way RANOVA was computed [factors: site selection (pre-selected, backward selected), duration and DoF pair (OpnCls-ExtFlx, OpnCls-RadUln, OpnCls-ProSup)]. The main effects of site selection [$F(1,8) = 2.0$, $p=0.20$] and DoF [$F(2,16) = 0.36$, $p=0.68$] were not significant, but duration [$F(8,64) = 40.6$, $p=0.0001$] was significant. *Tukey post hoc* comparisons for duration are not reported since our primary interest in this sub-analysis was in the site selection techniques.

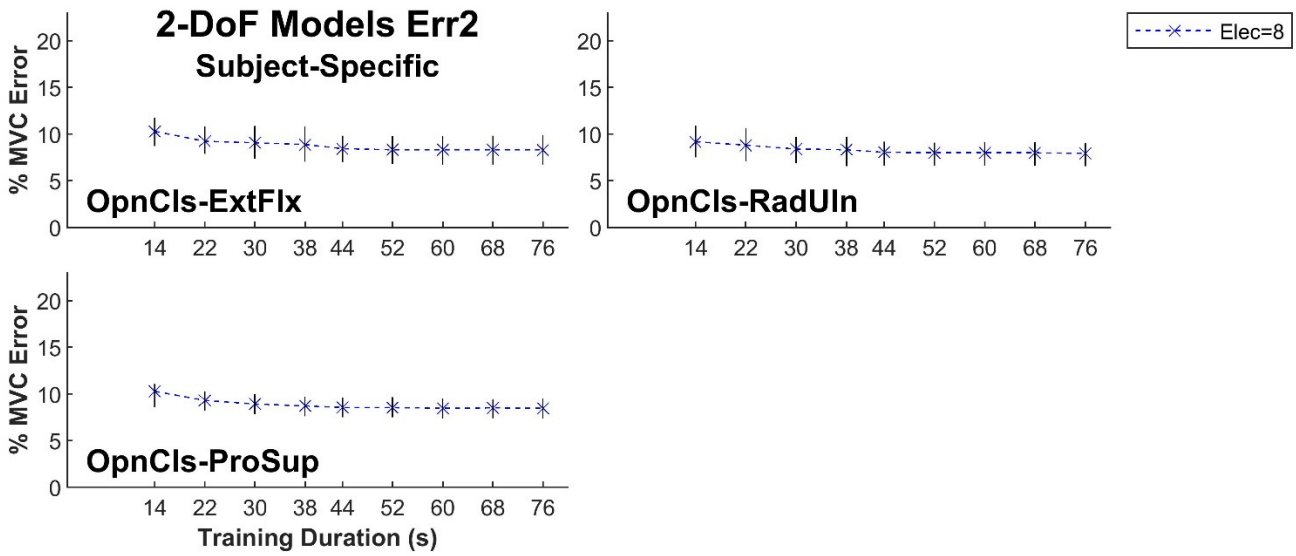

Fig. A-4. 14. Two-DoF summary error results for preselected eight electrodes versus duration, presented separately for each DoF as a function of training duration. Mean values shown by markers. Vertical lines show standard deviation.

REFERENCES

[1] C. Dai, Z. Zhu, C. Martinez-Luna, T. R. Hunt, T. R. Farrell, and E. A. Clancy, "Two degrees of freedom, dynamic, hand-wrist EMG-force using a minimum number of electrodes," *J. Electromyo. Kinesiol.,* vol. 47, pp. 10–18, 2019.

[2] L. Ljung, "System Identification: Theory for the User," Upper Saddle River, NJ: Prentice-Hall, 1999, pp. 1–8, 408–452, 491–519.

[3] E. A. Clancy, O. Bida, and D. Rancourt, "Influence of advanced electromyogram (EMG) amplitude processors on EMG-to-torque estimation during constant-posture, force-varying contractions," *J. Biomech.,* vol. 39, pp. 2690–2698, 2006.

[4] K. Koirala, M. Dasog, P. Liu, and E. A. Clancy, "Using the electromyogram to anticipate torques about the elbow," *IEEE Trans. Neural Sys. Rehabil. Eng.,* vol. 23, no. 3, pp. 396–402, 2015.

[5] E. A. Clancy, L. Liu, P. Liu, and D. V. Moyer, "Identification of constant-posture EMG-torque relationship about the elbow using nonlinear dynamic models," *IEEE Trans. Biomed. Eng.,* vol. 59, no. 1, pp. 205–212, 2012.

[6] W. H. Press, B. P. Flannery, S. A. Teukolsky, and W. T. Vetterling, "Numerical Recipies in C," 2nd ed., New York: Cambridge Univ. Press, 1994, pp. 671–681.

[7] E. A. Clancy, C. Martinez-Luna, M. Wartenberg, C. Dai, and T. Farrell, "Two degrees of freedom quasi-static EMG-force at the wrist using a minimum number of electrodes," *J Electromyogr Kinesiol,* vol. 34, pp. 24–36, 2017.

[8] E. A. Clancy, F. Negro, and D. Farina, "Single-channel techniques for information extraction from the surface EMG signal," in *Surface Electromyography: Physiology, Engineering, and Applications*, R. Merletti and D. Farina, Eds.: John Wiley & Sons, Inc., 2016, pp. 91–125.

[9] A. L. Hof and J. Van den Berg, "EMG to force processing I: An electrical analogue of the Hill muscle model," *J. Biomech.,* vol. 14, no. 11, pp. 747–758, 1981.

[10] V. T. Inman, H. J. Ralston, J. B. Saunders, B. Feinstein, and E. W. Wright, "Relation of human electromyogram to musculuar tension," *EEG Clin. Neurophysiol.,* vol. 4, no. 2, pp. 187–194, 1952.

[11] D. A. Winter and H. J. Yack, "EMG profiles during normal human walking: Stride-to-stride and inter-subject variability," *Electroenceph Clin Neurophysiol,* vol. 67, pp. 402–411, 1987.

[12] D. A. Winter, "Biomechanics and Motor Control of Human Movement, 3rd edition," Hoboken, NJ: John Wiley & Sons, Inc., 2005, pp. 203–260.

[13] E. R. Girden, "ANOVA: Repeated Measures," Sage Publications, 1992, p. 21.

Appendix 5: Backward Selection Electrodes' Comparison

FOUR ELECTRODES

FULL CALIBRATION

Number of electrode matches between cross-validations (exact match, off by <= 1, off by <= 2, off by <= 3).

	Exact Match	Within One Electrod	Within Two Electrode	Within Three Electrodes
1	3	3	4	4
2	4	4	4	4
3	3	4	4	4
4	3	3	4	4
5	2	3	3	4
6	2	3	4	4
7	3	3	4	4
8	3	4	4	4
9	3	3	4	4
10	2	2	3	4
11	1	1	2	2
12	2	2	4	4
13	3	3	4	4
14	3	4	4	4
15	3	3	3	3
16	3	3	3	3
17	0	2	3	4
18	3	3	3	3
19	4	4	4	4
20	3	4	4	4
21	2	3	4	4
22	3	3	3	4
23	3	4	4	4
24	1	3	3	3
25	4	4	4	4
26	2	3	4	4
27	3	3	4	4
Mean	2.63	3.11	3.63	3.78
Std	0.93	0.75	0.56	0.51

Between repeated backward selection iterations (i.e. run the iteration twice) 1-9 Flx-Ext & Opm-Cls, 10-18 Rad-Uln & Opn-Cls 19-27 Pro-Sup & Opn-Cls

UNIVERSAL FILTER

Number of electrode matches between cross-validations (exact match, off by <= 1, off

	Exact Match	Within One Electrod	Within Two Electrode	Within Three Electrode
1	3	3	4	4
2	4	4	4	4
3	4	4	4	4
4	3	3	4	4
5	2	3	3	4
6	2	3	4	4
7	2	3	4	4
8	2	4	4	4
9	2	2	3	3
10	3	3	4	4
11	1	1	2	2
12	2	2	4	4
13	3	3	3	4
14	1	4	4	4
15	3	3	3	3
16	2	3	3	4
17	0	2	2	2
18	1	2	2	2
19	3	3	3	3
20	2	3	4	4
21	1	4	4	4
22	3	4	4	4
23	3	4	4	4
24	0	3	3	4
25	3	3	3	3
26	2	3	3	4
27	3	3	4	4
Mean	2.22	3.04	3.44	3.63
Std	1.05	0.76	0.70	0.69

SIX ELECTRODES

FULL CALIBRATION

Number of electrode matches between cross-validations (exact match, off by <= 1, off by <= 2, off by <= 3).

	Exact Match	Within One Electrod	Within Two Electrode	Within Three Electrodes
1	5	5	5	5
2	6	6	6	6
3	3	5	5	6
4	5	5	5	5
5	4	4	4	5
6	5	6	6	6
7	5	6	6	6
8	5	6	6	6
9	5	5	6	6
10	3	4	5	5
11	3	4	5	5
12	4	6	6	6
13	5	5	6	6
14	4	5	6	6
15	5	6	6	6
16	4	5	5	5
17	0	3	5	6
18	6	6	6	6
19	6	6	6	6
20	3	4	5	5
21	4	6	6	6
22	6	6	6	6
23	3	4	4	4
24	3	5	5	5
25	5	5	5	6
26	3	5	5	5
27	5	5	6	6
Mean	4.26	5.11	5.44	5.59
Std	1.35	0.85	0.64	0.57

Between repeated backward selection iterations (i.e. run the iteration twice) 1-9 Flx-Ext & Opn-Cls, 10-18 Rad-Uln & Opn-Cls 19-27 Pro-Sup & Opn-Cls

UNIVERSAL FILTER

Number of electrode matches between cross-validations (exact match, off by <= 1, off

	Exact Match	Within One Electrod	Within Two Electrode	Within Three Electrode
1	4	4	4	4
2	6	6	6	6
3	4	4	4	5
4	4	4	4	4
5	4	5	5	5
6	5	6	6	6
7	3	5	6	6
8	3	4	5	5
9	5	5	5	6
10	4	4	4	4
11	3	3	4	4
12	4	4	6	6
13	5	5	5	5
14	2	5	6	6
15	4	5	5	6
16	3	4	6	6
17	0	5	5	5
18	5	6	6	6
19	5	5	6	6
20	4	5	5	5
21	3	5	5	5
22	5	5	5	5
23	4	5	5	5
24	3	6	6	6
25	3	4	4	5
26	3	5	6	6
27	6	6	6	6
Mean	3.85	4.81	5.19	5.33
Std	1.26	0.79	0.79	0.73

FOUR ELECTRODES

FULL CALIBRATION

Number of electrode matches between cross-validations (exact match, off by <= 1, off by <= 2, off by <= 3).

	Exact Match	Within One Electrod	Within Two Electrode	Within Three Electrodes
1	4	4	4	4
2	4	4	4	4
3	3	4	4	4
4	3	4	4	4
5	4	4	4	4
6	2	2	4	4
7	4	4	4	4
8	3	4	4	4
9	4	4	4	4
10	4	4	4	4
11	4	4	4	4
12	4	4	4	4
13	4	4	4	4
14	2	4	4	4
15	4	4	4	4
16	2	4	4	4
17	2	2	2	3
18	2	4	4	4
19	4	4	4	4
20	3	3	4	4
21	3	3	4	4
22	4	4	4	4
23	4	4	4	4
24	3	4	4	4
25	2	3	3	3
26	3	3	3	3
27	4	4	4	4
Mean	3.30	3.70	3.85	3.89
Std	0.82	0.61	0.46	0.32

Between backward selection cross validation (i.e. run the selection once and compare between two cross validated electrodes) 1-9 Flx-Ext & Opn-Cls,10-18 Rad-Uln & Opn-Cls 19-27 Pro-Sup & Opn-Cls

UNIVERSAL FILTER

Number of electrode matches between cross-validations (exact match, off by <= 1, off

	Exact Match	Within One Electrod	Within Two Electrode	Within Three Electrode
1	4	4	4	4
2	4	4	4	4
3	4	4	4	4
4	4	4	4	4
5	4	4	4	4
6	4	4	4	4
7	3	4	4	4
8	3	4	4	4
9	3	3	3	3
10	3	3	3	3
11	4	4	4	4
12	4	4	4	4
13	4	4	4	4
14	4	4	4	4
15	4	4	4	4
16	4	4	4	4
17	3	3	4	4
18	4	4	4	4
19	3	3	3	3
20	3	3	3	3
21	4	4	4	4
22	3	3	3	4
23	4	4	4	4
24	3	3	3	3
25	2	2	2	3
26	1	2	2	2
27	4	4	4	4
Mean	3.48	3.59	3.63	3.70
Std	0.75	0.64	0.63	0.54

SIX ELECTRODES

FULL CALIBRATION

Number of electrode matches between cross-validations (exact match, off by <= 1, off by <= 2, off by <= 3).

	Exact Match	Within One Electrod	Within Two Electrode	Within Three Electrodes
1	5	5	5	5
2	6	6	6	6
3	5	6	6	6
4	4	5	5	5
5	5	5	5	5
6	6	6	6	6
7	5	5	5	6
8	5	5	5	5
9	5	5	5	5
10	5	5	5	5
11	6	6	6	6
12	6	6	6	6
13	5	5	5	5
14	4	6	6	6
15	5	5	5	5
16	4	5	6	6
17	5	5	5	6
18	5	6	6	6
19	5	5	5	5
20	4	4	6	6
21	6	6	6	6
22	6	6	6	6
23	6	6	6	6
24	4	5	6	6
25	4	6	6	6
26	4	4	6	6
27	5	5	5	6
Mean	5.00	5.33	5.56	5.67
Std	0.73	0.62	0.51	0.48

Between backward selection cross validation (i.e. run the selection once and compare between two cross validated electrodes) 1-9 Flx-Ext & Opn-Cls,10-18 Rad-Uln & Opn-Cls 19-27 Pro-Sup & Opn-Cls

UNIVERSAL FILTER

Number of electrode matches between cross-validations (exact match, off by <= 1, off

	Exact Match	Within One Electrod	Within Two Electrode	Within Three Electrode
1	6	6	6	6
2	6	6	6	6
3	5	5	5	5
4	4	4	4	4
5	5	5	5	5
6	6	6	6	6
7	4	5	5	5
8	4	5	5	5
9	5	5	5	5
10	5	5	5	5
11	6	6	6	6
12	6	6	6	6
13	6	6	6	6
14	6	6	6	6
15	6	6	6	6
16	6	6	6	6
17	6	6	6	6
18	6	6	6	6
19	5	5	5	6
20	5	5	6	6
21	6	6	6	6
22	4	4	5	6
23	5	5	5	5
24	5	5	5	6
25	5	5	5	6
26	4	5	5	5
27	6	6	6	6
Mean	5.30	5.41	5.48	5.63
Std	0.78	0.64	0.58	0.56

Appendix 6: Clinical Documents

A-6.1: Informed Consent

INFORMED CONSENT TO TAKE PART IN A RESEARCH STUDY

TITLE OF THIS STUDY:	**Relating Arm Muscle Electrical Activity to Hand/Finger Forces for use in Prosthesis Control and Stroke Rehabilitation Devices**
STUDY PRINCIPAL INVESTIGATOR:	**Edward A. Clancy, Ph.D.** **508-831-5778**
PROJECT SPONSOR:	**Worcester Polytechnic Institute (WPI)**

Introduction
You are being asked to participate in a research study to be conducted at Worcester Polytechnic Institute. It is important that you read the following explanation of the proposed procedures. This form describes the purpose, procedures, benefits, risks, discomforts and precautions of the study. It also describes the alternative procedures that are available to you and your right to withdraw from the study at any time.

Purpose of the Study
When muscles in your forearm contract, they produce a small electrical signal that can be recorded. Some individuals who wear a prosthetic hand are able to control their hand using the electrical activity of remnant muscles from their forearm. Some people who have a stroke lose some of their ability to move their hands properly. In each condition, electrical activity in the forearm is related to forces produced in the hand/fingers. In this project, we are trying to develop a new technique for using these electrical signals to control a hand prosthesis and/or to aid therapy in stroke victims. This particular study will collect forearm muscle electrical activity and hand/wrist force recordings. These recordings will be used to develop our new technique in able-bodied people, such as yourself, who do not wear a hand prosthesis and have not experienced a stroke. If successful, the new technique may be tested in the future by prosthesis users and/or stroke patients. A total of up to 50 able-bodied people will volunteer as subjects in this experiment.

Experimental Protocol
You will be asked to complete a short subject questionnaire. After completing this questionnaire, you will be seated in a chair and secured using quick-release belts (similar to tightly worn seat-belts in an automobile). Your arm will be held in front and the side of you, supported at the elbow. Your hand and fingers will be tightly secured into a measurement device. Your forearm will be wiped with an alcohol wipe and then approximately 16 surface

recording electrodes will be secured around your forearm. These electrodes measure the electrical activity as represented at the surface of your skin. Then, you will be asked to perform a variety of muscle force tasks by pushing/pulling with your fingers, hand and/or wrist against the measurement device. A few of the tasks will require your maximum possible effort for a few seconds. Most tasks will require much less effort. Rest (2–3 minutes) will be provided between tasks, as necessary, so that you can easily maintain your muscle effort while competing all of the contraction tasks. Your participation will last for about four hours.

Benefits
There is no direct benefit to you for participating in this study.

Risks
There is some possibility of minor discomfort due to the postural restraints. There is a risk of skin irritation from the skin preparation required for the electrodes and from the tape used to secure the electrodes to your skin. You should expect some muscle soreness to develop as a consequence of contracting your muscles. You may also experience mental fatigue from the concentration required to complete the tasks. The risks to pregnant women and fetuses are unknown and therefore pregnant women should not participate in the study.

Medical Care if Injured
WPI assumes no responsibility to pay for any injuries that you might receive as a result of participating in this research study. No funds have been set aside for payments or other forms of compensation (such as for lost wages, lost time, or discomfort). If you suffer a physical injury as a result of your participation in this study, you may chose to seek medical care in the same way as you would normally. If your insurance does not cover the cost then you may be responsible for this cost. However, you do not give up any of your legal rights by signing this consent form.

Participation
Your participation in the study is voluntary. You are free to withdraw consent and discontinue participation at any time without penalty. You are free to seek further information regarding the experiment at any time. The project investigators retain the right to cancel or postpone the experimental procedures at any time they see fit.

Confidentiality
Records of your participation in this study will be held confidential so far as permitted by law. However, the study investigators and, under certain circumstances, the Food and Drug Administration (FDA) and the Worcester Polytechnic Institute Institutional Review Board (WPI IRB) will be able to inspect and have access to confidential data that identify you by name. Any publication or presentation of the data will not identify you.

Withdrawal
Data obtained in this experiment will become the property of the investigators and WPI. If you withdraw from the study, data already collected from you will remain in the study.

Data Reuse and Contribution of Your Data to a Public Data Archive

The data from this experiment will also be contributed to publicly available databases and/or reused by the study investigators in future research. The purpose of this data reuse is to share your data with other researchers (or reuse the data ourselves) to make further advances in medicine, science and teaching. Your data could be used for many different purposes. Most researchers will gain access to your data over the Internet. Before contributing your data, all information that identifies you as a subject in this experiment (including your name) will be coded using a random code. The only way to relate the code to yourself is by a "key" that the study investigators will maintain private. We will never reveal your identity, unless required to do so by law. The public database will not provide any direct access to your identity.

Questions
This study will be directly supervised by Edward A. Clancy. Questions or comments about participation should be directed to Edward A. Clancy at (508) 831-5778 (E-mail: ted@wpi.edu). You may also contact the Chair of the WPI IRB, Professor Kent Rissmiller at (508) 831-5019 (E-mail: kjr@wpi.edu); or the University Compliance Officer, Michael J. Curley at (508) 831-6919 (E-mail: mjcurley@wpi.edu).

Cost/Payment
You will receive $25 for completion of the study. If the experimental session is not completed, you will be paid $8 per completed hour (not to exceed $25).

For Employees of WPI:
Your participation in this study is voluntary. You are free to withdraw your consent and discontinue participation in this study at any time without prejudice or penalty. Your decision to participate or not participate in this study will in no way affect your continued employment or your relationship with individuals who may have an interest in this study. _____initials

(*Please note you will be participating in this study on your own time; not during regular working hours*)

VOLUNTEER'S STATEMENT:

I have been given a chance to ask questions about this research study. These questions have been answered to my satisfaction. I may contact Dr. Clancy if I have any more questions about taking part in this study.

I understand that my participation in this research project is voluntary. I know that I may quit the study at any time without losing any benefits to which I might be entitled. I also understand that the investigator in charge of this study may decide at any time that I should no longer participate in this study.

If I have any questions about my rights as a research subject in this study I may contact:

Prof. Kent J. Rissmiller, Chair
WPI Institutional Review Board
100 Institute Road
Worcester, MA 01609
(508) 831-5296 [E-mail: irb@wpi.edu]

By signing this form, I have not waived any of my legal rights.

I have read and understand the above information. I agree to participate in this study. I have been given a copy of this signed and dated form for my own records.

Study Participant (signature)	Date
Print Participant's Name	
Person who explained this study (signature)	Date

A-6.2: SOP-001 Procedure for Conducting an Informed Consent with a Potential Subject

See: Jennifer Keating, "Relating forearm muscle electrical activity to finger forces," M.S. thesis, Worcester Polytechnic Institute, Worcester, MA, May 2014, pp. 162–164.

A-6.3: Subject Questionnaire

Subject Questionnaire and Data Collection Sheet
(Completed by Verbal Interview After Informed Consent)

Relating Arm Muscle Electrical Activity to Hand/Finger Forces for use in Prosthesis Control and Stroke Rehabilitation Devices

Subject Identification Code: _____
(to be filled out by study staff)

Age (in years):	Height: _____ ft _____ in
Weight (in lbs):	Gender (circle one): Male Female
Ethnic category (circle one): Hispanic or Latino Not Hispanic or Latino Not reported	Racial category (circle one): American Indian/Alaska Native Asian Native Hawaiian or Other Pacific Islander Black or African American White More Than One Race Not reported

Do you have any condition affecting the function of your hands, arms or shoulders? Yes No If yes, please describe:
Do you have any past injuries to your right elbow or shoulder? Yes No If yes, please describe:
Do you have any limitations to your range of motion in your right elbow or shoulder? Yes No If yes, please describe:

TURN

Do you have any scars on your arms? Yes No If yes, please describe:
Do you have any physical limitations that would hinder your ability to complete this experimental work? Yes No If yes, please describe:
If female: Are you pregnant or could you be pregnant? Yes No [If yes, exclude as subject.]

A-6.4: Source Document for Clinical Procedure

See: Jennifer Keating, "Relating forearm muscle electrical activity to finger forces," M.S. thesis, Worcester Polytechnic Institute, Worcester, MA, May 2014, pp. 167–177.

A-6.5: Hand-Wrist and Finger Projects Subject Active Subject ID's

Hand-Wrist Project Subject ID's		Finger Project Subject ID's	
LZ41		ww02	ww12
LZ42		ww03	ww13
LZ43		ww04	ww14
LZ45		ww05	ww15
LZ46		ww06	ww17
LZ47		ww07	ww18
LZ48		ww08	ww19
LZ49		ww09	ww20
LZ50		ww10	ww21
		ww11	